

c.2



Lawrence Berkeley Laboratory

UNIVERSITY OF CALIFORNIA

EARTH SCIENCES DIVISION

RECEIVED
LAWRENCE
BERKELEY LABORATORY

APR 19 1988

LIBRARY AND
DOCUMENTS SECTION

Seismic Body Waves and the Earth's Inner Core

P. Cummins
(Ph.D. Thesis)

December 1987

TWO-WEEK LOAN COPY

*This is a Library Circulating Copy
which may be borrowed for two weeks.*



LBL-24735
c.2

DISCLAIMER

This document was prepared as an account of work sponsored by the United States Government. While this document is believed to contain correct information, neither the United States Government nor any agency thereof, nor the Regents of the University of California, nor any of their employees, makes any warranty, express or implied, or assumes any legal responsibility for the accuracy, completeness, or usefulness of any information, apparatus, product, or process disclosed, or represents that its use would not infringe privately owned rights. Reference herein to any specific commercial product, process, or service by its trade name, trademark, manufacturer, or otherwise, does not necessarily constitute or imply its endorsement, recommendation, or favoring by the United States Government or any agency thereof, or the Regents of the University of California. The views and opinions of authors expressed herein do not necessarily state or reflect those of the United States Government or any agency thereof or the Regents of the University of California.

**Seismic Body Waves and the Earth's
Inner Core**

by

Phillip Cummins

(Ph.D. Thesis)

**Department of Geology and Geophysics and
Center for Computational Seismology at Lawrence Berkeley Laboratory
University of California
Berkeley, California 94720**

Seismic Body Waves and the Earth's Inner Core

Phillip Cummins

ABSTRACT

In this study short-period body wave seismograms are numerically modeled to investigate the sensitivity of core phase waveforms to structure near the Earth's inner core boundary (ICB). A calculation technique is developed which is a hybrid combination of asymptotic and discrete-layer reflectivity methods, the former being applicable to the smoothly-varying layers of the mantle and outer core, whereas the latter is used for the more complicated structure near the ICB. This technique facilitates the consideration of a large number of different models for structure near the ICB.

The numerical results indicate that the frequency content of reflected short-period PKiKP waveforms observed at distances less than 40° is very sensitive to the thickness of the transition zone, with published data constraining the thickness to be less than 5 km. In the distance range $60 - 90^\circ$, effective decoupling of short-period PKiKP and PKJKP is achieved for transition zones as thin as 3 km, resulting in substantial distortion of the PKiKP waveform. The results indicate that the PKIKP+PKiKP waveforms in the distance range $120 - 130^\circ$ used in this study are not as sensitive to the transition thickness, so that it is reasonable to treat the ICB as a true discontinuity in the modeling procedure used here.

The data used in this study consist of PKIKP+PKiKP waveforms recorded by the Regional Seismic Test Network for 10 events in the south Pacific. Results indicate that the low Q_α in the inner core is associated with an absorption band on the high-frequency side of the short-period seismic band. The data determine the P-velocities above and below the ICB

to within a trade-off that is well constrained by the data: with a P-velocity above the ICB given by PREM, the P-velocity below the ICB is $11.03 \pm .03$ km/s. Similarly, for these data the estimate of the S-velocity at the top of the inner core trades off with the estimate of Q_α , but it is reasoned that the jump in S-velocity at the ICB is not likely to be less than 3 ± 1 km/s.

**This thesis is dedicated to Prof. Lane Johnson's
faith in his students**

Acknowledgments

I am greatly indebted to Prof. Lane Johnson for his excellent advice and support, as well as for setting an impeccable example in the human and technical aspects of responsible scientific endeavor. I am also grateful to Prof. Thomas V. McEvelly for many enthusiastic discussions and help in obtaining data and programs, and to Prof. H.F. Morrison for his help and advice. I thank Dr. E.L. Majer for his friendship and hard work in maintaining the outstanding work environment at Lawrence Berkeley Laboratory, and Shimon Cohen and Dahlia Rose Harper for their guidance and sage counsel.

I want to thank my fellow graduate students for the many open and frank discussions about geophysics, science, and life. Although it is difficult to name them all I can certainly try. I thank Tom Daley, Fred Eastwood, Joel Ita, Ann Kirkpatrick, Mike Leonard, Jim Nelson, Dan O'Connell, Jay Pulliam, Jonathan Scheiner, Lupe Severenson, Mary Templeton, and Dave Tralli for their friendship and support. I am especially indebted to Lee Hirsch, John Peterson, and Don Vasco for making my time in graduate school a wonderful personal experience as well as an educational one.

I would like to thank all of the people at the Earth Sciences Division of Lawrence Berkeley Laboratory, as well as those at the U.C. Berkeley Seismographic Station and the Geology and Geophysics Dept. who made this research possible. This work was supported by the Institute of Geophysics and Planetary Physics at Lawrence Livermore Laboratory under grant 87-15, and through the U.S. Department of Energy Contract No. DE-AC03-76SF00098 by the Assistant Secretary for Energy Research, Office of Basic Energy Sciences.

Finally, I would like to express my appreciation to my family for their personal interest and emotional support. My parents have always encouraged me to seek out new and exciting challenges and my grandparents backed even my more dubious undertakings. Both my brother Chris and sister Karen have extended much concern and companionship. I would also like to thank Lisette van Vliet for teaching me about love and beauty in a world of numbers and computer terminals, and for her late-night xeroxing efforts. There actually are things in life more important than sex, drugs, and rock and roll!

Table of Contents

Dedication	i
Acknowledgements	ii
Chapter 1: Introduction	1
1.1 A Resumé of Seismological Investigations of Core Structure	2
1.2 Phenomenological Interpretations of Structure Near the ICB	8
1.3 The Approach to the Seismological Investigation of Core Structure Adopted Here	10
References	13
Chapter 2: Synthetics Seismograms for an Inner Core Transition of Finite Thickness	18
Summary	18
2.1 Introduction	18
2.2 The Asymptotic Method	20
2.3 The Earth Flattening Transform and Invariant Imbedding	22
2.4 The Hybrid Method	27
2.5 Numerical Results	30
2.5.1 Pre-critical PKiKP: $0^\circ - 100^\circ$	33
2.5.2 PKiKP and PKIKP near the D cusp: $120^\circ - 130^\circ$	36
2.6 Conclusions	37
References	39
Chapter 3: Short Period Body Wave Constraints on Properties	

of the Earth's Inner Core Boundary	51
Summary	51
3.1 Introduction	51
3.2 Data	54
3.3 Analysis Procedure and Models of the ICB	58
3.4 Results	61
3.4.1 Frequency Dependence of Q_α in the Inner Core	63
3.4.2 P-velocity structure near the ICB:	
Distance Range (a) $120^\circ - 125^\circ$	65
3.4.3 P-velocity structure near the ICB:	
Distance Range (b) $128^\circ - 132^\circ$	66
3.4.4 P-velocity structure near the ICB:	
Distance Range (c) $133^\circ - 135^\circ$	67
3.4.5 S-velocity and Q_α below the ICB	68
3.5 Conclusions	70
References	74
Chapter 4: Conclusions	94
Appendix A: (β_i , Q_α) Waveform Comparisons for	
Distance Range (b)	98
Appendix B: (α_i , α_o) Waveform Comparisons for	
Distance Range (b)	109
Appendix C: Translation of M.A. Isakovich's Article on Thermal Dispersion	117
Appendix D: A Detailed Derivation of Isakovich's Formulas in Section 5	127

Chapter 1: Introduction

Knowledge of the major structural boundaries in the Earth is crucial to our understanding of its physics and chemistry. For example, the question of two-layer or one-layer mantle convection is directly connected with the question of the thermodynamic nature of the upper mantle discontinuities: are they due to changes of phase or composition? The nature of convection in both the mantle and core is to some extent determined by the strength and distribution of heat sources within the Earth, of which the heat produced (or absorbed) by phase changes at the core-mantle boundary (CMB) and the inner core boundary (ICB) may form an integral part. The Earth's magnetic field is produced by motion in the fluid outer core which is driven by these same thermodynamic processes at either the ICB or the CMB. Also, temperature profiles in the Earth are inferred by extrapolating the known geotherm at the surface of the Earth to the melting and freezing temperatures of iron at the CMB and the ICB, respectively.

This study is a seismological investigation of material properties near the Earth's inner core boundary. As described below, there is some evidence for complexity in the change of material properties at the ICB, i.e. evidence for an extended transition zone rather than a sharp boundary separating two homogeneous media. Complementing the general importance that our knowledge of the nature of the ICB has for our understanding of the Earth as a whole, there are some important implications which may derive from the existence of an extended transition zone at the ICB. Observational evidence for a gradual transition between the inner and outer cores may have important implications for our understanding of the effects of alloying on the solidification of inner core material. Similarly, an interpretation of anomalous material properties near the ICB in terms of thermal structure may indicate the presence of heat-producing dioxides at the base of the outer core. Specific phenomenological

models for a complicated transition are described below. It is the purpose of this study to decide if there is indeed evidence for a revision of the current simple picture of the inner core boundary as the point where the temperature profile of the Earth intersects the solidus of the liquid material in the outer core.

A historical survey of seismological investigations of the inner core is given below, with special attention being given to the inference of anomalous structure (i.e., strong velocity gradients) near the ICB. This survey is by no means complete (in particular, no mention is made of free oscillation studies, which have yielded extremely valuable information about the average properties of the core), but is merely intended to give a representative picture of the present state of affairs regarding our knowledge of the velocity structure of the Earth's core. This survey is followed by a description of some models for a complex inner core transition that have appeared in the literature, and a description of the approach to a seismological investigation of the ICB adopted here.

1.1. A Resumé of Seismological Investigations of Inner Core Structure

The history of seismological studies of core phases provides an interesting picture of the development of seismic observations as a tool for studying the Earth's interior. Prior to Lehman's (1936) and Gutenberg and Richter's (1938) studies of short-period core phases, it was thought that the first-arriving long-period P waves in the distance range $110^\circ - 142^\circ$ represented energy diffracted from the caustic at point B (see Figure 1) on the PKP travel-time curve. This seemed a reasonable assumption as ray theory predicts that the caustic surface associated with outer core PKP phases intersects the Earth's surface at $\approx 142^\circ$, and it was known that long-period energy diffracted from the caustic should be observable at considerable distances into the 'shadow zone' ($\Delta < 142^\circ$). With the advent of short-period instruments, however, it was noticed that even short period PKP energy could be observed at 123° , and Lehman (1936) and Gutenberg and Richter (1938) recognized that this observation required the presence of a high-velocity inner core in which strong refraction could give rise to short-period arrivals at this distance. Jeffreys (1939a) proved that it was indeed impossible for

short-period energy diffracted from the B caustic to be observable at distances more than a few degrees from the caustic, and that even long-period energy should not be observable at 110° .

At this point the situation was ripe for using the correct interpretation of PKP in the distance range $147^\circ - 180^\circ$ to estimate the P-velocities in the Earth's core, which Jeffreys did in 1939 (Jeffreys, 1939b). Jeffreys did this by using the travel time curves for the mantle phases PcP and ScS to subtract the mantle times from the outer core phases SKS and PKP, yielding a travel time curve for the outer core alone, and this latter curve could be inverted for outer core structure using the Herglotz-Wiechert method. This could only be done for the AB and EF portions of the travel time curve however, as the BC and CD phases are generally obscured by the first-arriving PKIKP phase. The BC and CD phases provide information about the velocity structure just above the inner core, and Jeffreys reasoned that it was necessary make some assumption about the P-velocity in this depth interval that was consistent with the observations for the BE and DF branches of the travel time curve. Unfortunately, Jeffreys chose to make this velocity distribution consistent with the 'refracted' PKIKP phase observed at 110° ; extrapolation of the DF travel time curve to this distance yielded a slowness of 2.12 s° . Thus, the reflected PKiKP phase had to arrive at 110° after the observed PKIKP phase and with a slowness greater than 2.12 s° ; moreover, since the reflected branch had to have a curvature that was concave upwards, the slowness for PKiKP grazing the top of inner core had to be even higher. This latter requirement led Jeffreys to assume a low velocity above the inner core that actually involved a decrease of velocity with depth, and this low velocity required a large inner core radius to result in a reflected phase that would arrive just after the 'refracted' phase observed at 110° . The results of later studies indicate that refracted PKIKP is not observable until 120° , so that the PKIKP phase described by Jeffreys was almost certainly a pre-critical PKiKP reflection arriving with a slowness that was considerably less than 2.12 s° . This misinterpretation resulted in an estimated P-velocity above the inner core that was too low ($\approx 9.8 \text{ km/s}$, while the PREM value is 10.356 km/s), an inner core radius that was too large (1256 km as opposed to 1221.5 km for

PREM), and a P-velocity just below the ICB that was too high (11.16 km/s opposed to 11.03 for PREM). While Jeffreys seems to have been aware that the observed phase at 110° may have been a pre-critical reflection, he nevertheless saw fit to introduce such a drastic feature in the velocity profile of the outer core without reconsidering his original assumption that the the observed phase was refracted.

It was not until 1952 that M.E. Denson (1952) observed that the increase in amplitude of 'PKIKP' near 120° indicated that PKIKP began at 120° , instead of 110° as Jeffreys had assumed, and Denson was one of the first to report observations of short-period precursors to PKIKP in the distance range $125^\circ - 140^\circ$. In 1958 Gutenberg published two studies (Gutenberg, 1958a and 1958b) of these short-period 'precursors' to PKIKP, in which the first suggestions of anomalous structure near the ICB appeared. In these two papers, Gutenberg suggested that material near the ICB was strongly dispersive, so that the short-period precursors represented high-frequency PKIKP energy that, near the transition between inner and outer cores, propagated with higher velocity than the lower-frequency energy of the main PKIKP pulse. This dispersion was manifest only in that part of the PKIKP travel time curve corresponding to rays with turning points at the transition. Gutenberg based his suggestion on work by Kuhn and Vielhauer (1953) on the propagation of elastic waves in material undergoing solidification, which indeed indicated that the solid-liquid boundary in the system they studied occurred closer to the liquid part of the system for high-frequency waves than was the case for low-frequency pulses. Gutenberg does not mention that the system studied by Kuhn and Vielhauer consisted of pine resin, a material whose properties may be very much different from those of geologic materials like Fe-FeS, especially at the melting point (Gutenberg's hypothesis was later given some theoretical basis by Anderson, 1980 and 1983, see below). He did note, however that 'the rather sudden end of the short-period waves at about the same distance and time where the long-period diffracted PKP begins looks suspicious' (Gutenberg, 1958b).

Two studies in the early 1960's rejected Gutenberg's dispersion hypothesis and instead postulated additional layering above the inner core to explain the PKIKP 'precursors'. Bolt

(1962 and 1964) added a single additional interface 420 km above the inner core and replaced Jeffreys' negative velocity gradient in this region with a constant velocity layer, reasoning that this still satisfied Jeffreys' travel time data within the statistical uncertainty. This increased the outer core P-velocity just above the inner core to a value of 10.31 km/s and also reduced the inner core radius to 1220 km, both of which were significant improvements over Jeffreys' model. These changes, together with an increase of inner core velocity to 11.22 km/s, appear to be consistent with Jeffreys original location of the D cusp at 110° . The study by Adams and Randall in 1964 suggested that yet another layer ≈ 300 km above the interface giving rise to Bolt's GH branch needed to be added to models of the core. Again, their model was tied to Jeffreys', in that the P-velocity above the transition zone was the same, and the D cusp had a similar slope and occurred at 110° . Given the hypothetical increases at the two interfaces above the inner core, it would seem that the latter two requirements alone would have forced the velocity gradients in the two shells to be negative, and in fact this is what Adams and Randall suggest. If the two shells had involved a substantial increase in average P-velocity, the D cusp would have been placed at a distance greater than 110° , where it had been erroneously located by Jeffreys (1939b).

The development of large seismic arrays and installation of the WWSSN led to a plethora of seismological studies of core structure. Pre-critical PKiKP reflections were observed at LASA by Engdahl *et al* (1970) and Bolt and Qamar (1970) at distances as small as 11° , and it was finally recognized that the phases observed at 110° which had previously been interpreted as PKiKP refractions were actually pre-critical PKiKP reflections (Buchbinder *et al* (1973)). Two independent studies by Buchbinder (1971) and Qamar (1973) resulted in very similar models of the core, in which they noted that the increase in PKiKP amplitudes fixed the D cusp at 120° (a result that had actually been obtained by Denson (1952) almost 20 years earlier). These studies were deficient in at least two respects, however. Both studies based their velocity structure just below the ICB on PKiKP travel time data in the distance range $\Delta < 140^\circ$, and it appears that some of these times may have instead been associated with PKiKP. For example, it is clear from Qamar's plot of PKiKP and

PKiKP amplitudes versus distance (Figure 16 in Qamar (1973)) that he thought PKiKP was the phase with higher amplitude in the distance range 120 – 130°; the results of this study indicate that the low Q_α in the inner core results in a PKiKP phase that is almost unobservable in this distance range, while the amplitude of PKiKP is strong. Buchbinder was aware that a low Q was required in the inner core, and that amplitudes of PKiKP should be less than those of PKiKP in the distance range 120 – 130° (see his Figure 22), but his analysis was based partly on Engdahl's (1968) earlier observations. In any case, it seems conceivable that a misidentification of PKiKP could have resulted in slowness measurements at the D cusp that were biased toward the slightly higher values of PKiKP. This would have led to the low velocity at the top of the inner core and introduced curvature into the travel time curve of the DF branch leading to the high P-velocity gradient at the top of the inner core that is apparent in their models.

The second deficiency in the Buchbinder (1971) and Qamar (1973) models was that their P-velocity structure just above the inner core was based on their interpretations of the PKiKP 'precursors' as being due to layering above the inner core. Other studies published at about the same time (e.g. Cleary and Haddon (1972), Haddon and Cleary (1974), Doornbos and Vlaar (1973), Husebye, King, and Haddon (1976)) established that these phases were the result of scattering of PKP where its caustic surface intersects the core-mantle boundary, and had nothing to do with structure near the ICB. Furthermore, Müller's (1973) study of long-period core phase amplitudes showed that, since no long-period reflections from the transition zone were observed, 'it is safe to conclude that the transition zone does not exist'. Müller also found it necessary to reduce the P-velocity jump at the ICB, and this led to a strong P-velocity gradient at the top of the inner core. In retrospect it seems that both his data and global travel time data may have been equally well satisfied by a higher P-velocity above the inner core (see below), the same jump in P-velocity that he obtained, and a weak gradient in P-velocity below the inner core boundary (in fact Müller points out that such a revision may be necessary).

Several studies conducted in the early 1980's suggested substantial modifications to previous models for the core. In 1981 Dziewonski and Anderson (1981) constructed the Preliminary Reference Earth Model (PREM), which attempted to satisfy both global travel time and free oscillation data in a consistent manner. This model had no region of high velocity gradients at the top of the inner core, and the P-velocity profile did not flatten out at the base of the outer core, as some previous models had suggested. Håge (1983) and Choy and Cormier (1983) conducted waveform studies of core phases which suggested some modifications to the PREM model. Håge used amplitude measurements of a large number of long-period core phase observations near the D cusp to place constraints on the jumps in P- and S-velocity at the inner core boundary. His results for the P-velocity were consistent with PREM, but his estimate for the S-velocity in the inner core was significantly lower than that of PREM (2-3 km/s as opposed to 3.5 km/s for PREM), indicating that the top of the inner core may be characterized by a strong gradient in S-velocity. Choy and Cormier (1983) studied short-period and broadband waveforms at several different points on the PKP travel time curve for a single event. Their results were consistent with PREM except for the P-velocity jump at the inner core boundary, which they reduced to $.52 \pm .07$ km/s from the PREM value of .67 km/s. They also suggested that the S-velocity may be zero at the top of the inner core, although this was poorly constrained by their data. Johnson and Lee (1985) performed an inversion of global travel time data which determined bounds for the velocity in the core. Their results showed that PREM could be brought into agreement with the global travel time data through changes in P-velocity that were never greater than .1 km/s, and that models such as those of Jeffreys (1939b) and Qamar (1973) (and presumably that of Müller (1973)) which had a transition zone of very weak velocity gradient above the inner core were not consistent with the global travel time data. They also pointed out that the small velocity jump obtained by Choy and Cormier (1983) fell outside their extremal bounds for P-velocity in the core.

In their 1985 study Johnson and Lee also published array measurements of core phase slownesses in the distance range 120 - 140° made at the Tonto Forest Seismological

Observatory. This was the first instance in which slowness measurements of *both* PKiKP and PKIKP at distances less than 140° were reported, so that there could be no question of confusion between PKiKP and PKIKP. Their results are roughly consistent with PREM, although they do not entirely rule out the relatively high slownesses for PKIKP measured by Qamar (1973) (For example, Johnson and Lee measure $1.94 \text{ s} / ^\circ$ at 123.9° , while Qamar estimated $1.99 \pm .04 \text{ s} / ^\circ$ at 120°).

1.2. Phenomenological Interpretations of Structure Near the Inner Core Boundary

The earliest interpretation of anomalous structure near the ICB was due to Gutenberg (1958a, 1958b). As mentioned above, he explained the short period precursors to PKIKP in terms of dispersion in a transition zone between the liquid outer core and an inner core of higher viscosity, with no real difference between the material of the outer and the inner core. This explanation was rejected as soon as the increasing quality of seismic data led to more plausible explanations for the precursors. Gutenberg does appear, however, to have been the first to suggest that the melting point curve of inner core material and the temperature profile intersect at a small angle (Gutenberg, 1958b), a hypothesis which has since received considerable support (Higgins and Kennedy, 1971, Doornbos, 1974, and Cormier, 1980).

Gutenberg's original idea of a viscoelastic inner core has been resurrected in the work of Anderson (1980 and 1983). Anderson points out that the observed bulk dissipation in the Earth's fundamental radial mode of free oscillation (${}_0S_0$) could be explained by viscous relaxation of the inner core, with the inner core boundary representing a glass transition at which the viscous relaxation time is equal to the period of the seismic waves interrogating it. In the latter paper (Anderson, 1983) he supports this hypothesis by referring to the work of Choy and Cormier (1983) and Håge (1983), both of which were body waveform studies suggesting the presence of strong gradients in seismic wave velocities at the top of the inner core. Anderson considers these results as suggestive of a broad transition region with a gradual increase in rigidity, with the high anelasticity that decreases with depth corresponding to a viscous relaxation band that sweeps through the frequency band for seismic body waves as

the relaxation time increases with pressure (i.e., depth). This model has profound implications for our understanding of the inner core: (a) since there is no crystallization of outer core material at the ICB, no latent heat or light rejected solute is produced at the base of the outer core, so that some other mechanism must be invoked for powering the geodynamo, (b) the Earth's temperature profile is no longer required to pass through the freezing point of an Fe-FeS mixture at the inner core boundary (although it must still pass through the melting point of iron at the core-mantle boundary), and (c) the inner core may not be rigid at all at the low frequencies associated with core convection.

Another interpretation of core structure which has important implications for our understanding of the thermal and chemical state of the core is that of Fearn *et al* (1981) and Loper and Fearn (1983). They consider (Fearn *et al* 1981) that the inner core is growing so fast that a substantial portion of the fluid outer core has become constitutionally supercooled, resulting in the growth of dendrites from the inner core which are broken off by convective motion in the outer core to eventually form a slurry of iron particles. In order to reconcile the small jump in P-velocity predicted by this model with the high jump in P-velocity inferred from seismic observations, Loper and Fearn (1983) modified this model to include a rigid matrix below the ICB which contains a large volume fraction (up to 0.47) of interstitial fluid. They conclude that this model can produce a sharp increase in both P- and S-velocity, as well as the observed P-wave attenuation in the inner core through bulk dissipation associated with thermal and material diffusion. This model has the following implications for the physics of the core: (a) both latent heat and light rejected solute are produced in a volume of considerable depth extent rather than at the surface of the inner core, complicating the relation between the growth rate of the inner core and its thermal and chemical history, (b) fluid convection occurs within the inner core as well as in the outer core, so that flow lines associated with outer core convection pass through the inner core, and (c) the inner core does not consist of pure iron.

While the above two models have by no means been generally accepted as valid representations of the physical state of the core, it does appear to be generally accepted that

the low Q_α observed for short-period body waves in the inner core is associated with the near coincidence of the melting curve for iron with the temperature profile in the top few hundred kilometers of the inner core. The original suggestion by Gutenberg (1958b) that this is the case was strengthened by the work of Higgins and Kennedy (1971), who found that both the adiabatic gradient and melting point gradient are very flat in the inner core, with a temperature at the center of the Earth that was only 15° below melting. This has led seismologists to invoke partial melting as an explanation for the low Q_α of seismic body waves observed in the top few hundred kilometers of the inner core (Doombos, 1974, Cormier, 1980). More recently, Stiller *et al* (1980) have attempted to describe this seismic anelasticity in terms of order parameter relaxation, which they reason could be of sufficiently low frequency near the melting point to be important in the seismic frequency band. In any case, obtaining more information about the attenuation of short period body waves in the inner core may yield some information about the temperature gradient below the ICB, which would have direct consequences for hypotheses on convection and heat sources in the inner core.

1.3. The Approach to the Seismological Investigation of Core Structure Adopted Here

The resumé of previous seismological studies presented here demonstrates that the anomalous structure near the ICB inferred by the earlier studies was often the result of erroneous interpretations of the available data and inconsistent a priori assumptions in the inversions for velocity structure. In the later studies the typically large amounts of data and more complicated analysis procedures make it difficult to assess how well the various models are constrained, but here also the inference of anomalous structure near the ICB seems questionable. In particular, it seems that few of the studies suggesting strong velocity gradients at the top of the inner core are based on data which is sensitive to velocity structure in this region of the Earth (i.e., observations of waves which bottom near the ICB). Nevertheless, the weak velocity gradients in the outer core and strong velocity gradients in the inner core that appear in many Earth models derived from seismological data have led to various phenomenological interpretations with vastly different implications for the physical state of

the Earth's core. Thus, it seems worthwhile to consider how well structure near the ICB is constrained by data which directly samples this region, and that is the purpose of the present study.

The data chosen for this study consist of short-period body-waveform data, since such data have good depth resolution and it is possible to use all of the information in the seismogram for the analysis. At the time this study was undertaken a new source of very high quality short-period digital waveform data became available in the form of recordings from the Regional Seismic Test Network (RSTN). The RSTN was deployed by the U.S. Department of Energy as a prototype network for monitoring nuclear test explosions in the Soviet Union. It consists of 5 stations in North America which employ state-of-the art seismic recording equipment emplaced in 100 m boreholes. More importantly, the sites selected for deployment were sites of low ambient seismic noise in areas of the North American continental shield having relatively simple crustal structure. Since an appropriate theoretical framework for the inversion of seismic body-waveform data does not exist at the present time, a modeling procedure was adopted.

In Chapter 2 a technique is developed for calculating synthetic seismograms for transitional models of the ICB. This technique is a hybrid combination of the 'full wave' and reflectivity algorithms which takes advantage of the speed and simplicity of the former for performing wavefield calculations in the mantle, outer core, and deep inner core where the smooth velocity structure is suitable for the asymptotic approximations used by the algorithm. Near the ICB the hybrid method uses an invariant imbedding algorithm to calculate the full reflectivity response of the transition zone, which can have an arbitrarily complex velocity structure. This technique is applied to the analysis of previously published data to demonstrate that the inner core transition has a scale length of at most 5 km, i.e., it is a very sharp feature. Waveform modeling of the RSTN data for the transition zone models indicates that the depth resolution of this data near the ICB is about 10 km, so that it is reasonable to consider it as a sharp transition in what follows.

Chapter 3 describes the details of the modeling procedure in which 4 parameters describing the transition at the ICB were systematically varied: P-velocity above the ICB, P-velocity below the ICB, S-velocity below the ICB, and Q_α at the top of the inner core. The effects of the former two are separated from those of the latter by considering that the position of the D cusp and travel time difference between PKIKP and PKiKP are dependent primarily on the P-velocities above and below the ICB, while the relative amplitudes of PKIKP and PKiKP are determined by the S-velocity and Q_α at the top of the inner core. No further separation of the parameter estimation process is possible and trade-off curves are established for the two groups of parameters.

References

- Adams, R.D., and M.J. Randall, The fine structure of the Earth's core, *Bull. Seism. Soc. Am.*, 54, 1299-1313, 1964.
- Anderson, D.L., A new look at the inner core of the Earth, *Nature*, 302, 660, 1983.
- Anderson, D.L., Bulk attenuation in the Earth and viscosity of the core, *Nature*, 285, 204-207, 1980.
- Anderson, O.L., Properties of iron at the Earth's core conditions, *Geophys. J. R. Astr. Soc.*, 84, 561-579, 1986.
- Bolt, B.A., Gutenberg's early PKP observations, *Nature*, 196, 122-124, 1962.
- Bolt, B.A., The velocity of seismic waves near the Earth's center, *Bull. Seism. Soc. Am.*, 54, 191-208, 1964.
- Bolt, B.A., and A. Qamar, Upper bound to the density jump at the boundary of the Earth's inner core, *Nature*, 228, 148-150, 1970.
- Buchbinder, G.G.R., A velocity structure of the Earth's core, *Bull. Seism. Soc. Am.*, 61, 429-456, 1971.
- Buchbinder, G.G.R., Wright, C. and G. Poupinet, Observations of PKiKP at distances less than 110°, *Bull. Seism. Soc. Am.*, 63, 1699-1707, 1973.
- Choy, G.L., and V.F. Cormier, The structure of the inner core inferred from short-period and broadband GDSN data, *Geophys. J. R. Astr. Soc.*, 72, 1-21, 1983.
- Cleary, J.R., and R.A.W. Haddon, Seismic wave scattering near the core-mantle boundary: a new interpretation of precursors to PKP, *Nature*, 240, 549-551, 1972.
- Cormier, V.F., Short-period PKP phases and the anelastic mechanism of the inner core, *Phys. Earth Planet. Inter.*, 24, 291-301, 1980.
- Cummins, P., and L.R. Johnson, Complete synthetic seismograms for an inner core transition of finite thickness, *Geophys. J. R. Astr. Soc.*, in press, 1988.

Denson, M.E. Jr., Longitudinal waves through the Earth's core, *Bull. Seism. Soc. Am.*, 42, 119-134, 1952.

Doombos, D.J., and N.J. Vlaar, Regions of seismic wave scattering in the Earth's mantle and precursors to PKIKP, *Nature Phys. Sci.*, 243, 58-61, 1973.

Doombos, D.J., The anelasticity of the inner core, *Geophys. J. R. Astr. Soc.*, 38, 397-415, 1974.

Doombos, D.J., Observable effects of a seismic absorption band in the Earth, *Geophys. J. R. Astr. Soc.*, 75, 693-711, 1983.

Dziewonski, A.M., and D.L. Anderson, Preliminary reference Earth model, *Phys. Earth Planet. Inter.*, 25, 297-356, 1981.

Engdahl, E.R., Core phases and the Earth's core, *Ph.D. Thesis*, Geophysics Dept., St. Louis University, 1968.

Engdahl, E.R., Flinn, E.A., and C.F. Romney, Seismic waves reflected from the Earth's inner core, *Nature*, 228, 852-853, 1970.

Fearn, D.R., and D.E. Loper, Structure of the Earth's inner core, *Nature*, 292, 232-233, 1981.

Gutenberg, B., and C.F. Richter, P' and the Earth's core, *M.N.R. Astr. Soc., Geophys. Supp.*, 4, 363-372, 1938.

Gutenberg, B., Caustics produced by waves through the Earth's core, *Geophys. J. R. Astr. Soc.*, 1, 238-247, 1958a.

Gutenberg, B., Wave velocities in the Earth's core, *Bull. Seism. Soc. Am.*, 48, 301-314, 1958b.

Haddon, R.A.W., and J.R. Cleary, Evidence for the scattering of PKP waves near the core-mantle boundary, *Phys. Earth. Planet. Int.*, 8, 211-234, 1974.

Husebye, E.S., D.W. King, and R.A.W. Haddon, Precursors to PKIKP and seismic wave scattering near the mantle-core boundary, *J. Geophys. Res.*, 81, 1870-1882, 1976.

- Häge H., Velocity constraints for the inner core inferred from long-period PKP amplitudes, *Phys. Earth Planet. Inter.*, 31, 171-185, 1983.
- Higgins, G., and G.C. Kennedy, The adiabatic gradient and the melting point gradient in the core of the Earth, *Geophys. J. R. Astr. Soc.*, 28, 97-109, 1971.
- Jeffreys, H., The times of core waves, *M.N.R. Astr. Soc., Geophys. Supp.*, 4, 549-561, 1939a.
- Jeffreys, H., The times of core waves (second paper), *M.N.R. Astr. Soc., Geophys. Supp.*, 4, 594-615, 1939b.
- Kuhn, W., and S. Vielhauer, Beziehungen zwischen der ausbreitung von longitudinal- und transversalwellen in relaxierenden medien, *Z. Physic. Chem.*, 202, 124, 1953.
- Johnson, L.R., and R.C. Lee, Extremal bounds on the P velocity in the Earth's core, *Bull. Seism. Soc. Am.*, 75, n1, 115-130, 1985.
- Lehman, I., "P" *Publ. Bur. Cent. Seism. Internat., Serie A*, 14, 87-115, 1936.
- Loper, D.E., and D.R. Feam, A seismic model of a partially molten inner core, *J. Geophys. Res.*, 88, 1235-1242, 1983.
- Müller, G., Amplitude studies of core phases, *J. Geophys. Res.*, 78, 3469-3490, 1973.
- Qamar, A., Revised velocities in the Earth's core, *Bull. Seism. Soc. Am.*, 63, 1073-1105, 1973.
- Stiller, H., S. Franck, and U. Schmit, On the attenuation of seismic waves in the Earth's core, *Phys. Earth Planet. Inter.*, 22, 221-225, 1980.

Figure 1. Travel time curve for core phases PKiKP, PKIKP, and PKP.

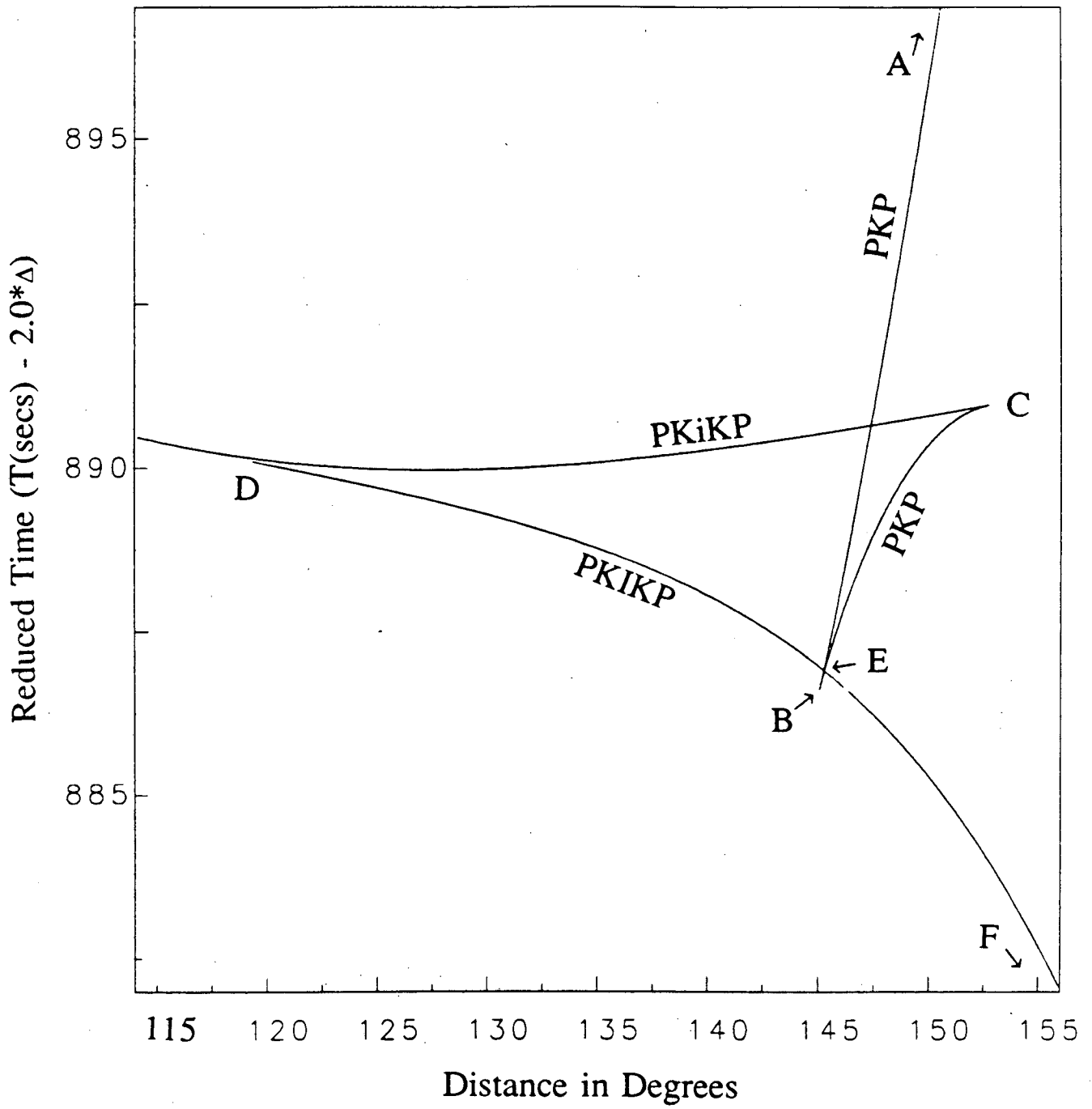


Figure 1

Chapter 2: Synthetic Seismograms for an Inner Core Transition of Finite Thickness

Summary

We describe calculations for short-period body waves that interact with an inner-outer core transition of finite thickness. This involves development of a hybrid full wave-reflectivity algorithm, which is used to calculate synthetic seismograms for Earth models having various transition thicknesses. The numerical results indicate that the frequency content of reflected short-period PKiKP waveforms observed at distances less than 40° is very sensitive to the thickness of the transition zone. Comparison with published data in this distance range indicates that the inner core transition must be less than 5 km thick. In the distance range $60 - 90^\circ$, effective decoupling of short-period PKiKP and PKJKP is achieved for transition zones as thin as 3 km, resulting in substantial distortion of the PKiKP waveform. PKIKP+PKiKP waveforms in the distance range $120 - 130^\circ$ are not as sensitive to the detailed properties of the transition, but the signal quality is good enough to constrain the transition thickness to be less than 10 km.

2.1. Introduction

The existence of transition zones in the Earth's mantle and core has been inferred from seismic data ever since the quality and quantity of such data were adequate for studies of global Earth structure. Our understanding of the nature of these transition zones, however, is still far from complete, and may be crucial to our knowledge of the composition and thermal state of the Earth. An essential feature of such a transition zone which can be constrained by seismic data is its thickness. For example, Lees *et al* (1983) used the frequency dependence of the body wave reflection coefficient for the 670 km upper mantle transition zone to

determine a maximum thickness of 5km. Interpreting this result in terms of phase diagrams for hypothesized mantle phase changes allowed them to conclude that this transition zone must involve a change in composition as well as phase.

Various investigators have postulated the existence of a transition zone between the Earth's inner and outer core, taking the form of either a dendritic 'mush' (Loper and Fearn, 1983) or a layer of adcumulates (Morse, 1986). While such models seem consistent with our theoretical understanding of the solidification process in multicomponent systems, studies of short period body waves reflected by the inner core indicate that "the inner core has a sharp boundary relative to 1-s period waves" (Engdahl *et al*, 1974). Clearly, some quantification of this latter statement is required if we are interested in using seismic data to estimate the thickness of the hypothesized transition zone and determine what its properties reveal about the the process of core solidification.

Unfortunately, precise quantification of the thickness constraint that seismic body wave data place on the properties of the inner core transition requires the calculation of synthetic seismograms for phases that have traversed the mantle and outer core and interacted with the high velocity and density gradients in the transition zone. Phinney (1970) and Hron and Chapman (1974) have considered this type of problem using analytic solutions of the scalar Helmholtz equation for special forms of the transition zone discovered by Epstein. While this approach allowed Phinney to estimate the scale length of the inner core transition to be about 1.5 km, these results applied only to the acoustic case, and could be applied only to the special forms of transition zones for which analytic solutions were available. The calculations for seismic waves interacting with a transition zone of arbitrary form have so far not been attempted.

For an infinitesimally thin transition this could be accomplished by calculating asymptotic solutions to the wavefields that satisfy appropriate boundary conditions at the top of the inner core (Richards, 1973, Cormier and Richards, 1977, and Chapman, 1978). However, if all of the reverberation and coupling phenomena that may occur in the presence of the high gradients of a transition zone of finite thickness are to be accounted for, a more complete

approach is necessary. Two such approaches have been considered in the literature: the iterative asymptotic treatment described by Chapman (1981), and a combination of the Earth flattening transform and a discrete layer approximation of the continuous transition (e.g. Müller, 1973). The asymptotic methods are computationally convenient when calculating the response of a few layers with smooth velocity profiles, but they become cumbersome and expensive when turning points occur in regions of high velocity gradients. While the homogeneous (Earth-flattened) layer approximations avoid the cumbersome expansions and time consuming tau integrations of the asymptotic methods, they do require a large number of layers to model the whole Earth. This problem is especially prohibitive if the results are to be compared with the short period body wave data that will provide the best resolution of the transition zone. To avoid the problems inherent in each of these techniques we have developed a hybrid method that will combine an asymptotic treatment of the few smoothly varying layers of the mantle and outer core with a reflectivity method that will calculate the full wavefield in the transition zone. This hybrid method is described below, preceded by brief reviews of the asymptotic and discrete layer methods.

2.2. The Asymptotic Method

The asymptotic method for calculating body wave seismograms used in this paper has been developed in Richards (1973), Cormier and Richards (1977), and Choy (1977), and we give only a brief review here of its application to the phase PKIKP. Following Richards (1973), we assume that the regions in which the asymptotics are used have sufficiently smooth variations in material parameters that the displacement can be represented by P and SV potentials ϕ and χ :

$$\mathbf{u}(\mathbf{r}, \omega) = \frac{1}{\rho^{1/2}} [\nabla\phi + \nabla \times (0, 0, -\frac{\partial\chi}{\partial\Delta})] + 0(\frac{\mathbf{u}}{\omega}) \quad (1)$$

where we are using the sign convention of Aki and Richards (1980), $\mathbf{u}(\mathbf{r}, \omega) = \int_{-\infty}^{\infty} \mathbf{u}(\mathbf{r}, t) e^{i\omega t} dt$. For a body force given by the gradient of the potential $F \delta(\mathbf{r}-\mathbf{r}_s) H(t)$, these potentials satisfy the decoupled Helmholtz wave equations:

$$\nabla^2 \phi + \frac{\omega^2}{\alpha^2} \phi = \frac{F}{(i\omega\rho_s^{1/2}\alpha_s^2)} \delta(\mathbf{r}-\mathbf{r}_s) + O\left(\frac{|\mathbf{u}|}{\omega}\right)$$

$$\nabla^2 \chi + \frac{\omega^2}{\beta^2} \chi = O\left(\frac{|\mathbf{u}|}{\omega^2}\right)$$

With this potential representation, the radial component of displacement due to P-wave motion when source and receiver radii are equal is:

$$u_r(r_s, \Delta_0, \omega) = \frac{F e^{i\pi/4}}{4\pi\rho_s \alpha_s^2 r_s^2} \left(\frac{\omega}{2\pi \sin \Delta_0}\right)^{1/2} \int_{\Gamma} p^{1/2} T_m(p, \omega) \frac{k^{(2)}(p, \omega)}{k^{(1)}(p, \omega)} R_o(p, \omega) e^{i\omega J(p)} dp \quad (2)$$

where Γ is a contour in the complex p plane and:

r_s = radius of source/receiver;

ρ_s = density at r_s ;

α_s = P velocity at r_s ;

$T_m(p, \omega)$ = product of transmission coefficients above the inner core;

$k^{(j)}(p, \omega)$ = up (1) and down (2) -going Langer asymptotic wave functions

$R_o(p, \omega)$ = reflection coefficient for the transition zone;

$J(p) = 2 \int_p^{r_s} \sqrt{1/\alpha(r) - p^2/r^2} dr + p \Delta_0 = T(p) - p \Delta(p) + p \Delta_0 =$ phase delay;

In the last expression $T(p)$ and $\Delta(p)$ have the interpretation of travel time and distance traveled by the ray with ray parameter p and turning point r_p . These quantities are calculated by numerically integrating functions of the complex velocity profile $\alpha(r)$, which is taken to be the polynomial in r specified by the PREM Earth model (Dziewonski and Anderson, 1981) in each layer of the mantle and outer core. All values of p which contribute to the integral have turning points below the core-mantle boundary, and when r_p lies inside or below the inner core transition zone it will be necessary to extrapolate the outer core velocity profile down to the level of r_p , i.e. $J(p)$ (and $k^{(j)}(p, \omega)$, see below) have contributions from a nonphysical velocity profile. When the turning point lies far below the transition zone, the asymptotic forms of $J(p)$ and $k^{(j)}(p, \omega)$ will be such that these contributions cancel, and when the turning point lies near the transition zone, the contributions due to the extrapolated profile

will be small. In either case, the solution should not be strongly dependent on the extrapolated velocity profile, as described in Chapman and Orcutt (1985, p. 123). Note that in the notation of Richards (1973) the wave function ratio $k^{(2)}/k^{(1)}$ would be included as part of the reflection coefficient $R_o(\omega, p)$, but we have written them separately to emphasize that they are calculated using different techniques.

Finally, the wave functions $k^{(j)}(p, \omega)$ are the Langer asymptotic wave functions described in Richards (1976):

$$k^{(j)}(p, \omega) = \frac{A^{(j)} \xi^{1/2} H_{1/3}^{(j)}(\omega \xi)}{r_o \sqrt{1/\alpha(r_o)^2 - p^2/r_o^2}} \quad (3)$$

Here, $A^{(j)}$ are chosen so that the $k^{(j)}(p, \omega)$ become Hankel functions in a homogeneous Earth, and $\xi = \int_p^{r_o} \sqrt{1/\alpha(r)^2 - p^2/r^2} dr$ is calculated for the the velocity profile in the outer core. The wave functions $k^{(j)}(p, \omega)$ are evaluated just above the transition zone at r_o and the phase is referenced to the same turning point r_p as the corresponding integral in $J(p)$. These wave functions are asymptotic approximations to the exact radial eigenfunctions even at the turning point, and their ratio serves to correct the phase factor $J(p)$ as described in Cormier and Richards (1977).

2.3. The Earth Flattening Transform and Invariant Imbedding

In order to accurately model the reverberation and coupling that occurs within the transition zone, we have chosen to transform the velocity and density profiles to a flat geometry and use the invariant imbedding algorithm of Kennett and Kerry (1979) to calculate the response of a stack of homogeneous layers that approximates the continuous transition. Various forms of the Earth flattening transform (EFT) have been used in the literature (e.g. Müller (1973), Kennett and Illingworth (1981)). We use the form:

$$\frac{r}{r_o} = e^{z/r_o} \quad , \quad \frac{r_o}{r} \alpha(r) = \alpha(z) \quad , \quad \frac{r_o}{r} \beta(r) = \beta(z) \quad , \quad \frac{r}{r_o} \rho(r) = \rho(z) \quad (4)$$

which, according to Chapman and Orcutt (1985), is a compromise between using a transform which is exact for horizontal displacement and one which exactly transforms dilatation. Note that we have chosen a reference radius r_0 at the top of the transition zone.

We use the spherical harmonic expansion of stress τ and displacement \mathbf{u} as defined in Aki and Richards (1980):

$$\mathbf{u} = \sum_{l,m} U \hat{\mathbf{r}} Y_l^m + V \frac{1}{\sqrt{l(l+1)}} \nabla_1 Y_l^m + W \left(-\frac{\hat{\mathbf{r}}}{\sqrt{l(l+1)}} \times \nabla_1 Y_l^m \right) \quad (5)$$

$$\tau = \sum_{l,m} R \hat{\mathbf{r}} Y_l^m + S \frac{1}{\sqrt{l(l+1)}} \nabla_1 Y_l^m + T \left(-\frac{\hat{\mathbf{r}}}{\sqrt{l(l+1)}} \times \nabla_1 Y_l^m \right)$$

where $\nabla_1 = \hat{\Delta} \frac{\partial}{\partial \Delta} + \hat{\phi} \frac{1}{\sin \Delta} \frac{\partial}{\partial \phi}$ and the Y_l^m are normalized surface spherical harmonics. The elastodynamic wave equation requires that the motion-stress vector for P-SV motion (U, V, R, S) satisfy:

$$\frac{d}{dr} \begin{bmatrix} U \\ V \\ R \\ S \end{bmatrix} = \begin{bmatrix} -\frac{2}{r}(1-2\beta^2/\alpha^2) & \frac{\omega\rho}{r}(1-2\beta^2/\alpha^2) & \frac{1}{\rho\alpha^2} & 0 \\ -\frac{\omega\rho}{r} & \frac{1}{r} & 0 & \frac{1}{\mu} \\ -\rho\omega^2 + \frac{4\mu}{r^2}(3-4\beta^2/\alpha^2) & -\frac{2\mu\omega\rho}{r^2}(3-4\beta^2/\alpha^2) & -\frac{4\mu}{r\rho\alpha^2} & \frac{\omega\rho}{r} \\ -\frac{2\mu\omega\rho}{r^2}(3-4\beta^2/\alpha^2) & -\rho\omega^2 - \frac{2\mu}{r^2} + \frac{4\omega^2\rho^2\mu}{r^2}(1-\beta^2/\alpha^2) & -\frac{\omega\rho}{r}(1-2\beta^2/\alpha^2) & -\frac{3}{r} \end{bmatrix} \begin{bmatrix} U \\ V \\ R \\ S \end{bmatrix}$$

where we have used $\sqrt{l(l+1)} = \omega\rho$ and $\mu = \rho\beta^2$ is the rigidity. Applying the EFT, this becomes:

$$\frac{d}{dz} \begin{bmatrix} U \\ V \\ R/\omega \\ S/\omega \end{bmatrix} = \omega \begin{bmatrix} 0 & \rho(1-2\beta^2/\alpha^2) & 1/\rho\alpha^2 & 0 \\ -\rho & 0 & 0 & 1/\rho\beta^2 \\ -\rho & 0 & 0 & \rho \\ 0 & 4\rho^2\rho\beta^2(1-\beta^2/\alpha^2)-\rho & -\rho(1-2\beta^2/\alpha^2) & 0 \end{bmatrix} \begin{bmatrix} U \\ V \\ R/\omega \\ S/\omega \end{bmatrix} \quad (6)$$

$$+ \frac{1}{r_0} \begin{bmatrix} -2(1-2\beta^2/\alpha^2) & 0 & 0 & 0 \\ 0 & 1 & 0 & 0 \\ 4\rho\beta^2(3-4\beta^2/\alpha^2)/\omega r_0 & -\rho 2\rho\beta^2(3-4\beta^2/\alpha^2) & -4\beta^2/\alpha^2 & 0 \\ -\rho 2\rho\beta^2(3-4\beta^2/\alpha^2) & 2\mu/\omega r_0 & 0 & -3 \end{bmatrix} \begin{bmatrix} U \\ V \\ R/\omega \\ S/\omega \end{bmatrix}$$

All of the quantities in the above equation now refer to the flat Earth, e.g. $p \rightarrow r_o p$, $\mu \rightarrow (r/r_o)\mu$. The first matrix on the right hand side is just the coefficient matrix of the system of equations for the flat Earth problem, and is the zeroth-order term in the asymptotic expansion of the layer matrix considered in Woodhouse (1978) and Chapman and Orcutt (1985). The second matrix contains the first and second order terms which will be neglected in what follows. We see that the block diagonal terms of this matrix are of order $(\omega p r_o)^{-1}$ compared to the diagonal terms of the zeroth-order matrix, and this quantity will usually be less than 2 % in the calculations presented here. The off-diagonal error terms are either of similar magnitude or of order $p \beta^2 / \omega r_o$, which is always less than .5 %. These error criteria depend on both slowness and frequency, and this dependence is conveniently summarized by the following inequality:

$$\frac{1}{\omega} < p r_o < \omega \left(\frac{r_o}{\beta} \right)^2$$

Thus, the error introduced by the EFT decreases with increasing frequency, and the above inequality is well satisfied for almost all of the calculations presented here (the low frequencies of the PKiKP phase at distances 0° – 50° may be adversely affected, however).

Aki and Richards (1980) note that the EFT should lead to a degree of approximation equivalent to that given by the Langer approximation that we use in the smoothly varying regions of the Earth. More difficult to assess is the error incurred by approximating the continuously varying flat Earth model by many homogeneous layers. We know that the exact and approximate solutions should converge in the limit of infinitesimally thin layers, and will simply use a layer thickness of 1/4 the P wavelength at the Nyquist frequency, since this seems to be a conservative estimate based on previous work (Chapman and Orcutt (1985), and references listed there). Moreover, test calculations using very thin layers of 0.1 km thickness were not noticeably different from the Green's functions that used a layer thickness of 1/4 the P wavelength at the Nyquist frequency.

Various methods exist for solving the system (6), the primary difference between them being the way in which they treat the numerical instability caused by the presence of

exponentially growing evanescent waves. We use Kennett's algorithm because it avoids this difficulty in a natural way that is typical of invariant imbedding algorithms (Meyer, 1973). In the derivation of this algorithm we follow Chin *et al* (1984), and note that the system (6),

$$\frac{dB}{dz} = \omega AB$$

where B is the motion stress vector and A is the layer matrix, is diagonalizable. We therefore set $B = Dv$, where D is the eigenvector matrix for A , and note that the four columns of D correspond to up- and down-going P and SV waves, each having an amplitude given by the respective component of v . In what follows we denote quantities associated with up- and down-going waves with + and - superscripts, respectively. The equations to be solved for a given homogeneous layer l , $z_l < z < z_{l+1}$, can now be expressed in terms of the up- and down-going waves as:

$$\begin{aligned} \frac{dv_l^+}{dz} &= i\omega\Lambda_l^+ v_l^+ & v_l^+ &= F_l v_l^- \text{ at } z = z_l \\ \frac{dv_l^-}{dz} &= i\omega\Lambda_l^- v_l^- & v_l^- &= v^0 \text{ at } z = z_{l+1} \end{aligned} \quad (7)$$

where $\Lambda_l^\pm = \text{diag}(\pm\sqrt{1/\alpha_l^2 - \rho^2}, \pm\sqrt{1/\beta_l^2 - \rho^2})$, and we have used boundary conditions appropriate to the problem being studied. That is, given the amplitudes of the down-going P and SV waves at z_{l+1} , and the continuity of stress and displacement at z_l (the form of F_l is given below), we must solve for the amplitudes of the up-going P and SV waves at z_{l+1} .

The problem for a given layer has now been phrased as a two-point boundary value problem that is amenable to solution via invariant imbedding. While the general theory involves considering (7) as the equation for a characteristic curve $(v_l^+(z), v_l^-(z))$ imbedded in the integral surface of a differential equation of higher dimension, for the linear case we only need the result that the characteristic curve has the form (Meyer, 1973):

$$v_l^+ = R_l v_l^- + T_l$$

where $T_l = 0$ for the homogeneous boundary condition in (7) (there are no sources in the

layer). \mathbf{R}_l satisfies a Riccati equation, which for our problem reduces to:

$$\frac{d\mathbf{R}_l}{dz} = i\omega(\Lambda_l^+\mathbf{R}_l - \mathbf{R}_l\Lambda_l^-) \quad , \quad \mathbf{R}_l(z_l) = \mathbf{F}_l$$

or

$$\mathbf{R}_l(z) = \mathbf{E}\mathbf{F}_l\mathbf{E} \quad , \quad \mathbf{E} = \text{diag}(e^{i\omega(z-z_l)\sqrt{1/\alpha_l^2-p^2}} \quad , \quad e^{i\omega(z-z_l)\sqrt{1/\beta_l^2-p^2}}) \quad \text{for } z_l < z < z_{l+1}$$

Note that growing exponentials in $\mathbf{R}_l(z)$ are avoided entirely provided the correct sign is chosen for the imaginary parts of the square roots (positive for our form of the Fourier transform).

In expressing the continuity of the stress-displacement vector \mathbf{B} at z_l , we follow Kennett and Kerry (1979) in decomposing the eigenvector matrix \mathbf{D} into its 2×2 up- and down-going components:

$$\mathbf{B}_l(z_l) = \mathbf{D}_l \mathbf{v}_l = \begin{bmatrix} \mathbf{M}_l^+ & \mathbf{M}_l^- \\ \mathbf{N}_l^+ & \mathbf{N}_l^- \end{bmatrix} \begin{bmatrix} \mathbf{v}_l^+ \\ \mathbf{v}_l^- \end{bmatrix} = \begin{bmatrix} \mathbf{M}_{l-1}^+ & \mathbf{M}_{l-1}^- \\ \mathbf{N}_{l-1}^+ & \mathbf{N}_{l-1}^- \end{bmatrix} \begin{bmatrix} \mathbf{v}_{l-1}^+ \\ \mathbf{v}_{l-1}^- \end{bmatrix} = \mathbf{B}_{l-1}(z_l) \quad (8)$$

or, using $\mathbf{v}_{l-1}^+(z_l) = \mathbf{R}_{l-1}(z_l)\mathbf{v}_{l-1}^-(z_l)$ we have:

$$\mathbf{M}_l^+ \mathbf{v}_l^+ + \mathbf{M}_l^- \mathbf{v}_l^- = (\mathbf{M}_{l-1}^+ \mathbf{R}_{l-1} + \mathbf{M}_{l-1}^-) \mathbf{v}_{l-1}^- \equiv \Psi_l \mathbf{v}_{l-1}^-$$

$$\mathbf{N}_l^+ \mathbf{v}_l^+ + \mathbf{N}_l^- \mathbf{v}_l^- = (\mathbf{N}_{l-1}^+ \mathbf{R}_{l-1} + \mathbf{N}_{l-1}^-) \mathbf{v}_{l-1}^- \equiv \Phi_l \mathbf{v}_{l-1}^-$$

These can be solved for \mathbf{v}_{l-1}^- to give the boundary condition of the form (7):

$$\mathbf{v}_l^+ = -[\mathbf{N}_l^+ - \Phi_l \Psi_l^{-1} \mathbf{M}_l^+]^{-1} [\mathbf{N}_l^- - \Phi_l \Psi_l^{-1} \mathbf{M}_l^-] \mathbf{v}_l^- = \mathbf{F}_l \mathbf{v}_l^-$$

If \mathbf{R}_{l-1} is zero, corresponding to only downgoing waves below z_l , we have the situation appropriate for the calculation of standard plane wave reflection coefficients:

$$\mathbf{v}_l^+ = -[\mathbf{N}_l^+ - \mathbf{N}_{l-1}^- \mathbf{M}_{l-1}^{-1} \mathbf{M}_l^+]^{-1} [\mathbf{N}_l^- - \mathbf{N}_{l-1}^- \mathbf{M}_{l-1}^{-1} \mathbf{M}_l^-] \mathbf{v}_l^- = \begin{bmatrix} R_{PP} & R_{PS} \\ R_{SP} & R_{SS} \end{bmatrix} \mathbf{v}_l^- \quad (9)$$

Finally, the recursion relation among the \mathbf{R}_l is

$$\mathbf{R}_l(z) = -\mathbf{E}[\mathbf{N}_l^+ - \Phi_l \Psi_l^{-1} \mathbf{M}_l^+]^{-1} [\mathbf{N}_l^- - \Phi_l \Psi_l^{-1} \mathbf{M}_l^-] \mathbf{E}, \quad (10)$$

where

$$\Phi_l \Psi_l^{-1} = [\mathbf{N}_{l-1}^+ \mathbf{R}_{l-1}(z_l) + \mathbf{N}_{l-1}^-][\mathbf{M}_{l-1}^+ \mathbf{R}_{l-1}(z_l) + \mathbf{M}_{l-1}^-]^{-1}$$

as obtained by Chin *et al* (1984). Note that evanescent waves cause no numerical problems because when \mathbf{R}_{l-1} vanishes the above formula reduces to the calculation of plane wave reflection coefficients as in Eq. (9). In conclusion we mention that (10) can alternatively be expressed as the sum of multiple interactions with the structure below r_l analogous to a Debye series (Kennet and Kerry, 1979), a property which facilitates the application of free surface boundary conditions and reflectivity approximations.

2.4. The Hybrid Method

We now outline a hybrid method that combines the computational convenience of the asymptotic methods in smoothly varying regions of the Earth with the full calculation of the wavefield in the transition zone afforded by the homogeneous layer approximations. The idea of using a hybrid algorithm is nothing new. The reflectivity algorithm of Fuchs and Müller, for example, typically splits the Earth into a 'reflectivity zone' and a 'propagation zone'. Also, Cormier (1986) has developed a hybrid method for connecting analytical and numerical ray theory calculations for efficient treatment of complicated near-source structure. More similar to the technique described here is the method developed by Baag and Langston (1985), which uses a WKBJ algorithm in the smoothly varying region and propagator matrices to model complicated near-source and near-receiver structure. Our method improves upon that of Baag and Langston in that the Langer approximation we use is valid even when the turning point is near the level at which the asymptotic and homogeneous layer solutions are connected, where the WKBJ approximation breaks down. Both of these methods follow directly from the formalism of Kennett (1983) and Chapman and Orcutt (1985).

We connect the asymptotic and homogeneous layer solutions simply by requiring that the components of the motion-stress vector are continuous across the connecting boundary. Thus we consider the uncoupled P and SV potentials ϕ and χ below the transition zone to be

given by Langer standing waves $i(p, \omega) = i^{(1)} + i^{(2)}$ and $h(p, \omega) = h^{(1)} + h^{(2)}$ respectively, where $i^{(j)}$ and $h^{(j)}$ are Langer traveling waves of the form (3), calculated for the appropriate P or S velocity profile in the inner core and evaluated at the bottom of the transition zone r_i . The motion stress vector immediately below the transition zone then becomes, using (1) and (5),

$$\begin{aligned} \begin{bmatrix} U \\ V \\ R/\omega \\ S/\omega \end{bmatrix} &= \begin{bmatrix} -i\omega\bar{q}_\alpha & \omega p/r_i \\ \omega p/r_i & -i\omega\bar{q}_\beta + 1/r_i \\ \rho\omega(2\beta^2 p^2/r_i^2 - 1) + i\bar{q}_\alpha 4\mu/r_i & -2\mu\omega p/r_i(i\omega\bar{q}_\beta - 1/r_i) \\ -2\mu\omega p/r_i(i\omega\bar{q}_\alpha - \frac{1}{r_i}) & \rho\omega(2\beta^2 p^2/r_i^2 - 1) + 2\mu/r_i(i\bar{q}_\beta - 1/\omega r_i) \end{bmatrix} \begin{bmatrix} A_P i(\omega, p) \\ A_S h(\omega, p) \end{bmatrix} \\ &\rightarrow \left\{ \omega \frac{r_o}{r_i} \begin{bmatrix} -iq_\alpha & p \\ p & -iq_\beta \\ \rho(2\beta^2 p^2 - 1) & -i2\mu p q_\beta \\ -i2\mu p q_\alpha & \rho(2\beta^2 p^2 - 1) \end{bmatrix} + \frac{1}{r_i} \begin{bmatrix} 0 & 0 \\ 0 & 1 \\ i4\mu q_\alpha & -2\mu p \\ -2\mu p & i2\mu(q_\beta - 1/\omega r_o) \end{bmatrix} \right\} \begin{bmatrix} A_P i(\omega, p) \\ A_S h(\omega, p) \end{bmatrix} \quad (11) \end{aligned}$$

where we have applied the EFT in the last expression and used the approximation $\sqrt{l(l+1)} \approx \omega p$. A_P and A_S are constants which as yet are undetermined, and the quantities $\bar{q}_\alpha = i/\omega \, di/dr \, 1/i(\omega, p)$ and $\bar{q}_\beta = i/\omega \, dh/dr \, 1/h(\omega, p)$ are generalized vertical slownesses whose flat Earth equivalents are denoted by $q_{\alpha\beta} = r_i/r_o \bar{q}_{\alpha\beta}$. Following the argument given below Eq. (6) in the previous section, the matrix on the far right can be neglected, and the first matrix on the right hand side has exactly the same form as the downgoing component of the matrix D in (8). Thus, providing that the $q_{\alpha\beta}$ are interpreted correctly, the boundary condition for the invariant imbedding algorithm at the bottom of the stack of layers z_0 can be expressed as:

$$\begin{aligned} \mathbf{M}_0^+ \mathbf{v}_0^+ + \mathbf{M}_0^- \mathbf{v}_0^- &= \omega \frac{r_o}{r_i} \mathbf{M}_i^- \begin{bmatrix} A_P i(\omega, p) \\ A_S h(\omega, p) \end{bmatrix} \\ \mathbf{N}_0^+ \mathbf{v}_0^+ + \mathbf{N}_0^- \mathbf{v}_0^- &= \omega \frac{r_o}{r_i} \mathbf{N}_i^- \begin{bmatrix} A_P i(\omega, p) \\ A_S h(\omega, p) \end{bmatrix} \end{aligned}$$

where we have use the subscript i for the matrices evaluated below the interface. Eliminating the vector of asymptotic wave functions below the stack, we arrive at the boundary condition at z_0 in the form (7):

$$\mathbf{v}_0^+ = [\mathbf{N}_0^+ - \mathbf{N}_i^- \mathbf{M}_i^{-1} \mathbf{M}_0^+]^{-1} [\mathbf{N}_0^- - \mathbf{N}_i^- \mathbf{M}_i^{-1} \mathbf{M}_0^-] \mathbf{v}_0^- = \begin{bmatrix} R_{PP} & R_{PS} \\ R_{SP} & R_{SS} \end{bmatrix} \mathbf{v}_0^-$$

and the asymptotic solutions for the wavefield below the transition zone are incorporated into the invariant imbedding calculation simply by using the generalized slownesses $q_{\alpha,\beta} = r_i/r_o \bar{q}_{\alpha,\beta}$ in place of the radicals $\sqrt{1/(\alpha,\beta)^2 - p^2}$ when calculating the plane wave reflection coefficients for the interface at the bottom of the stack. If the Langer standing wave is used for the asymptotic solution below the stack of layers, then all of the multiple reverberations (e.g. PKmIKP $m \geq 2$) will be included in the invariant imbedding solution, and this is the case for the P wave potential used in the calculations of Green's functions for the distance range $100 - 130^\circ$ presented here. In practice however, we will generally use the usual flat Earth vertical slowness $\sqrt{1/\beta^2 - p^2}$ for the S waves. This amounts to making a Debye expansion of the S waves below the transition zone and ignoring those phases which arrive outside the time interval of interest (i.e., since the PKJKP phases arrive long after PKIKP, they may be neglected). Similarly, we use the flat earth vertical slowness for the P potential for the distance range $0 - 100^\circ$, which includes only the effect of PKIKP.

The connection at the top of the stack of layers z_N is even more simple. Only P waves are present in the fluid outer core above the transition, and the motion-stress vector can be expressed as in (11):

$$\begin{bmatrix} U \\ V \\ R/\omega \\ S/\omega \end{bmatrix} = \omega \begin{bmatrix} i\bar{q}_\alpha^+ & -i\bar{q}_\alpha^- \\ p & p \\ \rho(2\beta^2 p^2 - 1) & \rho(2\beta^2 p^2 - 1) \\ i2\mu p \bar{q}_\alpha^+ & -i2\mu p \bar{q}_\alpha^- \end{bmatrix} \begin{bmatrix} A_p^+ k^{(1)}(\omega, p) \\ A_p^- k^{(2)}(\omega, p) \end{bmatrix} = \begin{bmatrix} iq_\alpha & -iq_\alpha \\ p & p \\ \rho(2\beta^2 p^2 - 1) & \rho(2\beta^2 p^2 - 1) \\ i2\mu p q_\alpha & -i2\mu p q_\alpha \end{bmatrix} \begin{bmatrix} R_N \\ 1 \end{bmatrix}$$

where again we have expressed everything in terms of Earth flattened quantities, A_p^\pm are the amplitudes of the up- (+) and down-going (-) P wave potentials in the outer core, and we denote by $\bar{q}_\alpha^\pm = -(\pm i/\omega k(\omega, p)) dk^{(1,2)}/dr$ the up- and down-going Langer vertical slownesses in the outer core, evaluated at r_o . Note also that the 2×2 matrix \mathbf{R}_i has become the scalar R_N in the fluid, and that we now use $q_\alpha = \sqrt{1/\alpha^2 - p^2}$. Since only the P waves are present, half of the above equations are redundant, and the remaining equations can be solved for the amplitude

A_p^+ in terms of A_p^- :

$$A_p^+ = - \frac{q_\alpha \frac{1-R_N}{1+R_N} - q_\alpha^-}{q_\alpha \frac{1-R_N}{1+R_N} + q_\alpha^+} \frac{k^{(2)}(\omega, p)}{k^{(1)}(\omega, p)} A_p^-$$

Thus, we see the origin of the ratio of outer core wavefunctions in (2), and can finally write the expression for $R_o(\omega, p)$:

$$R_o(\omega, p) = - \frac{q_\alpha \frac{1-R_N}{1+R_N} - q_\alpha^-}{q_\alpha \frac{1-R_N}{1+R_N} + q_\alpha^+}$$

2.5. Numerical Results

The method described in the previous section leads to a fairly general algorithm for calculating synthetic seismograms for body waves that have interacted with the inner-outer core transition. The method is appropriate for a broad frequency band and the variation of physical parameters within the transition zone can be essentially arbitrary. It is beyond the scope of this paper, however, to attempt an inversion of seismic data for all of the possible variations of physical parameters that may occur. We have therefore concentrated our attention on a single property of the transition, its thickness. In this section we use the method described previously to explore the sensitivity of a number of different seismic waves to this property of the transition, and we find that by comparing the calculations with observations presently in the literature, as well as with short-period waveform data, it is possible to arrive at some preliminary conclusions concerning the thickness of the inner core transition.

All of the Earth models considered in this study will consist of small perturbations of the Preliminary Reference Earth Model (PREM), described in Dziewonski and Anderson (1981), and so our analysis depends on the assumption that PREM adequately describes the variation of elastic parameters outside the transition zone. This seems to be a reasonable assumption, especially as far as the P-velocity profile is concerned. The recent studies by

Müller (1973) and Häge (1983) resulted in estimates of the P-velocity jump at the inner core boundary that were not significantly different from that of PREM, and Johnson and Lee's (1985) inversion of ISC travel times for the inner and outer cores found that the P-velocity profile of PREM could be brought into agreement with the ISC data through modifications that nowhere exceed .1 km/s. There is some suggestion in the studies of Qamar (1973), Buchbinder (1971), and Choy and Cormier (1983), that the P-velocity jump may be somewhat smaller than the PREM value, and both the Choy and Cormier (1983) and Häge (1983) studies suggest that the S-velocity at the top of the inner core may be lower than that of PREM. But there does not seem to be general agreement on any model which fits the available data better than PREM, so this was chosen as a reference model for the calculations.

Four models were considered in this study, with one model being PREM which has a sharp inner core transition zone of zero thickness. The other three models use PREM above and below the transition zone, but have smooth increases in $1/Q$, density, and P- and S-velocities within the transition between outer and inner cores. This increase is a cosine interpolation of the PREM values above and below the transition zone which keeps the model parameters and their first derivatives continuous. We use three models of this type with transition thicknesses of 3.0, 5.0 and 10.0 km, but note that due to the particular shape of transition we have chosen, the model parameters undergo 90% of the transition in depth intervals of 1.5, 3.6 and 7.1 km, respectively.

While we use PREM to describe the variation of elastic parameters with depth outside the inner core transition zone, we have not included attenuation in the mantle and crust in the calculation of the Green's functions. Since the body waves we are modeling all have nearly vertical raypaths in the mantle and crust, they should experience very nearly the same attenuation effects there, and these as well as the contributions due to the source time function and instrument response will be modeled by convolution with an empirical source/attenuation operator. This empirical operator is derived from an observed pre-critical PKiKP reflection recorded at a receiver whose instrument response is consistent with the data being modeled. There will be a small amount of distortion in the data due to the non-zero

phase of the pre-critical reflection coefficient for an inner core transition of finite thickness, but the calculations can be made consistent by removing this distortion through a spectral division of the source/attenuation operator by the Green's function for the same distance. Thus, if $S(\omega, \Delta)$ is the synthetic spectrum for distance Δ , $G(\omega, \Delta)$ is the Green's function for distance Δ , and $D(\omega, \Delta)$ is the spectrum for an observed pre-critical PKiKP reflection recorded at distance Δ , then we obtain the synthetic spectrum at distance Δ_1 via:

$$S(\omega, \Delta_1) = \frac{G(\omega, \Delta_1)}{G(\omega, \Delta_0)} \times D(\omega, \Delta_0)$$

In the inner core itself the rays bottom in a region of low Q that has not been modeled by the source/attenuation operator. Unless stated otherwise, we use the Q_α model of Doombos (1974) in this region, which has a Q_α of about 200 in the top 200 kilometers of the inner core with a monotonic increase to a value of about 1000 at 700 km radius. While Doombos (1983) has also shown that Q_α in the inner core decreases with increasing frequency, we have used a frequency independent Q_α for computational convenience. Q_α in the outer core was taken to be 10000, which should have very little effect on the synthetics, and Q_β in the inner core was set equal to Q_α .

Finally, it is necessary to perform the inverse transforms over frequency and slowness in order to obtain results in the time domain. We use a discrete Fourier transform for inverting the frequency transformation and perform a numerical integral over slowness, taking the contour Γ in (2) to be a finite interval along the real axis and using cosine tapers at the ends to avoid spurious arrivals associated with sharp truncations of the integrand. The cosine tapers had very little effect on the synthetics, but a better procedure would be to use an integration path that begins and ends in regions of the complex ray parameter plane where the integrand is small, as described in Richards (1973), Cormier and Richards (1977), and Choy (1977). This technique avoids spurious truncation phases by exploiting the exponential behavior of the asymptotic wave functions for complex ray parameter, but it also requires a somewhat more complicated computer program to accommodate the complex integration path. We used the cosine tapering because it had very little effect on the synthetics and was easy to

implement.

2.5.1. Pre-critical PKiKP: $0^\circ - 120^\circ$

One of the most important constraints on the thickness of the inner core transition is implied by the data presented in Engdahl *et al* (1970) and Engdahl *et al* (1974). These data consist of PKiKP waves detected at the LASA array at distances between 11° and 36° . It was noted that, in the passband centered at 1 Hz, these pre-critically reflected signals exhibit very little distortion when compared with either direct P or PcP phases from the same event. In Figure 1 are displayed the displacement Green's functions calculated for a 5.0 km transition zone in the form of spectral amplitude versus distance curves for frequencies of 0.5, 1.0, and 2.0 Hz. Note the decrease in spectral amplitude with increasing frequency at distances less than 40° . The short-period LASA records contained significant energy in the 0.5-2.0 Hz band, and it is clear from the figure that the LASA waveforms in the $11^\circ - 36^\circ$ distance range would have been strongly low-pass filtered upon reflection by an inner core boundary of 5.0 km thickness. Since the waveforms in this distance range were not distorted relative to the direct P and PcP phases, the LASA data constrains the inner core transition to be less than 5.0 km thick. As mentioned previously, the material parameters of this model undergo 90% of the inner core transition within a depth range of about 3.6 km, so that this result is in good agreement with that of Phinney (1970).

Another fairly complete study of pre-critical PKiKP phases is that of Buchbinder *et al* (1973). They consider the identification of PKiKP arrivals at distances between 30° and 105° . In Figure 2, we show peak-to-peak short-period PKiKP amplitudes as a function of distance calculated for PREM and for 3.0, 5.0, and 10.0 km transitions, where we have convolved the Green's functions with an empirical source/attenuation operator taken from a pre-critical PKiKP reflection observed at the DWWSSN station TOL (see Table 1). Also plotted in Figure 2 are the amplitudes observed by Buchbinder *et al* for Event 1 in Table 2 of their paper, which were measured using short-period WWSSN or Canadian Seismic Network records, both of which have short-period responses similar to that of the DWWSSN. The synthetics

were generated for an explosion source, and this should be consistent with the Buchbinder *et al* data since the event studied was a Novaya Zemlya nuclear test explosion. Both the event studied by Buchbinder *et al* and the event we use for our empirical source/propagation operator have m_b 's of 6.7, and visual inspection of the U.C. Berkeley short-period records for the Novaya Zemlya explosion indicated that they have similar dominant period and waveform complexity.

Since there was very little difference in the amplitudes predicted for the three models at distances greater than 105° , we used the predicted amplitudes in this distance range to normalize the Buchbinder *et al* data. Inspection of Figure 2 indicates that the predicted amplitudes for the 10.0 km transition are not consistent with the data, so that the amplitudes observed by Buchbinder *et al* constrain the transition to be less than 10.0 km thick. On the other hand, the scatter in the amplitudes at distances less than 40° does not preclude a transition thickness of 5.0 km. What could be an indication that the transition is less than 5.0 km thick is given by the lack of data in the $43^\circ - 105^\circ$ distance range. We quote from Buchbinder *et al*'s analysis of single-station short period records:

Curiously, no possible PKiKP phases were observed on standard records at distances beyond 43° even though stations were abundant, but they could be identified again at distances greater than 105° , where PKiKP precedes PP, and the theoretical amplitudes start to increase rapidly.

It is not clear whether the lack of observations between 43° and 105° was due to a decrease in amplitude, interference with the PP coda, or both. Using data from the Yellowknife array, the authors were able to detect PKiKP energy for several events in the distance range $70^\circ - 100^\circ$, but the amplitudes are not published. In any case it is clear from Figure 2 that observational evidence for a decrease in PKiKP amplitudes between 40° and 105° would favor a transition thickness of less than 5.0 km.

Perhaps the most interesting result of this study however, is the drastic change in waveform that the pre-critical reflection undergoes in the distance range $60^\circ - 90^\circ$. Figure 3a-c

illustrates the differences in pre-critical PKiKP waveforms for three of the models used in this study. In Figure 3a can be seen the very low amplitudes and phase reversal around 80° which is to be expected for an inner core with a sharp boundary and non-zero shear modulus. This property of PKiKP was used in the studies by Müller (1973) and Häge (1983) to constrain the shear modulus of the inner core. In Figures 3b and 3c, where we present the displacement Green's functions for 3.0 km and 5.0 km transitions respectively, we see that there is no 'transparent zone' of very low amplitude reflection and that instead of causing a simple phase reversal the extended transition zones have given rise to more complicated pulse distortion.

The absence of a 'transparent zone' in the results for the transition zone models is due to the decoupling of PKiKP and PKJKP achieved by the smooth transition zone models. This is illustrated in Figure 4, where moduli of the 1 Hz P-P reflection coefficients for PREM and for a transition zone 3 km thick are plotted as a function of distance along with their respective P-S transmission coefficients. These coefficients represent the effect of reflection from or transmission through the stack of layers between 1205 km and 1235 km radius that was used in the invariant imbedding calculations. Unlike all of the other calculations presented in this paper, both Q_α and Q_β were taken to be 10000 in the inner core in order to isolate the effects of decoupling from those of attenuation. Using realistically low Q's would have had little effect on PKiKP, but the high-frequency PKJKP energy that we use to illustrate decoupling would be so severely attenuated that decoupling would be difficult to discern. It can be seen in Figure 4 that the modulus of the P-S transmission coefficient for PREM has a maximum in the distance range $60 - 90^\circ$, where the PREM P-P reflection coefficient decreases in modulus and undergoes a phase reversal. The modulus of the P-S transmission coefficient for the 3 km transition zone is 5 times smaller than that of the corresponding PREM coefficient, while the modulus of the P-P reflection coefficient has increased in the distance range $60 - 90^\circ$, indicating that some of the incident PKiKP energy which no longer couples to the shear wave in the inner core has been reflected by the smooth transition (the modulus of the P-P transmission coefficient also increases at the expense of the

P-S transmission coefficient in this distance range). The decoupling of PKiKP and PKJKP results in a PKiKP waveform that is very sensitive to the thickness of the transition, as was seen in Figure 3.

2.5.2. PKiKP and PKIKP near the D cusp: $120^\circ - 130^\circ$

While some of the most interesting effects of an inner core transition zone are manifest in the pre-critical distance range, the PKiKP arrivals at these distances have very small amplitudes and are often obscured by phases such as PP which arrive earlier than PKiKP. At distances greater than about 100° , however, PKiKP increases in amplitude and becomes the first arriving phase, and it is in this distance range that waveform analysis becomes practical. While waveform modeling should provide the best resolution of the inner core transition zone when applied to short-period data, the sensitivity of short-period waveform data to scattering makes this type of analysis difficult. This problem has been mentioned in the studies by Müller (1973), Choy and Cormier (1983), and Häge (1983), but we note that a large portion of the scattering of short-period energy may occur in the crust. We therefore attempt to minimize the effects of scattering by considering only deep earthquakes that have been recorded by stations having very simple crustal structures. The best data set we could find which fit these criteria consisted of 5 earthquakes in the southwest Pacific which were recorded by the Regional Seismic Test Network (RSTN) stations in the Northwest Territory, Canada (RSNT) and Ontario, Canada (RSON) (see Table 1). Station RSNT recorded a pre-critical PKiKP reflection for each event, and we used this recording as an empirical source/attenuation operator to model the PKIKP+PKiKP phase recorded by RSON at around 130° .

The resulting synthetics generated for PREM and for 5.0 km and 10.0 km transition zone models are compared with the RSON recordings in Figure 5. The data have been aligned and normalized so that the peak amplitudes of the synthetics and the data arrive simultaneously and have the same amplitude; this should remove the crustal corrections to both travel time and amplitude. The agreement of both sets of synthetics with the data is

unusually good for short-period waveforms, but we notice that there is a systematic discrepancy in the synthetics generated for the transition zone models. This discrepancy consists of a slight decrease in the width of the wavelet as well as a disparity in the amplitudes of some of the peaks and troughs. In Figure 6 are plotted the surface focus displacement Green's functions for PKiKP+PKIKP in the distance range 120 – 130°. It can be seen that just past the D cusp at 120° in the PKP travel time curve the refracted PKIKP phase splits apart from the reflected PKiKP, so that by 130° the time difference between PKIKP and PKiKP is about 0.8 seconds for PREM. The Green's functions for the transition zone models are almost identical, except that at 130° the time difference between PKIKP and PKiKP is 0.7 seconds for the 5.0 km transition and 0.6 seconds for the 10.0 km transition zone. When convolved with the source/attenuation operator this change in differential arrival time leads to a slight decrease in the wavelet duration and a change in the interference pattern of PKIKP+PKiKP as the transition zone becomes thicker. While the resulting discrepancy between observed waveforms and synthetics is very slight for the 5.0 km transition, it is clearly distinguishable for the 10.0 km transition. Hence we conclude that these data constrain the transition to be less than 10.0 km thick.

2.6. Conclusions

We have shown that by using a hybrid combination of two different methods, it is possible to treat the calculation of body waves that have interacted with the Earth's inner core in an accurate, complete, and efficient manner. This approach allows one to explore completely general models of the interesting transition zone between the inner and outer core. Synthetic seismograms generated with this new hybrid method have provided quantitative measures of how properties of the transition zone might affect body waves, have indicated what types of experimental data are needed to better constrain this transition zone, and have led to some preliminary conclusions based on data already available.

The results of this study agree well with those of Phinney (1970), who used results for the acoustic case to infer that the presence of 1 Hz near-vertical reflections from the inner

core imply that the transition has a scale length of 1.5 km or less. Our estimate was slightly more conservative; we arrived at a scale length 5.0 km or less through reasoning similar to Phinney's. Some interesting phenomena unique to the elastic case have emerged from this study, however. Principle among these is the interesting effect that the decoupling of PKiKP and PKJKP has on the amplitudes and waveforms of PKiKP in the distance range $60^\circ - 90^\circ$. For a transition as thin as 3 km this decoupling is so effective that high frequency energy containing valuable information about the detailed structure of the transition zone is reflected instead of being transmitted into the inner core as shear wave energy.

The strongest constraint on the thickness of the inner core transition zone is implied by the data of Engdahl *et al* (1970 and 1974), in which the authors show that PKiKP phases observed at less than 40° from the source undergo reflection with very little waveform distortion in the short-period frequency band. These data constrain the transition thickness to be less than 5.0 km. Because of the large scatter in short-period amplitudes, data of the type presented in Buchbinder *et al* (1973) provide a somewhat weaker constraint, but a transition as thick as 10.0 km is inconsistent with the observations. Short-period waveform data recorded at post-critical distances near the D cusp have similar depth resolution, with a transition thickness of 10.0 km producing a reduction of the travel time difference between PKiKP and PKIKP of about 0.2 s. This is detectable using some of the best quality short-period data available.

References

- Aki, K., and P.G. Richards, 1980. *Quantitative Seismology, Theory and Methods*, W.H. Freeman, San Francisco, Calif.
- Baag C. and C.A. Langston, 1985. A WKBJ spectral method for computation of SV synthetic seismograms in a cylindrically symmetric medium, *Geophys. J. R. astr. Soc.*, 80, 387-417.
- Buchbinder, 1971. A velocity structure of the Earth's core, *Bull. Seism. Soc. Am.*, 61, 429-456.
- Buchbinder, G.G.R., Wright, C. and G. Poupinet, 1973. Observations of PKiKP at Distances less than 110°, *Bull. Seism. Soc. Am.*, 63, 1699-1707.
- Chapman, C.H., and J.A. Orcutt, 1985. The computation of body wave synthetic seismograms in laterally homogeneous media, *Rev. Geophys.*, 23, 105-163.
- Chapman, C.H., 1981. Long-period corrections to body waves: theory, *Geophys. J. R. astr. Soc.*, 64, 321-372.
- Chapman, C.H., 1978. A new method for computing synthetic seismograms, *Geophys. J. R. astr. Soc.*, 54, 481-518.
- Chin, R.C.Y., Hedstrom, G.W., and L. Thigpen, 1984. Matrix methods in synthetic seismograms, *Geophys. J. R. astr. Soc.*, 77, 483-502.
- Choy, G.L., and V.F. Cormier 1983. The structure of the inner core inferred from short-period and broadband GDSN data, *Geophys. J. R. astr. Soc.*, 72, 1-21.
- Choy, G.L., 1977. Theoretical seismograms of core phases calculated by frequency-dependent full wave theory, and their interpretation, *Geophys. J. R. astr. Soc.*, 51, 275-312.
- Cormier, V.F., 1986. An application of the propagator matrix of dynamic ray tracing: the focusing and defocusing of body waves by three-dimensional velocity structure in the source region, *Geophys. J. R. astr. Soc.*, 87, 1159-1180.

- Cormier, V.F., and P.G. Richards, 1977. Full wave theory applied to a discontinuous velocity increase: the inner core boundary, *J. Geophys.*, 43, 3-31.
- Doombos, D.J., 1983. Observable effects of a seismic absorption band in the Earth, *Geophys. J. R. astr. Soc.*, 75, 693-711.
- Doombos, D.J., 1974. The anelasticity of the inner core *Geophys. J. R. astr. Soc.*, 38, 397-415.
- Dziewonski, A.M., and D.L. Anderson, 1981. Preliminary reference Earth model, *Phys. Earth Planet. Inter.*, 25, 297-356.
- Engdahl, E.R., Flinn, E.A., and R.P. Masse, 1974. Differential PKiKP travel times and the radius of the inner core, *Geophys. J. R. astr. Soc.*, 39, 457-463.
- Engdahl, E.R., Flinn, E.A., and C.F. Romney, 1970. Seismic waves reflected from the Earth's inner core, *Nature*, 228, 852-853.
- Hron M., and C.H. Chapman, 1974. Seismograms from Epstein transition zones, *Geophys. J. R. astr. Soc.*, 37, 305-322.
- Häge H., 1983. Velocity constraints for the inner core inferred from long-period PKP amplitudes, *Phys. Earth Planet. Inter.*, 31, 171-185.
- Johnson, L.R., and R.C. Lee, 1985. Extremal bounds on the P velocity in the Earth's core, *Bull. Seism. Soc. Am.*, 75, n1, 115-130.
- Julian, B.R., Davies, D., and R.M. Sheppard, 1972. PKJKP, *Nature*, 235, 317-318.
- Kennett B.L.N., 1983. *Seismic Wave Propagation in Stratified Media*, Cambridge University Press, Cambridge.
- Kennett B.L.N., and M.R. Illingworth, 1981. Seismic waves in a stratified half space - III. Piecewise smooth models, *J. Geophys. Res.*, 66, 663-675.
- Kennett B.L.N., and N.J. Kerry, 1979. Seismic waves in a stratified half space, *J. Geophys. Res.*, 57, 557-583.

- Lees, A.M., Bukowinski, M.S.T., and R. Jeanloz, 1983. Reflection properties of phase transition and compositional change models of the 670-km discontinuity, *J. Geophys. Res.*, 88, 8145-8159.
- Loper, D.E., and D.R. Fearn, 1983. A seismic model of a partially molten inner core, *J. Geophys. Res.*, 88, 1235-1242.
- Meyer, G.H., 1973. *Initial Value Methods for Boundary Value Problems* Academic Press, New York and London.
- Morse, S.A., 1986. Adcumulus growth of the inner core, *Geophys. Res. Lett.*, 13, 1557-1560.
- Müller, G., 1973. Amplitude studies of core phases, *J. Geophys. Res.*, 78, 3469-3490.
- Phinney, R.A., 1970. Reflection of acoustic waves from a continuously varying interfacial region, *Rev. Geophys. Space Phys.*, 8, 517-532.
- Qamar, A., 1973. Revised velocities in the Earth's core, *Bull. Seism. Soc. Am.*, 63, 1073-1105.
- Richards, P.G., 1973. Calculation of body waves, for caustics and tunnelling in core phases, *Geophys. J. R. astr. Soc.*, 35, 243-264.
- Richards, P.G., 1976. On the adequacy of plane-wave reflection/transmission coefficients in the analysis of seismic body waves *Bull. Seism. Soc. Am.*, 66, n3, 701-717.
- Woodhouse, J.H., 1978. Asymptotic results for elastodynamic propagator matrices in plane-stratified and spherically-stratified earth models *Geophys. J. R. astr. Soc.*, 54, 263-280.

Figure 1. Spectral amplitude of displacement Green's functions for PKiKP versus distance calculated for a 5.0 km transition zone centered at 1221.5 km radius. The decrease in spectral amplitude between 0° and 5° is due to the wavenumber taper applied when generating the synthetics.

Figure 2. Peak-to-peak amplitudes of synthetic short-period records as a function of distance. The synthetics were generated using a source/attenuation operator taken from the event listed in Table 1, and the results for PREM (heavy), 3.0 km (solid), 5.0 km (dashed), and 10.0 km (dot-dashed) are shown. Also plotted are the short-period amplitudes from Buchbinder *et al*'s (1973) Table 2 which have been normalized so that they agree with all three models in the distance range 110°–115°. The decrease in amplitude between 0° and 5° is due to the wavenumber taper applied when generating the synthetics.

Figure 3. Displacement Green's functions calculated for three models: (a) PREM, (b) a 3.0 km transition zone, and (c) a 5.0 km transition zone. Some degradation of the low frequency energy at 95° and 100° degrees is evident due to the wavenumber tapering. The frequency band is .3-5.0 Hz. The traces have been approximately aligned, so that they do not have a common origin time. All trace amplitudes in this figure are true relative amplitudes.

Figure 4. 1 Hz P-P reflection coefficients (solid) and P-S transmission coefficients (dot-dashed) for two inner core models: PREM (heavy) and a 3 km transition (light). These coefficients describe reflection from and transmission through the stack of layers between 1205 km and 1235 km radius that was used in the invariant imbedding calculations. Both Q_α and Q_β were set equal to 10000 in order to illustrate decoupling of PKiKP and PKJKP.

Figure 5. Short-period synthetics (dashed traces) compared with recordings from the RSTN station RSON (solid traces) at distances near 130° . The source attenuation operators were obtained from pre-critical PKiKP phases recorded by station RSNT, and the events used are listed in Table 1. The models used to generate the synthetics are: PREM, a 5.0 km thick transition zone, and a 10.0 km thick transition zone.

Figure 6. PKIKP+PKiKP displacement Green's functions calculated for PREM, a 5.0 km thick transition zone, and a 10.0 km thick transition zone. The frequency band is 0.3-5.0 Hz. All trace amplitudes in this figure are true relative amplitudes.

Table 1. Earthquakes used in this study

Event Information						
Label	Date	Origin time (UT)	Location (Lat-Lon)	Depth (km)	m_b	Distance to RSON
*	1984 Mar. 5	03:33:51.2	8.1S-123.8E	650.6	6.7	
event 1	1984 Jan. 17	02:09:04.9	7.7S-117.4E	303.9	5.7	129.9°
event 2	1985 Aug. 8	16:18:03.4	6.2S-113.5E	603.0	5.7	130.0°
event 3	1985 Aug. 8	16:29:57.5	6.2S-113.4E	588.7	5.7	130.0°
event 4	1985 Aug. 12	04:18:58.0	7.0S-117.2E	583.7	5.7	129.3°
event 5	1986 Oct. 18	22:09:31.2	5.3S-110.0E	634.1	5.7	130.8°

* TOL recording used for calculations in Figure 2

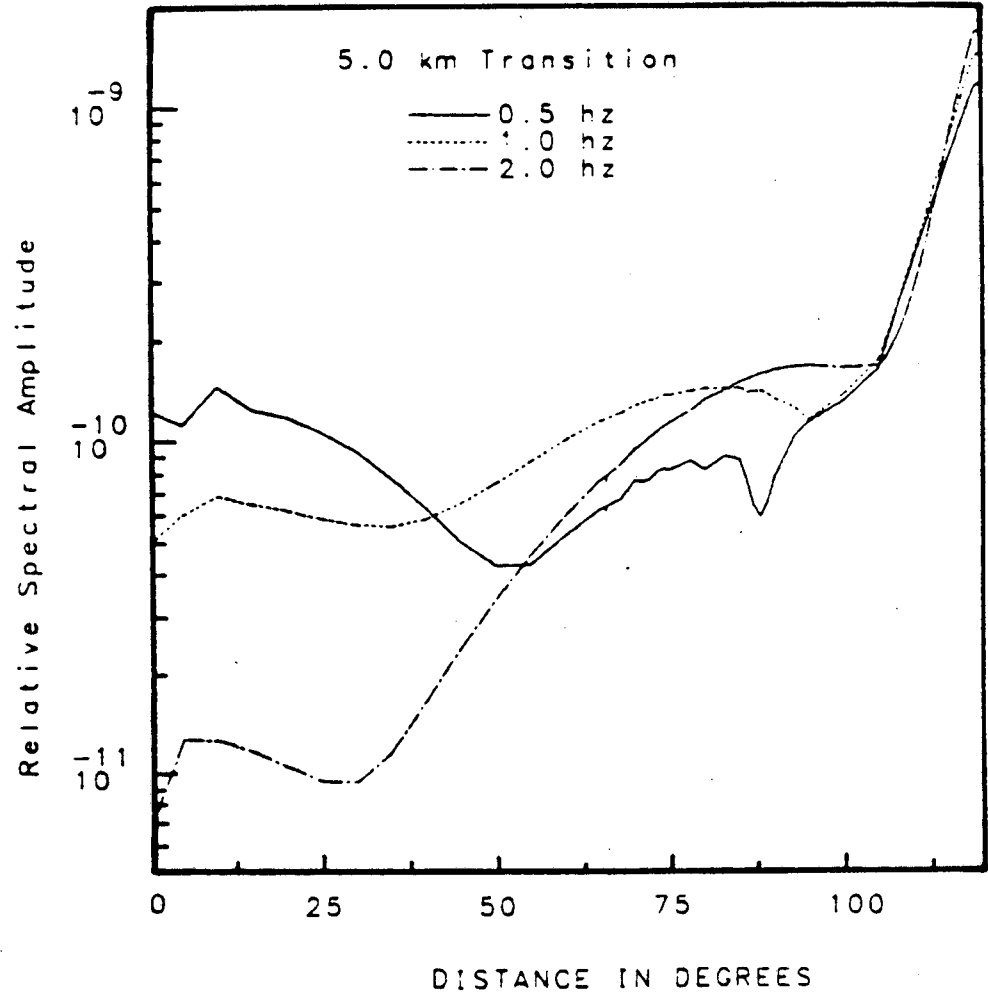


Figure 1

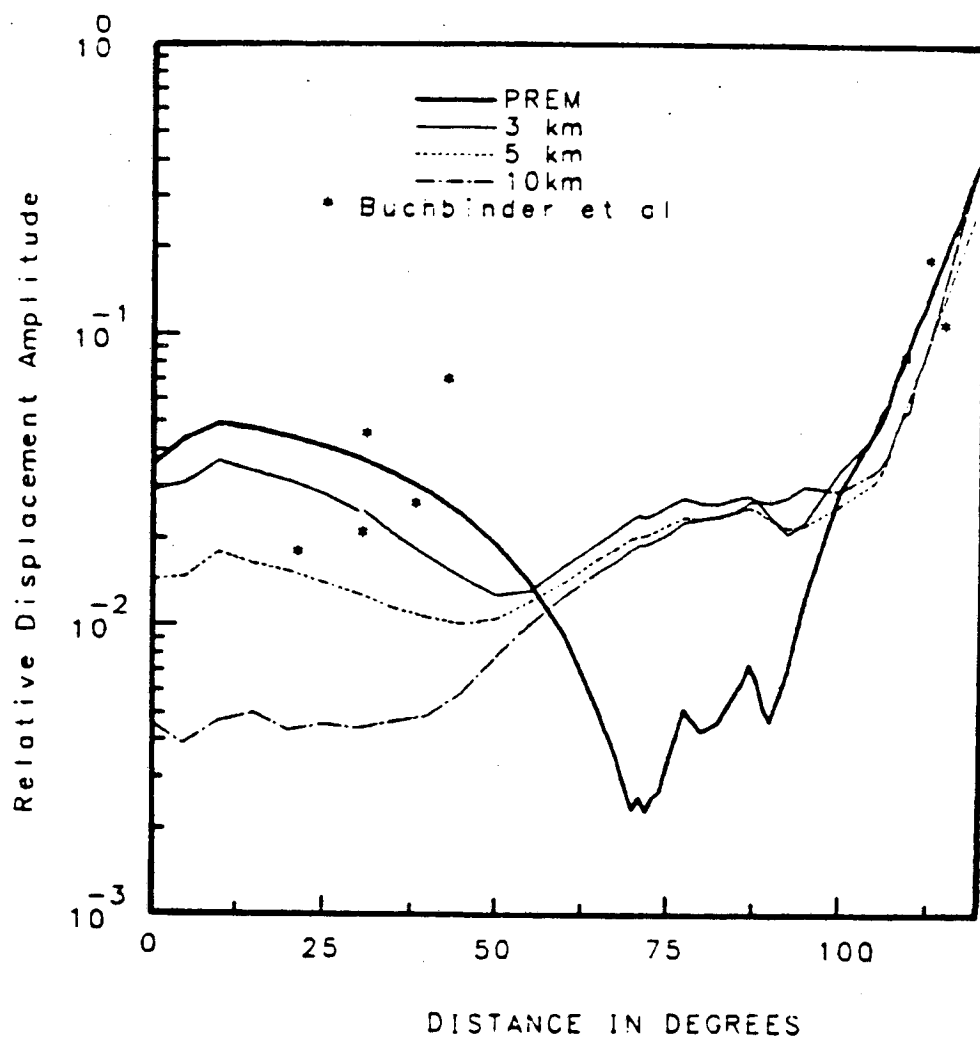


Figure 2

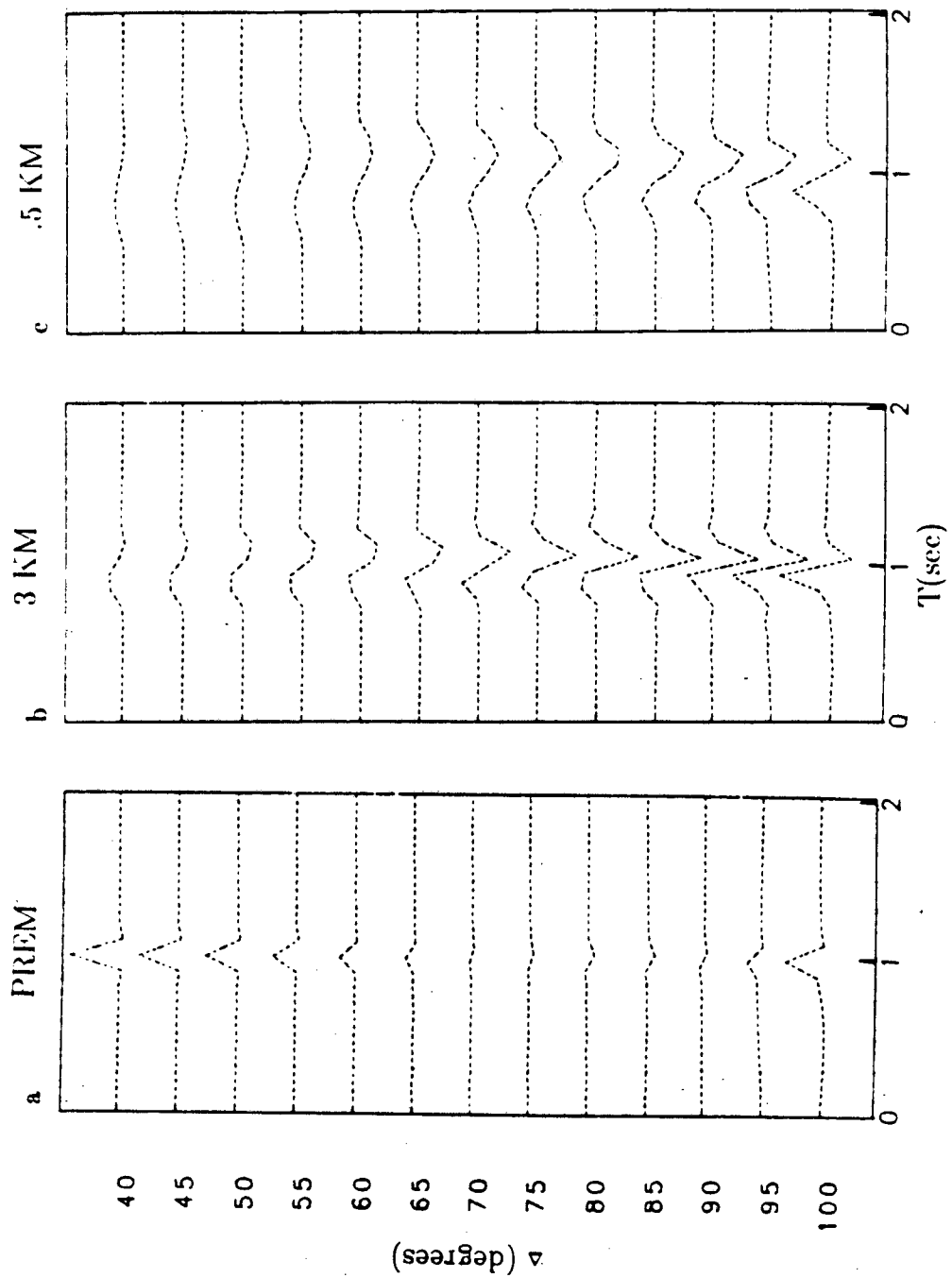


Figure 3

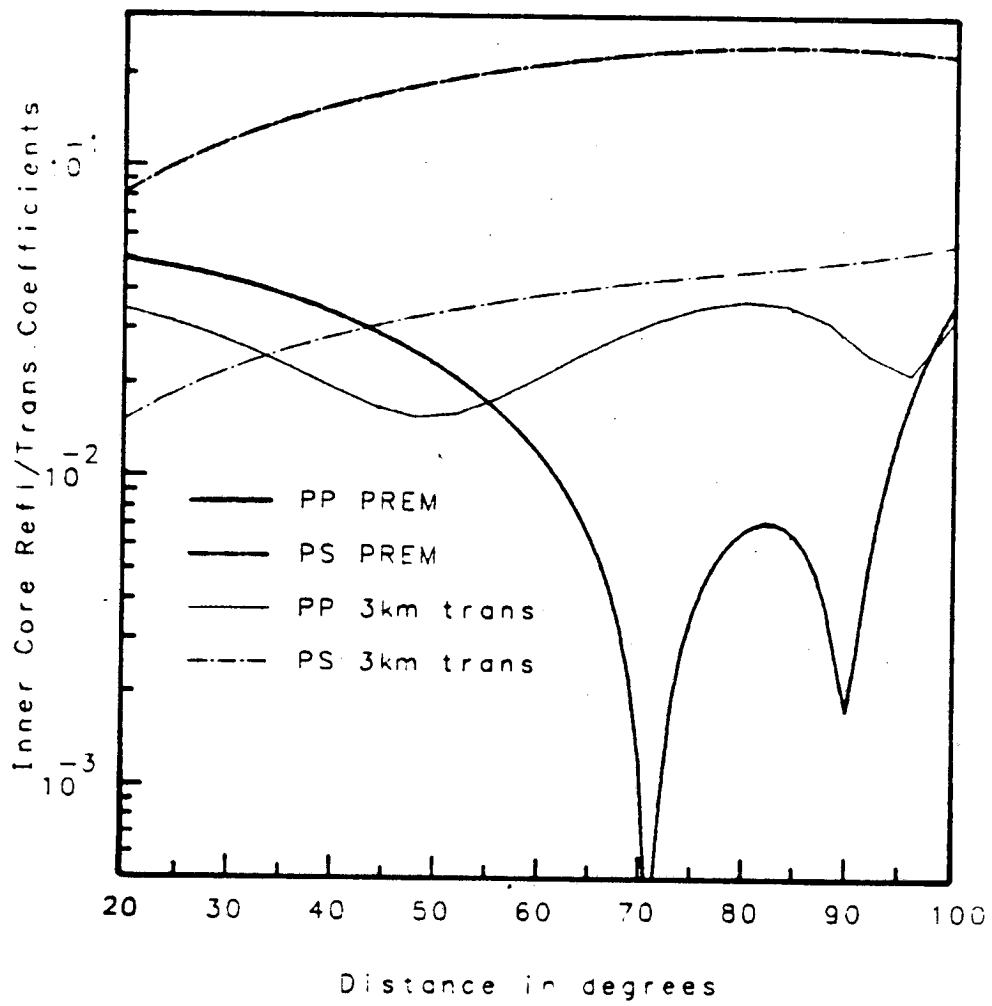


Figure 4

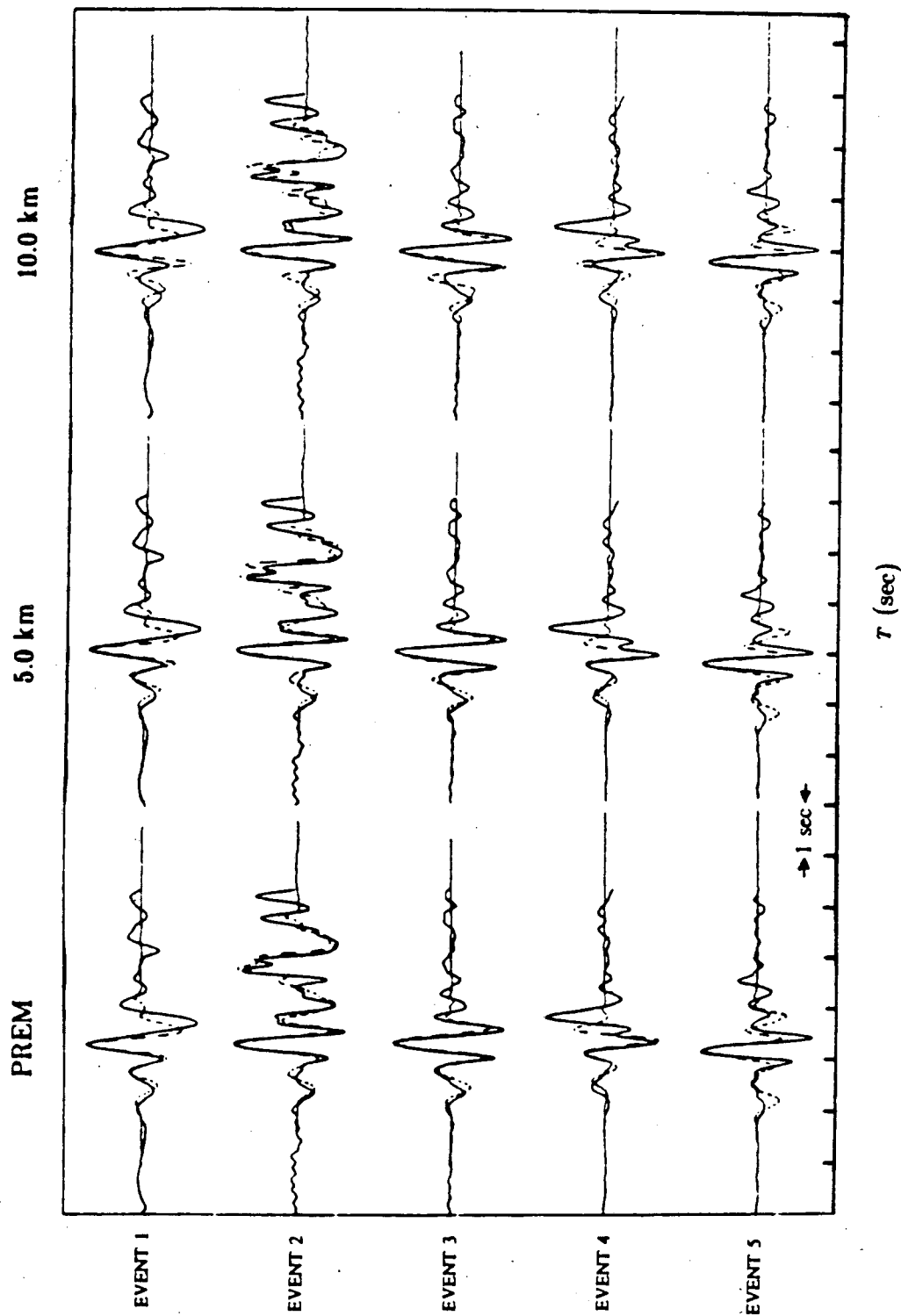


Figure 5

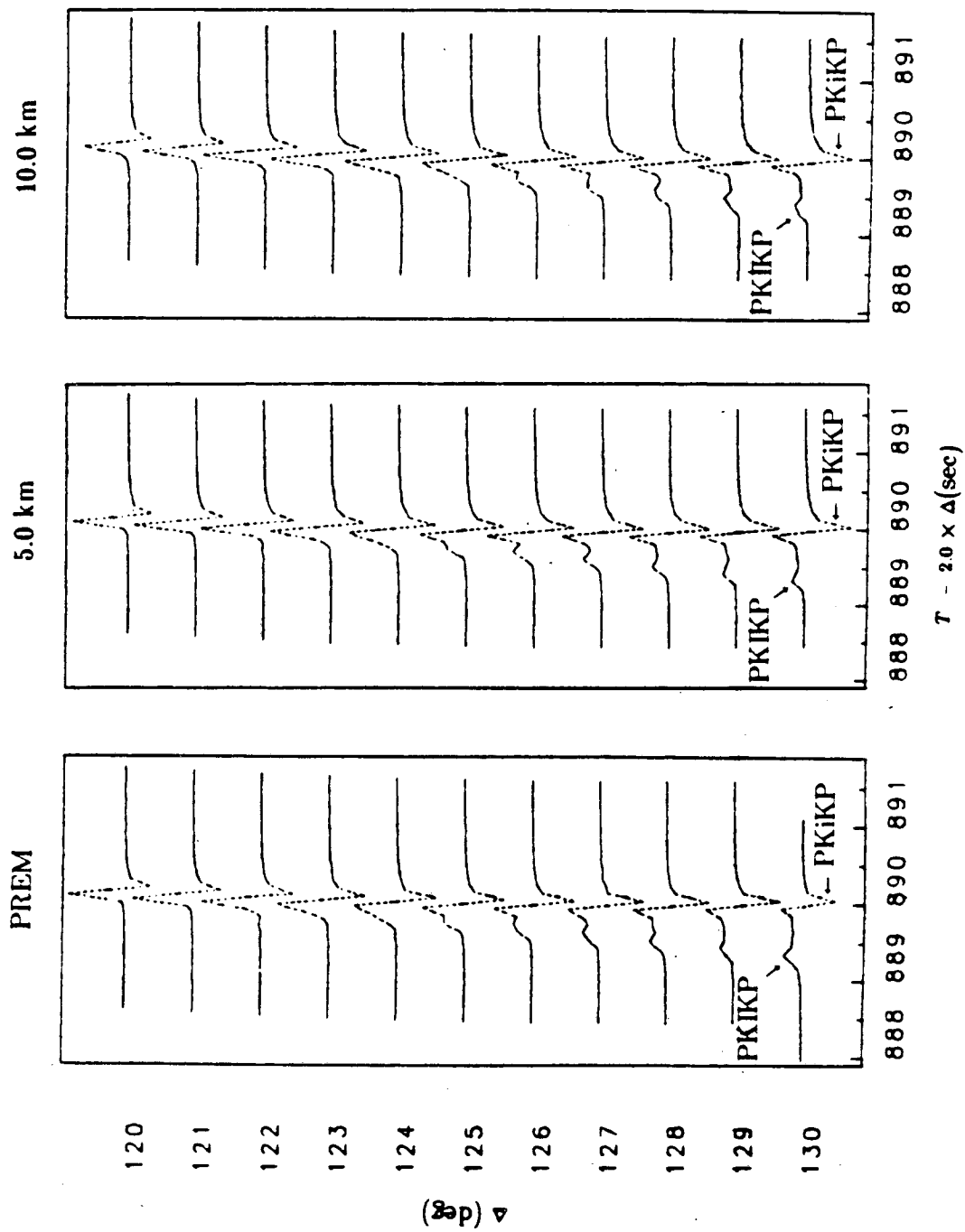


Figure 6

Chapter 3: Short-period Body Wave Constraints on Properties of the Earth's Inner Core Boundary

Summary

In this study we model short-period waveform data in an attempt to constrain the P- and S-velocity structure at the Earth's inner core boundary (ICB). The data set consists of recordings from 10 events in the south Pacific, and the data selection criteria as well as methods of analysis were designed to avoid problems with receiver response often associated with short-period waveform data. These data are modeled using a calculation technique that facilitates the consideration of a wide variety of models for the ICB. Results indicate that Q_α in the inner core has the frequency dependence suggested by Doornbos (1983). The data determine the P-velocities above and below the ICB to within a trade-off that is well constrained by the data. For example, with a P-velocity structure above the ICB given by PREM, the P-velocity below the ICB is $11.03 \pm .03$ km/s. Similarly, for the data analyzed here the estimate of the S-velocity at the top of the inner core trades off with the estimate of Q_α , but we use the Q_α model of Doornbos (1983) to estimate the jump in S-velocity to be 3 ± 1 km/s.

3.1. Introduction

Seismological models of the Earth's core have often suggested the presence of anomalous structure near the Earth's inner core boundary (ICB). One of the earliest models due to Jeffreys (1938), for example, includes a pronounced zone of negative velocity gradient just above the ICB. Later models due to Bolt (1962) and Adams and Randall (1964) include layering above the ICB. More recent studies have shown that the anomalous features of

these models could be eliminated through different interpretations of the data. Jeffreys' low velocity zone was required to accommodate the appearance of refracted PKIKP phases at 110° ; later studies (Denson, 1952, Buchbinder, 1971 and Qamar, 1973) indicate that this phase first appears at 120° . Similarly, Bolt (1962) and Adams and Randall (1964) required layering above the inner core to account for supposed reflections that were later found to constitute energy scattered near the core-mantle boundary (Cleary and Haddon, 1972).

More recent studies by Buchbinder (1971) and Qamar (1973) of short-period core phase amplitudes and travel times, as well as Müller's (1973) study of long-period PKIKP waveforms indicated a relatively small jump in P-velocity at the inner core boundary (ICB), suggesting that the upper portion of the inner core is characterized by a high P-velocity gradient. These studies relied on a combination of amplitude and travel time data to infer the presence of anomalous structure at the top of the inner core: amplitudes of precritical PKiKP indicated that the P-velocity jump at the ICB is about 0.6 km/s, while travel times of PKP and PKIKP were thought to constrain the P-velocities immediately above and 200 km below the ICB to be about 10.2 km/s and 11.1 km/s respectively. Thus, a high P-velocity gradient in the outer 200 km of the inner core (about $.0045 \text{ s}^{-1}$) was required to make up the difference. The large quantities of data and complex analysis procedures used in these studies make it difficult to ascertain the extent to which the structure at the top of the inner core is actually constrained by the data and to what extent it is determined by *a priori* assumptions and non-unique interpretations of the data. For example, Qamar's (1973, figure 16) plot of PKIKP and PKiKP amplitudes versus distance indicates that PKiKP has larger amplitude for $\Delta > 125^\circ$, while the corresponding figure in Buchbinder (1971, figure 22) shows the opposite, indicating a possible misidentification of phases in this distance range (Buchbinder uses a low Q_α in the inner core, which is confirmed by the present study).

Häge (1983) performed an analysis of long-period waveforms from 16 earthquakes in which he used model 1066B (Gilbert and Dziewonski, 1975) to represent the Earth above the inner core, and systematically varied the jumps in density, P-, and S-velocity at the ICB to

obtain estimates of the parameters which best fit the observed amplitudes. He found that no strong gradients in P-velocity were required at the top of the inner core, although there was a suggestion that the S-velocity gradient may be large there. It is not clear, however, how sensitive his results were to changes in the outer core P-velocity, which he assumed *a priori*. In contrast, the study by Choy and Cormier (1983) of short-period waveforms suggested a small P-velocity jump (0.52 km/s) at the ICB, and the authors tentatively suggested that the S-velocity jump may be zero, which leads to the inference of strong velocity gradients below the ICB.

Although the presence of anomalous velocity gradients near the ICB has not been firmly established, several physical interpretations for this phenomenon have appeared in the literature. Gutenberg (1958b), in his study of precursors to PKIKP, seems to have been the first to suggest that the state of matter in the inner core was anomalous. This suggestion has since reappeared with Anderson's (1980 and 1983) idea of a 'glassy-type' transition at the ICB, and Fearn and Loper's (1981, see also Loper and Fearn (1983)) model of a dendritic 'mushy zone'. Our poor knowledge of the phase diagram of Fe-FeS at core conditions does not rule out the possibility of a gradual change in composition near the ICB, and this idea receives some support in theoretical studies of the properties of binary liquid alloys at core temperatures and pressures (Alder and Trigueros, 1977, and Stevenson, 1980). The most plausible hypothesis concerning anomalous material properties near the ICB, however, suggests that the temperature profile in the inner core is very close to the melting curve for iron. This was first suggested by Gutenberg (1958a), and seems consistent with both theoretical studies (Higgins and Kennedy, 1971) and recent shock wave data (Anderson, 1986, Brown and McQueen, 1986, Williams *et al.*, 1987). All of these models have interesting implications for core dynamics and thermal history. Anderson (1983) suggests that if his model of a glassy core is valid, the effective size of the inner core would decrease with decreasing frequency of motion, so that a rigid inner core may not exist at the low frequencies associated with outer core convection. Fearn and Loper (1981) argue that their model involves the

production of a substantial amount of light fluid in the inner core that will have a profound effect on the pattern of convective motion in the outer core. The validity of the latter two propositions would have interesting implications for the thermal state of the Earth's core. Thus, confirming and explaining the anomalous nature of the upper portion of the inner core is a problem of some geophysical importance.

This study focuses on the determination of velocity structure near the ICB. A critical appraisal of the constraints which our data place on this structure requires that the structural parameters be varied in a systematic manner, so that the sensitivity of the data to the model parameters can be reliably assessed, and that the least number of *a priori* assumptions be included in the analysis. We reason that in order to attain a resolution in both velocity and depth that will be valuable in discriminating between the various phenomenological models for the inner core transition we must use short-period body waveform data.

3.2. Data

There are four types of seismological data available for a study of this type: free oscillation data, travel-time data, and long- and short-period body waveform data. Free oscillation data provide valuable constraints on the average properties of the inner core, but are incapable of achieving the depth resolution required to determine detailed structure. The scatter in global travel time data prevents a precise determination of the sharp change in velocity that takes place at the ICB; in their study of ISC travel time data, Johnson and Lee (1985) found that these data were satisfied by models having a velocity increase of between 0.4 and 1.1 km/s over a depth interval of 50 km at the ICB. Long-period body waveform data achieve better depth resolution than free oscillation data, and their use of all of the information contained in a seismogram yields more powerful constraints on the velocity jumps at the inner core boundary than are available from travel time data; e.g., the studies by Müller (1974), and Häge (1983) claim to achieve a resolution of $\pm .05$ km/s in the P velocity jump at the ICB. But the wavelengths of long-period body waves in the inner core are of the order of

100 km, and this may still be inadequate for discriminating between the various models of the inner core transition zone. This study requires the use of short-period body wave data, which should in theory be capable of providing even more powerful constraints on the velocity jump at the ICB than long period data, and which also should have a depth resolution of tens of kilometers.

There are very serious problems encountered when using short-period waveform data, however, and these have been the subject of some discussion in several recent seismological studies of the inner core. Both Müller (1973) and Häge (1983) note that the large observed scatter of short-period PKP amplitudes mitigates the usefulness of this data in constraining inner core structure, and they hypothesize that this scatter is due to inhomogeneities located along the whole ray path between source and receiver. Choy and Cormier (1983) include short-period data in their analysis, but they rely on broadband waveforms obtained from merged long- and short-period data in order to avoid the sensitivity to scattering that is inherent in the short-period data. While we consider the objections to using short-period waveform data to be well-founded, our persistence in relying on this data is based on the premise that it contains important information that is not emphasized in analyses based on long-period data. Only the short period data are capable of obtaining the resolution that is critical for the application of our results to constraining phenomenological models of the inner core transition, and this data may also contain valuable information on the frequency dependence of Q in the inner core (Doombos, 1974). Some support for the idea of modeling short-period teleseismic data may be found in Choy's (1982) study using Grafenburg array data, in which he found that phase coherence in the short-period band was considerably stronger than amplitude coherence, although his assessment of the efficacy of modeling short period data was not optimistic. We also note that Choy's study indicated that, for the deep teleseism he examined at Grafenburg, the scatter in short period amplitude data was due to upper mantle or crustal structure near the receiver.

In an attempt to avoid some of the problems associated with modeling short-period waveforms and obtain the maximum possible resolution for determining core structure, we have chosen to use data from the Regional Seismic Test Network (RSTN). This network, installed in North America by the U.S. Department of Energy as a prototype network for monitoring nuclear test explosions in the Soviet Union, has several properties that make its data well suited to studies of deep Earth structure. The response of its short-period band is the same for all stations and is flat to velocity between 2 and 10 Hz, so that the high end of the signal spectrum for PKP phases is undistorted. This data is continuously recorded so that no data is discarded due to failure of an event-detection algorithm. The instruments are emplaced in 100 m boreholes, and an attempt was made to locate the stations at low-noise sites on Precambrian rock of the Canadian shield (Taylor and Qualheim, 1983) - this should minimize degradation of signal quality due to noise and site effects. Finally, the location of the network in North America places it in the distance range of 100–140° with respect to a number of deep earthquakes in the southwest Pacific. This distance range straddles the D cusp in the PKP travel time curve, where PKiKP undergoes critical reflection and PKIKP phases sampling the top of the inner core are observed.

The siting of the two stations RSNT and RSON was particularly ideal. Both of these stations have their seismometer packages clamped directly into Precambrian rock of the Canadian shield (see Figure 1), and, according to the study by Owens *et al* (1987), the crustal structure at each site is very simple. The results of their study indicated that the crustal structures at both sites are characterized by two or three flat layers, with the discontinuities at mid-crustal depths. Thus, the steeply-incident PKP phases considered in this study should generate very little converted energy, and any reverberations of P wave energy will arrive well outside the time window of interest (the first 1-2 sec of the waveform). These considerations as well as the excellent fits obtained with the data from these two stations allow us to feel justified in treating the crust at RSNT and RSON as transparent, i.e. there is no need to incorporate corrections for receiver structure at either of these sites. Furthermore, the

locations of RSNT and RSON with respect to the south Pacific earthquakes we selected for study were generally such that RSNT recorded a pre-critically reflected PKiKP phase, whereas RSON was at a larger distance where PKIKP and the post-critically reflected PKiKP phase were observed (see Figure 2). This allowed us to use the RSNT recordings as empirical source/attenuation operators which could be used as an input for the modeling procedure, as described below.

The siting of the other three stations of the network was not so favorable for our study. Stations RSCP and RSNY were usually at distances of 140° or greater from the selected earthquakes, and this distance range is close to the B caustic in the PKP travel time curve where the outer core PKP phases are sharply focused. The amplification of the PKP energy is so great that outer core phases scattered at the core-mantle boundary often interfere with the inner core phases of interest (Cleary and Haddon, 1972). This phenomenon is well documented, and was at one time thought to represent energy reflected from a transition zone above the inner core (Bolt, 1962). For our purposes it represents signal-generated noise that so severely degraded signal quality at RSNY and RSCP that only a few recordings from RSNY could be used in the analysis. Station RSSD, on the other hand, recorded many events at distances between 120° and 140° , but its site response appears to be relatively complicated. This is no surprise, as RSSD is the one station for which Owens *et al* (1987) were unable to obtain a reliable model of crustal structure. As described in their paper, station RSSD is located on the western flank of the Black Hills in South Dakota, where a layer of limestone sediments thought to be less than 1 km thick overlies the Precambrian basement which dips to the west. Thus, the seismometer package at RSSD is likely to be very close to a dipping interface of high impedance contrast, and both converted energy and reverberations are expected to arrive within a narrow time window.

Finally, we feel that some description of the criteria we used for selecting events is called for. As explained below, the modeling procedure required that we restrict the events geographically to include only those for which the RSTN stations straddled the D cusp of the

PKP travel time curve, i.e. those for which the RSTN sampled the distance range $100 - 120^\circ$ and also the distance range $120 - 140^\circ$. The events were required to be deep (at least 100 km depth) in order to minimize the influence of near-source crustal structure. The most restrictive criteria we applied, however, were that the signal-to-noise ratio be good and that the source time functions be relatively simple, criteria which we found to be almost mutually exclusive. Application of these criteria to all of the data recorded on the GDSN event tapes distributed by the National Earthquake Information Center resulted in the selection of 10 events, although it was often necessary to obtain more complete recordings of the RSTN data from the RSTN's System Control and Receiving Station in Albuquerque, NM. We also examined the radiation patterns of the remaining events, and none of the events had nodal planes closer than 10° to the take-off angles of interest in this study. A list of the events used in this study appears in Table 1.

3.3. Analysis Procedure and Models of the ICB

Modeling of the data described in the previous section requires the calculation of synthetic seismograms for short-period body waves that interact with the ICB at angles of incidence near the critical angle. The method of calculation employed here has been described at length in Cummins and Johnson (1988), and will be only briefly sketched here. This method is a hybrid combination which uses the 'full wave' theory of Richards (1973) in the smoothly varying layers of the mantle and outer core as well as in the deep inner core, where the asymptotic WKBJ and Langer wave functions adequately describe the wavefield. In the vicinity of the ICB the method uses the invariant imbedding algorithm of Kennett (1983), which includes all of the reverberation and coupling phenomena that occur in the presence of the large velocity gradients which may characterize the underside of the ICB. Thus, calculations for arbitrary models for the ICB can be performed very efficiently as the full wave asymptotic wave functions for the mantle and outer core need be calculated only once, and can then be combined with a large number of reflectivity calculations for various models of

the inner core transition.

Calculation of the short-period synthetics will also require an adequate representation of the earthquake source time function as well as the propagation and attenuation effects of the mantle and outer core. We avoid the difficult problem of modeling these phenomena by obtaining a source/attenuation operator directly from the pre-critical PKiKP reflections recorded at RSNT for the events studied. All of the core phases analyzed leave the source in a very narrow cone of takeoff angles and have steep raypaths in the mantle, so that the influence of the source radiation pattern and propagation in the mantle should be very nearly the same for core phases arriving at the different stations in the network. This assumption may not apply to regional variations of Q in the upper mantle beneath central and eastern North America, but we note that the four stations used in the analysis (RSNT, RSNY, RSON, and RSSD) are all located on the Canadian shield. The high Q values typical of such continental shield areas should have little effect on the waveforms, i.e. while the regional variation in amplitudes may be significant, the corresponding variation in dispersion will be small. Thus, assuming the crust at RSNT to be transparent, the recorded signal represents the earthquake source time function and attenuation effects in the mantle and outer core, convolved with the Green's function appropriate for a given model of the ICB. If $S(\omega, \Delta)$ is the synthetic spectrum for distance Δ , $G(\omega, \Delta)$ is the corresponding Green's function, and $D_{RSNT}(\omega, \Delta)$ is the data spectrum for the pre-critical PKiKP reflection recorded by RSNT, then we obtain the synthetic spectrum at distance Δ_1 via:

$$S(\omega, \Delta_1) = \frac{G(\omega, \Delta_1)}{G(\omega, \Delta_0)} \times D_{RSNT}(\omega, \Delta_0)$$

This procedure removes the slight distortion which may have been introduced into the precritical reflection by structure immediately below the ICB, and then convolves the resulting source/attenuation operator with the Green's function for the post-critical distance Δ_1 , producing a synthetic seismogram which may be directly compared with the data.

All of the Earth models considered in this study are variations of the Preliminary Reference Earth Model (PREM) described in Dziewonski and Anderson (1981). PREM is used in the full wave calculations for the variation in elastic parameters above 1500 km and below 1000 km radius. In the intervening depth interval, henceforth referred to as the transition zone, the $\alpha(r)$, $\beta(r)$, $\rho(r)$, and $1/Q(r)$ profiles will consist of cubic interpolations between the specified parameter values at the top and bottom of the transition zone that are constrained to keep the material parameters and their derivatives continuous except for the jump at 1221.5 km radius which represents the ICB. Each transition zone model is then discretized into layers 0.5 km thick which are subjected to a version of the earth flattening transformation before their reflectivity response is calculated via the invariant imbedding algorithm. The jump in material parameters at the ICB will be represented as a sharp discontinuity, which is consistent with the pre-critical PKiKP reflections observed by Engdahl *et al* (1974). Cummins and Johnson (1988) have shown that these data constrain the transition at the ICB to be less than 5.0 km, and that the depth resolution of the RSTN short-period waveform data considered here is about 10.0 km for the distance range 120 – 140°. Thus, the thickness of the ICB is less than the data can resolve, and a model with a sharp discontinuity is appropriate.

While the Earth models considered in this study use PREM for the variation of elastic parameters with depth outside the transition zone, no anelasticity was included in the mantle or outer core, as this will be introduced into the synthetics by our empirical source/attenuation operators. For anelasticity in the lower 1000 km of the inner core, we use a Q_α profile similar to that of Doombos (1974), which involves an increase in Q_α with depth, and we also incorporate the frequency dependence suggested by Doombos' later study (1983), which involves a decrease in Q_α with increasing frequency. We note however, that the Q_α model used in the inner core below 1000 km radius has little effect on the synthetics; it is the behavior of Q_α within the top two hundred kilometers that has a very strong influence on the synthetics, and this behavior will be varied in the modeling procedure. Finally, in all of the models considered here we assume that all of the attenuation occurs in

shear, that is:

$$Q_{\beta} = \frac{4\beta^2}{3\alpha^2} Q_{\alpha}$$

This seems to be a reasonable assumption as it is consistent with our knowledge of the anelastic properties of most solids. Even if most of the attenuation were in bulk, then the weaker shear attenuation would have little effect on our estimate of Q_{α} , since our data are not very sensitive to the shear modulus of the inner core.

3.4. Results

Before describing the results of our numerical modeling in detail, we felt that some discussion of the quality of the data and its sensitivity to the modeling parameters is warranted. In Figure 2 are plotted 3 sets of recordings typical of those used in this study (only stations RSNT, RSSD, RSON, and in one case, RSNY are used here). The first two suites of seismograms (Figure 2a and b) each include an RSNT recording of a pre-critically reflected PKiKP phase that was used as a source/attenuation operator, as well as data from RSSD and RSON recorded at distances greater than 120° . The third suite (Figure 2c) includes a RSON recording of a post-critically reflected PKiKP phase which was used as a source/attenuation operator for the RSNY recording at 135° . Each of these three suites of seismograms represents one of the three distance ranges into which we have grouped the data: (a) $120.0\text{--}125.0^{\circ}$, (b) $128.0\text{--}132.0^{\circ}$, and (c) $133.0\text{--}135.0^{\circ}$. Distance range (a) lies just beyond the D cusp in the PKP travel time curve, where the reflected PKiKP phase undergoes critical reflection and the refracted PKiKP begins to emerge from the PKiKP+PKiKP wavelet (see Figure 3). Because the travel time difference between PKiKP and PKiKP in this distance range is too small (about .1-.3 sec for PREM) for an interference pattern to develop, we must rely on subtle features of the waveforms, such as the relative amplitudes of peaks and troughs, to judge the quality of the fit with observed data. Distance range (b) lies far enough past the D cusp that the PREM travel time difference between PKiKP and PKiKP is about .6

sec, and since the dominant energy in the observed waveforms occurs at a frequency of about 2.0 Hz this phase difference was large enough to cause the interference pattern between PKiKP and PKIKP to be very sensitive to small perturbations of the material parameters below the ICB. We rely primarily on the data recorded at distance range (b) to establish the tight constraints on material contrasts at the ICB claimed in this paper. Distance range (c) lies well past the D cusp, but it is close to the B caustic where the outer core PKP phase is sharply focused. PKP energy that is presumably scattered by inhomogeneities near the core-mantle boundary can arrive at times preceding and coincident with PKIKP having sufficiently strong amplitudes that the PKIKP+PKiKP signal quality is severely degraded. Nevertheless, information can be derived from the time difference between PKIKP and PKiKP that helps constrain the P-velocity structure near the ICB.

With three exceptions (see section 3.4.4) the data to be analyzed here have RSNT at a distance less than the D cusp and both RSSD and RSON at distances beyond the D cusp. The fits obtained at RSSD were reasonably good for short-period data, but our ability to fit the RSON waveforms was excellent. As explained in the previous section, we attribute this to the very simple crustal structure at both RSNT and RSON, whereas the crustal structure at RSSD is known to be more complicated. Because of the degrading effect that complex crustal structure appears to have on the RSSD data, we rely almost exclusively on comparisons of our synthetic waveforms with the RSON recordings to infer inner core structure. While the trend from more poor to better fits are consistent between both the RSON and RSSD data sets, few of the results we obtain would be possible based on comparisons with the RSSD data alone. Thus, an objection to the conclusions reached in the following paragraphs is that we are fitting the crustal structure at RSON rather than inner core structure; i.e., waveform modeling relying on either RSON or RSSD data will be biased by the crustal structure, and only a study relying on the largest possible number of receivers can claim to be independent of receiver structure at any one site. We have three answers to this objection: (a) our hypothesis that the crustal structure at RSSD is much more complex than that at RSON is

based on numerous independent studies (e.g. Owens *et al.*, 1987, Taylor and Qualheim, 1983, Hall and Hajnal, 1959), and not solely on our study of the data set considered here, (b) the energy appearing coincident with PKIKP on the horizontal component seismograms at RSSD is significant and indicative of some interaction with near-receiver structure, while the very small amplitudes on the horizontals at RSON (in all but one case, see below) is consistent with uncontaminated PKIKP arriving at the receiver from nearly vertically below, and (c) the close agreement between synthetics and RSON waveforms is ubiquitous in our data set and is not limited to any one distance range or characteristic waveform. In any case we display comparisons of synthetics with both the RSON and the RSSD data so that readers may make their own judgements.

3.4.1. Frequency dependence of Q_α in the inner core

Figures 4a-c compare the data from RSON and RSSD at distance range (b) with synthetics generated using three different models. Figures 4a and 4c use PREM for the variation of elastic parameters with depth, including the jumps in material properties at the ICB. The calculation in Figure 4a uses a Q_α in the inner core that is constant with frequency and has the value 297, which is slightly higher than the value suggested by Cormier (1980) and used by Choy and Cormier (1983). In Figure 4c, however, the calculation has used a Q_α for the inner core having a frequency dependence similar to Doornbos' (1983) relaxation band model, with cut-off relaxation times of .07 and .01 s, i.e. on the high side of the short-period seismic band. The absorption band was chosen with Q_α having a value of 215 at 1.0 Hz, which is slightly lower than that proposed by Doornbos (1983). Both of the models in Figures 4a and 4c were determined as the best fit to the data obtained by using PREM with the given frequency-dependence of Q_α and varying its 1.0 Hz value alone; the agreement of the values for Q_α with those obtained by Doornbos (1974) and Cormier (1980) is interesting. The depth dependence of Q_α was similar to that proposed by Doornbos (1974) but this had little effect on the synthetics, as PKIKP for this distance range bottoms in the top 25 km of

the inner core where Q_α does not change significantly.

It seems clear upon comparing Figure 4a and 4c that the frequency-dependent Q_α fits the data better than a constant Q_α model when PREM is assumed to describe the jump in P- and S-velocities at the ICB. The synthetics in Figure 4 have been aligned and normalized so that the first peak or trough in the PKIKP pulse is coincident with and has the same amplitude as that in the data. We note that the dominant period in the first part of the waveform for the synthetics in Figure 4a is slightly shorter than that of the data, and the relative amplitudes of the RSON waveforms are inconsistent; the amplitudes of the synthetic PKiKP pulses are too small for EV184 and EV585 and too large for EV485 and EV785. Both of these features match the RSON data when the frequency-dependent Q_α model is used. It is not clear, however, whether the dispersion introduced by this model actually distorts the waveform of PKIKP or merely shifts it in time, altering its interference with PKiKP. The former effect would be a clear indication of dispersion, whereas the latter could also be produced by changing the P-velocity just below the ICB. To test this hypothesis, we calculated the synthetics displayed in Figure 4b, using a model identical to that used in 4(a) except that the P-velocity at the top of the inner core was raised by .03 km/s. This slight change in P-velocity brought both the onset of PKIKP and the peak amplitude of PKiKP into alignment with the data, but careful inspection reveals that the PKIKP wavelet is too narrow to agree with the observed data. The effect is slight but is discernible and consistent from event to event. We thus regard the frequency dependence of Q_α proposed by Doombos (1983) as confirmed by our data, and note that his analysis depended on the waveforms alone, not travel time differences. As noted by Doombos (1983), many frequency dependent models should fit the data equally well as long as Q_α decreases with increasing frequency in the short-period frequency band, but we use the relaxation model for Q_α described above in what follows.

3.4.2. P-velocity structure near the ICB: Distance range (a), 120 – 125°

As discussed above, this distance range lies just past the D cusp in the PKP travel time curve where the travel time difference between PKIKP and PKiKP is very small (see Figure 3). Perturbations in the P-velocity above (α_o) and below (α_i) the ICB can change the waveforms in this distance range in two ways: lowering α_o or increasing α_i will cause the D cusp to occur at smaller distances, increasing the travel time difference between PKIKP and PKiKP at any given distance; on the other hand, increasing α_o or lowering α_i will cause the D cusp to occur at greater distances, decreasing the travel time difference between PKIKP and PKiKP and reducing the phase distortion in PKiKP caused by post-critical reflection. Thus, an increase or decrease in both velocities simultaneously will tend to keep the position of the D cusp stationary, without affecting the PKIKP+PKiKP waveform. This trade-off and the degree of misfit caused by opposing perturbations of P-velocity above and below the ICB are illustrated in Figure 5a-d. The synthetics in Figure 5 are aligned and normalized so that the maximum amplitudes of the synthetics are coincident with those of the data, a procedure which should correct for any time delay or amplification due to local crustal structure. In Figures 5a and 5b we have plotted comparisons of the observed waveforms in distance range (a) with synthetic seismograms calculated for models with (α_i , α_o) equal to (10.95, 10.2) km/s (Figure 5a), and (11.1, 10.5) km/s (Figure 5b). Both models fit the data equally well. In Figure 5c, however, is illustrated a comparison between the observed waveforms and synthetics calculated for (α_i , α_o) equal to (10.9, 10.4) km/s, and here it can be seen that the phase distortion of the post-critical reflection is not strong enough to match the relative amplitudes of the first peak and trough of the observed waveforms. Similarly, Figure 5d illustrates the comparison of observed waveforms with synthetics calculated for a model with (α_i , α_o) equal to (11.1, 10.3) km/s, and it can be seen that for this model the travel time difference between PKIKP and PKiKP is too large to agree with the data. The region of the (α_i , α_o) model space corresponding to good fits to the observed waveforms is illustrated in Figure 8, where we have considered reasonable perturbations in P-velocity above and below

the ICB. The bounds of this region were established via a subjective determination of unacceptable misfit between observed and synthetic waveforms in distance range (a). The conclusions reached here using the RSON data would have been impossible based solely on a comparison of synthetics with the observed RSSD waveforms, as the complex receiver response distorts the waveform to a far greater extent than the perturbations in (α_i, α_o) considered here.

3.4.3. P-velocity structure near the ICB: Distance range (b), 128 – 132°

In Figure 6 are displayed comparisons of the data in distance range (b) with the synthetics generated for four Earth models similar to those considered in the section 3.4.2. The waveforms in this distance range consist of an interference pattern between the refracted PKIKP phase and the reflected PKiKP phase which arrives about 0.6 seconds later and has greater amplitude (see Figure 3). Information may be extracted from this type of wavelet in two ways: by comparing the relative amplitudes of PKIKP and PKiKP and by comparing their relative phase. The relative amplitudes are strongly influenced by the S-velocity and Q_α at the top of the inner core as well as by the contrast in P-velocity, so that a comparison of relative amplitudes does not provide an unambiguous determination of the P-velocity below the ICB. On the other hand the relative phase, or more specifically the travel time difference between PKIKP and PKiKP, is not sensitive to the S-velocity or Q_α in the inner core (it is sensitive to the dispersion, but this has been considered in section 3.4.1 above). Thus, the travel time difference between PKIKP and PKiKP provides an unambiguous measurement of the P-velocity at the top of the inner core. It is this property of the observed and synthetic waveforms that will be considered now.

The synthetics in Figure 6 are aligned with the first prominent peak or trough in the observed PKIKP wavelet and normalized to its amplitude. so that the mismatch in phase between observed and synthetic waveforms will appear as a misalignment in the amplitude maximum of PKiKP. Figures 6a and 6b illustrate the comparisons between observed and

synthetic waveforms for values of (α_i, α_o) equal to (10.95, 10.2) and (11.13, 10.5) km/s, respectively. Again, the synthetics for both of these models fit the data equally well, implying that there is a trade-off between values of α_i and α_o which are consistent with the data. In Figure 6c and 6d are displayed similar comparisons for models with (α_i, α_o) equal to (11.0, 10.35) and (11.06, 10.35), respectively. These synthetics do not fit the data because of the mismatch in phase of the PKiKP arrivals, which has opposite sign for (α_i, α_o) values on opposite sides of the trade-off curve. We note that this is true only for the first half of the waveform for event EV785, while the fit for the rest of the waveform is poor. Examination of the horizontal component data for this event indicated that at about 1.5 s after the first arrival on the vertical component a second arrival is evident with a slowness considerably greater than that of the first-arriving PKiKP. There were no obvious candidates for phases that may arrive coincident with PKiKP at 130° for an earthquake 584 km deep. We do not speculate about what this later arrival may be; we merely note its existence and disregard the latter half of the waveform for this event. The fit is also poor for EVT86. The horizontals were not available for this event, but the fit is so anomalously poor that we suspect a similar phenomenon may obscure the first part of the waveform.

The phase mismatch illustrated in Figures 6c and 6d is slight, but its consistency from event to event has led us to use this slight phase mismatch as the criterion for determining the bounds on region of (α_i, α_o) space which is consistent with the data (see Figure 8). Similar conclusions could be reached by comparing the synthetics with the observed RSSD waveforms, but the fit is not as good.

3.4.4. P-velocity structure near the ICB: Distance range (c), $133 - 135^\circ$

To obtain RSTN recordings in the distance range $133-135^\circ$ it was necessary to consider different geographic regions in which the absence of any suitable deep earthquakes forced us to consider shallow events (see Table 1). Three such events had simple source time functions and were recorded by either station RSNT or station RSON at distances near 120° . These

recordings were used as source/attenuation operators to model the waveforms recorded by another station (RSSD, RSON, or RSNY) at 133 – 135°. While the waveforms in this distance range are affected by changes in (α_i, α_o) in the same manner as those in distance range (b), the signal quality of the data is considerably poorer due to the arrival of scattered PKP energy preceding and coincident with PKIKP+PKiKP. Nevertheless, the differential travel time between PKIKP and PKiKP is still clearly discernible.

Thus, it is possible to constrain the trade-off curve for the (α_i, α_o) values which are consistent with the data, and the same pattern that we obtained in sections 3.4.2 and 3.4.3 is verified: values of (α_i, α_o) which lead to the best fits with the observed waveforms lie between (10.9, 10.2) and (11.15, 10.5) (Figures 7a and b), while the width of the trade-off region is characterized by the poor fits obtained at (11.025, 10.3) and (11.0, 10.4) (Figures 7c and d). This region is plotted in Figure 8, along with the corresponding regions for distance ranges (a) and (b).

3.4.5. S-velocity and Q_α below the ICB

As mentioned in section 3.4.3 of this section, both Q_α and the S-velocity in the inner core influence the relative amplitudes of PKIKP and PKiKP. The effect of decreasing Q_α in the inner core is to lower the amplitude of the refracted PKIKP phase. The effect of decreasing the S-velocity at the top of the inner core is to increase the amplitude of the reflected PKiKP phase (see e.g. Müller, 1974). Since we can determine only the relative amplitudes of PKIKP and PKiKP, our data is at best capable of constraining Q_α and the S-velocity at the top of the inner core to within a trade-off: high Q_α and low S-velocity should fit the data as well as a low Q_α and high S-velocity. This trade-off is illustrated in Figure 9, which compares the observed waveforms with the synthetics generated for models identical to PREM except that in Figure 9a the S-velocity at the top of the inner core has been perturbed to the value 4.0 km/s and Q_α has the value 170 at 1 Hz, and in Figure 9b the S-velocity was perturbed to zero and a Q_α of 297 was used at the top of the inner core. Both of these models fit the data

equally well, and either fit is very nearly as good as that in Figure 3c, which used the PREM value of 3.5 km/s for the S velocity at the top of the inner core and a Q_α of 215 at 1 Hz.

We have made an attempt to quantify the trade-off between Q_α and the S-velocity of the inner core in Figure 10, where for each of four values of Q_α (170, 215, 255, and 297) we have plotted the S-velocity corresponding to the best fit to the observed data. We estimate the uncertainty in the values for S-velocity in this figure to be ± 1 km/s, based on a subjective determination of the models for which we obtained unreasonable fits to the data when the S-velocity was perturbed from the values plotted in Figure 10. Also plotted in Figure 10 are the bounds on the inner core S-velocity determined by Häge (1983) in his study of long-period pre-critical PKiKP reflections, as well as Doornbos's (1983) proposed 1 Hz value for Q_α at the top of the inner core, and the combination of S-velocity and Q_α proposed by Choy and Cormier (1983) (0 km/s and 285, respectively). We note that the data Choy and Cormier (1983) used to infer a zero S-velocity at the top of the inner core was quite similar to that used here, and may be subject to the same trade-off between Q_α and S-velocity. The pre-critical PKiKP data analyzed by Häge (1983) were not subject to this trade-off, but it seems likely that the 0.05 Hz energy predominant in the long-period waveforms may average over depth intervals considerably larger than the resolution length possible in this study and that of Choy and Cormier (1983). The study by Doornbos (1983) used short-period waveforms in the distance range 148 – 150°, where the relative amplitudes of PKiKP and PKiKP are not influenced by the S-velocity at the top of the inner core. Since his estimate of Q_α represents an average over the top two hundred kilometers of the inner core, and since several studies indicate that Q_α increases with depth in the inner core (Doornbos, 1974, Choy and Cormier (1983)), it seems reasonable to accept Doornbos' (1983) estimate as an upper bound for Q_α at the top of the inner core that is independent of the S-velocity. Based on this assumption we estimate the shear velocity at the top of the inner core to be 3 ± 1 km/s.

3.5. Conclusions

In this paper we have attempted to infer velocity structure near the ICB via the modeling of teleseismic body waves, using as few *a priori* assumptions as seemed reasonable. The primary assumption used was that PREM accurately describes the average structure of the Earth's core both above and below the transition zone. Since our analysis depends on the change in waveform over a small interval of ray parameters corresponding to waves traveling almost vertically through the crust and mantle, deviations of the true structure from PREM in these regions should have little effect on the results. Furthermore, our calculations indicate that the data are not sensitive to small deviations from PREM near the ICB with scale lengths of the order of 10km or less (Cummins and Johnson, 1988). The data are clearly sensitive to perturbations in structure with scale lengths of 50 km or more, and it is such perturbations which have been considered in the analysis. We find that a systematic variation of all of the relevant model parameters, P-velocity above the ICB (α_o), as well as P-velocity (α_i), S-velocity (β_i), and attenuation Q_α below the ICB, leads to regions of the model space which roughly define trade-off curves in (α_i , α_o) and (β_i , Q_α) (see Figures 8 and 10). Any combination of model parameters which lies near these curves satisfies the data considered here.

Because of the lack of an appropriate statistical framework for the analysis of seismic body waves, the regions of (α_i , α_o) and (β_i , Q_α) space represented in Figures 8 and 10, respectively, do not represent confidence intervals. They are merely a subjective determination of the different combinations of model parameters which are consistent with the data. Furthermore, the separation of the ((α_i , α_o) and (β_i , Q_α) parts of the model space achieved by separately considering relative travel times and relative amplitudes is not rigorous: using a point other than PREM on the (α_i , α_o) trade-off curve in section 3.4.5 above may have lead to a slightly different trade-off curve for (β_i , Q_α), although the converse is not true.

While our results concerning the P-velocity profile near the ICB agree well with those of Müller (1973) and Häge (1983), and are consistent with the wide body of geophysical data

that led to the construction of PREM, they do not agree with the results of Choy and Cormier (1983). This discrepancy is very interesting, and it is important to seek possible explanations. We note that all of our data, almost all of the data used in Müller's (1973) study, and most of the data used in Häge's (1983) study consisted of North American recordings from events in the southwest Pacific. More specifically, our data consists of North American recordings from events (except one, EVB84, see Table 1) within an areal extent of about 20° in longitude and 10° in latitude in the southwest Pacific, so that our data only sample a solid angle on the ICB of about 5° in the northwest Pacific. Choy and Cormier's (1983) estimate of the P-velocity below the ICB was based on recordings from the SRO stations MAIO and CTAO of a deep earthquake in South America, so that their data sampled completely different regions of the ICB. Thus, the possibility that lateral heterogeneity of the velocity structure in the inner core may explain the discrepancy between Choy and Cormier's (1983) result and that obtained here cannot be ruled out. A similar situation may explain the disagreement between PREM and the results of Choy and Cormier (1983). The detailed structure in PREM was determined from travel time data, and the high density of seismographic stations in North America may result in a bias in this data towards structure along the path from North America to the only region of deep seismicity that lies in the distance range appropriate for core phases, the southwest Pacific.

Similarly, the estimate of 3 ± 1 km/s for the S-velocity below the ICB obtained here agrees with the results of Müller (1973) and Häge (1983), but does not agree with the result of Choy and Cormier (1983). However, our result for the S-velocity is based on Doornbos' (1983) model for Q_α at the top of the inner core, while Choy and Cormier's (1983) result would seem to be dependent on the higher value for Q_α in the inner core obtained by Cormier (1981). We preferred the Doornbos (1983) model over that of Cormier (1981) for two reasons: (a) the frequency dependence of Q_α that was taken into account in Doornbos' (1983) model fit both his waveform data and ours better than the frequency-independent Q_α used by Cormier (1981), and (b) Doornbos's (1983) model was chosen as the best model which fit

data sampling the top two hundred kilometers of the inner core, whereas Cormier's (1981) model was based on data sampling a much broader depth interval, so that his estimate may be biased towards the high Q_α values typical of the lower part of the inner core (Doombos, 1974, Choy and Cormier, 1983). In any case the discrepancy between our S-velocity estimate and that of Choy and Cormier (1983) can probably be explained by the trade-off between S-velocity and Q_α discussed in section 3.4.5 above. Either the high Q_α used by Choy and Cormier (1983) caused them to underestimate the S-velocity below the ICB, or the low Q_α used here has caused us to overestimate the S-velocity.

Finally, we turn to the geophysical implications of our study. Some of the most interesting implications follow from the result that the low Q_α in the inner core is associated with an absorption band on the high-frequency side of the frequency band for short-period body waves. While the dispersion indicated by Figure 3c is a subtle feature of the observed waveforms that may be affected by our choice of elastic parameters, we noted during the modeling procedure that a frequency-dependent Q_α always resulted in a better fit to the observed waveforms. Moreover, the observation that short-period core phases sample the low-frequency flank of the absorption band in the inner core was first made by Doombos (1983) in an analysis that was much less sensitive to elastic effects. This observation leads to the conclusion that the observed absorption peak is not due to the mechanism of viscous relaxation proposed by Anderson (1980 and 1983), since this mechanism requires an absorption peak on the low frequency side of the seismic band. Also, the Q_α model proposed by Loper and Fearn (1983) involves dissipation via thermal and material diffusion. For this mechanism to be operative at frequencies as high as 1 Hz would require liquid inclusions of the order of .01-.1 cm or smaller, so that the large-scale mixing of fluid and solid in the top few hundred kilometers of the inner core proposed by them is not likely to be associated with the observed absorption peak. Of course, either of these mechanisms may be associated with an as yet undetected absorption peak on the low frequency side of the seismic band, in which case they are not constrained by the seismic data.

The trade-offs demonstrated in this study for elastic and anelastic properties at the ICB imply a certain amount of nonuniqueness in any geophysical interpretation. However, the trade-off curve in Figure 8 can be used to argue as follows: a strong P-velocity gradient in the top of the inner core would require that the P-velocity just below the ICB be considerably lower than the PREM value, and this would require that the velocity above the ICB be correspondingly lower than the PREM value. Seismological models which have such a transition zone at the bottom of the outer core have been proposed in the past (e.g. Jeffreys (1938) and Qamar (1973)), but the recent study by Johnson and Lee (1985) shows that such models are inconsistent with global travel time data. Also, the studies by Cormier (1980) and Choy and Cormier (1983) indicate that such models are inconsistent with the body waveform data. Thus, the existence of a strong P-velocity gradient at the top of the inner core does not seem likely, although it is not completely ruled out by the analysis presented here. While our estimate for the S-velocity jump at the ICB is not significantly different from that of PREM, it is not well determined by our data, so that an S-velocity gradient considerably stronger than that predicted by PREM is also not ruled out by our analysis (indeed, Håge (1983) claims that this must be the case). The density cannot be determined by our data; according to Müller (1973) a change in density of $\pm 1 \text{ gm/cm}^3$ is equivalent to a change in S-velocity of $\pm 0.3 \text{ km/s}$, so that the uncertainty in our determination of S-velocity precludes a meaningful estimation of the jump in density.

References

- Adams, R.D., and M.J. Randall, The fine structure of the Earth's core, *Bull. Seism. Soc. Am.*, 54, 1299-1313, 1964.
- Aki, K., and P.G. Richards, *Quantitative Seismology, Theory and Methods*, W.H. Freeman, San Francisco, Calif., 1980.
- Alder, B.J., and M. Trigueros, Suggestion of a eutectic region between the liquid and solid core of the Earth, *J. Geophys. Res.*, 82, 2535-2539, 1977.
- Anderson, D.L., A new look at the inner core of the Earth, *Nature*, 302, 660, 1983.
- Anderson, D.L., Bulk attenuation in the Earth and viscosity of the core, *Nature*, 285, 204-207, 1980.
- Anderson, O.L., Properties of iron at the Earth's core conditions, *Geophys. J. R. Astr. Soc.*, 84, 561-579, 1986.
- Bolt, B.A., Gutenberg's early PKP observations, *Nature*, 196, 122-124, 1962.
- Brown, J.M., and R.G. McQueen, Phase transitions, Grüneisen parameter, and elasticity for shocked iron between 77 GPa and 400 GPa *J. Geophys. Res.*, 91, 7485-7494, 1986.
- Buchbinder, G.G.R., Wright, C. and G. Poupinet, Observations of PKiKP at distances less than 110° *Bull. Seism. Soc. Am.*, 63, 1699-1707, 1973.
- Choy, G.L., and V.F. Cormier, The structure of the inner core inferred from short-period and broadband GDSN data, *Geophys. J. R. Astr. Soc.*, 72, 1-21, 1983.
- Choy, G.L., Experiments with SRO and GRF-array data, *U.S. Geological Surv., Open-File Rept.*, 82-216, 1983.
- Cleary, J.R., and R.A.W. Haddon, Seismic wave scattering near the core-mantle boundary: a new interpretation of precursors to PKP, *Nature*, 240, 549-551, 1972.

- Cormier, V.F., Short-period PKP phases and the anelastic mechanism of the inner core, *Phys. Earth Planet. Inter.*, 24, 291-301, 1980.
- Cummins, P., and L.R. Johnson, Complete synthetic seismograms for an inner core transition of finite thickness, *Geophys. J. R. Astr. Soc.*, in press, 1988.
- Denson, M.E. Jr., Longitudinal Waves through the Earth's core, *Bull. Seism. Soc. Am.*, 42, 119-134, 1952.
- Doornbos, D.J., Observable effects of a seismic absorption band in the Earth, *Geophys. J. R. Astr. Soc.*, 75, 693-711, 1983.
- Doornbos, D.J., The anelasticity of the inner core *Geophys. J. R. Astr. Soc.*, 38, 397-415, 1974.
- Dziewonski, A.M., and D.L. Anderson, Preliminary reference Earth model, *Phys. Earth Planet. Inter.*, 25, 297-356, 1981.
- Engdahl, E.R., Flinn, E.A., and C.F. Romney, Seismic waves reflected from the Earth's inner core, *Nature*, 228, 852-853, 1970.
- Fearn, D.R., and D.E. Loper, Structure of the Earth's inner core, *Nature*, 292, 232-233, 1981.
- Gilbert, F. and A.M. Dziewonski, An application of normal mode theory to the retrieval of structural parameters and source mechanisms from seismic spectra, *Phil. Trans. R. Soc. London, Ser. A*, 278, 1265-1276, 1975.
- Gutenberg, B., Caustics produced by waves through the Earth's core, *Geophys. J. R. Astr. Soc.*, 1, 238-247, 1958.
- Häge H., Velocity constraints for the inner core inferred from long-period PKP amplitudes, *Phys. Earth Planet. Inter.*, 31, 171-185, 1983.
- Hall, D.H. and Z. Hajnal, Crustal structure of northwest Ontario: refraction seismology, *Can. J. Earth Sci.*, 6, 81-99, 1959.

- Higgins, G., and G.C. Kennedy, The adiabatic gradient and the melting point gradient in the core of the Earth, *Geophys. J. R. Astr. Soc.*, 28, 97-109, 1971.
- Jeffreys, H., The time of core waves, *M.N.R. Astr. Soc., Geophys. Supp.*, 4, 594-615, 1938.
- Julian, B.R., Davies, D., and R.M. Sheppard, PKJKP, *Nature*, 235, 317-318, 1972.
- Kennett, B.L.N., *Seismic Wave Propagation in Stratified Media*, Cambridge University Press, Cambridge, 1983.
- Lee, R.C. and L.R. Johnson, Extremal bounds on the P velocity in the Earth's core, *Bull. Seism. Soc. Am.*, 75, 115-130, 1985.
- Lees, A.M., Bukowinski, M.S.T., and R. Jeanloz, Reflection properties of phase transition and compositional change models of the 670-km discontinuity, *J. Geophys. Res.*, 88, 8145-8159, 1983.
- Loper, D.E., and D.R. Fearn, A seismic model of a partially molten inner core, *J. Geophys. Res.*, 88, 1235-1242, 1983.
- Morse, S.A., Accumulus growth of the inner core, *Geophys. Res. Lett.*, 13, 1557-1560, 1986.
- Müller, G., Amplitude studies of core phases, *J. Geophys. Res.*, 78, 3469-3490, 1973.
- Owens, T.J., S.R. Taylor, and G. Zandt, Crustal structure at Regional Seismic Test Network stations determined from inversion of broadband Teleseismic P waveforms, *Bull. Seism. Soc. Am.*, 77, 631-662, 1987.
- Qamar, A., Revised velocities in the Earth's core, *Bull. Seism. Soc. Am.*, 63, 1073-1105, 1973.
- Richards, P.G., Calculation of body waves, for caustics and tunnelling in core phases, *Geophys. J. R. Astr. Soc.*, 35, 243-264, 1973.
- Stevenson D.J., Anomalous bulk viscosity of two-phase fluids and implications for planetary interiors, *J. Geophys. Res.*, 88, 2445-2455, 1983.

Stevenson D.J., Applications of liquid state physics to the Earth's core, *Phys. Earth Planet. Inter.*, 22, 42-52, 1980.

Stoker, R.L., and R.B. Gordon, Velocity and internal friction in partial melts, *J. Geophys. Res.*, 80, 4828-4836, 1975.

Taylor, S.R., and B.J. Qualheim, Regional Seismic Test Network site descriptions, *Rep UCID-19769*. Lawrence Livermore Laboratory, Livermore, Calif., 1983.

Vaišnys, J.R., Propagation of acoustic waves through a system undergoing phase transitions, *J. Geophys. Res.*, 73, 7675-7683, 1968.

Williams, Q., R. Jeanloz, J. Bass, B. Svendsen, and T.J. Arhens, The melting curve of iron to 250 Gigapascals: a constraint on the temperature at the Earth's center, *Science*, 236, 181-182, 1987.

Zener, C., Theory of elastic polycrystals with viscous grain boundaries, *Phys. Rev.*, 60, 906-908, 1941.

Figure 1. RSTN station locations and the major crustal provinces of North America as indicated by the age of basement rocks (modified from Owens *et al.*, 1987).

Figure 2. RSTN recordings from three of the events listed in Table 1. The tick marks on the horizontal axis in each figure represent seconds of a time scale reduced at 2.0 s/deg. Superposed are PREM travel times calculated for the appropriate source depth and shifted to align with the RSON recordings.

Figure 3. Displacement Green's functions calculated for PREM with a frequency-dependent Q_α in the inner core, illustrating the position of the D cusp and the three distance ranges used in this study.

Figure 4. Comparisons of synthetics (dashed traces) with observed RSSD and RSON recordings (solid traces) for (a) an inner core model in which the velocity and density jumps at the ICB are specified by PREM and Q_α in the inner core is constant with frequency with a value of 297; (b) a model identical to that in (a) except that the P-velocity jump at the ICB is 0.7 km/s, 0.03 km/s greater than the PREM value, and (c), a model identical to PREM except that the relaxation model of Doombos (1983) was used for the frequency-dependence of Q_α in the inner core, with a 1 Hz value of 215.

Figure 5. Comparisons of synthetics (dashed traces) with observed RSSD and RSON recordings (solid traces) in distance range (a) for four different pairs (α_i, α_o) : (a) (10.95, 10.2)

km/s, (b) (11.1 , 10.5) km/s, (c) (10.9 , 10.4) km/s, and (d) (11.1 , 10.3) km/s.

Figure 6. Comparisons of synthetics (dashed traces) with observed RSSD and RSON recordings (solid traces) in distance range (b) for four different pairs (α_i , α_o): (a) (10.95 , 10.2) km/s, (b) (11.13 , 10.5) km/s, (c) (11.00 , 10.35) km/s, and (d) (11.06 , 10.35) km/s.

Figure 7. Comparisons of synthetics (dashed traces) with observed RSSD and RSON recordings (solid traces) in distance range (c) for four different pairs (α_i , α_o): (a) (10.9 , 10.2) km/s, (b) (11.15 , 10.5) km/s, (c) (11.0 , 10.4) km/s, and (d) (11.025 , 10.3) km/s.

Figure 8. Graph illustrating the trade-off between values of P-velocity in the outer core α_o and those in the inner core α_i for the three distance ranges considered here. *'s denote values of (α_i , α_o) for which calculations produced a poor fit to the data in distance range (a), O's denote values of (α_i , α_o) for a poor fit was obtained to the data in distance range (b), and X's denote values of (α_i , α_o) corresponding to poor fits to the data in distance range (c).

Figure 9. Comparisons of synthetics (dashed traces) with observed RSSD and RSON recordings (solid traces) for models identical to PREM except that Q_α in the inner core has the frequency dependence proposed by Doornbos (1983), and: in (a) the Q_α value at 1 Hz is 297, and the S-velocity jump at the ICB is 0.0 km/s, while in (b) the 1 Hz value of Q_α is 170 and the S-velocity jump is 4.0 km/s.

Figure 10. Graph illustrating the trade-off between the 1 Hz value of Q_α in the inner core with the S-velocity jump at the ICB for the data considered in this paper. Also shown are the bounds on the S-velocity jump at the ICB proposed by Häge (1983) and the 1 Hz value of Q_α proposed by Doornbos (1983), as well as the model for the S-velocity jump at the ICB proposed by Choy and Cormier (1983) and the Q_α value used in their frequency-independent model for Q_α .

Table 1. Earthquakes used in this study

Label	Event Information					Distance to Stations			
	Date	Origin time (UT)	Location (Lat-Lon)	Depth (km)	m_b	RSNT	RSSD	RSON	RSNY
ev184	1984 Jan. 17	02:09:04.9	7.7S-117.4E	303.9	5.7	113.2	128.5	129.4	141.3
ev284	1984 Apr. 1	09:59:00.3	5.6S-124.8E	585.0	5.7	108.8	122.7	124.7	
ev384	1984 Apr. 17	14:16:49.6	6.7S-126.8E	455.6	5.7	108.9	122.2	124.6	137.9
evb84	1984 Apr. 26	10:11:10.2	6.9S-71.5E	10.0	6.0	124.3	142.7	134.4	132.3
ev584	1984 Sep. 16	10:23:41.7	7.1S-117.5E	637.6	5.5	113.1	128.3		141.2
ev485	1985 Aug. 8	16:18:03.4	6.2S-113.5E	603.0	5.7	113.8	130.0	130.0	141.2
ev585	1985 Aug. 8	16:29:57.5	6.2S-113.4E	588.7	5.7	113.8	130.0	130.1	141.1
ev785	1985 Aug. 12	04:18:58.0	7.0S-117.2E	583.7	5.7	113.1	128.4	129.3	141.2
evb85	1985 Jul. 9	13:27:00.3	8.6S-110.3E	81.1	5.6	117.2	133.7	143.9	149.5
eve85	1985 Apr. 21	13:53:00.5	5.2S-130.5E	78.5	6.0		118.6	121.5	135.1

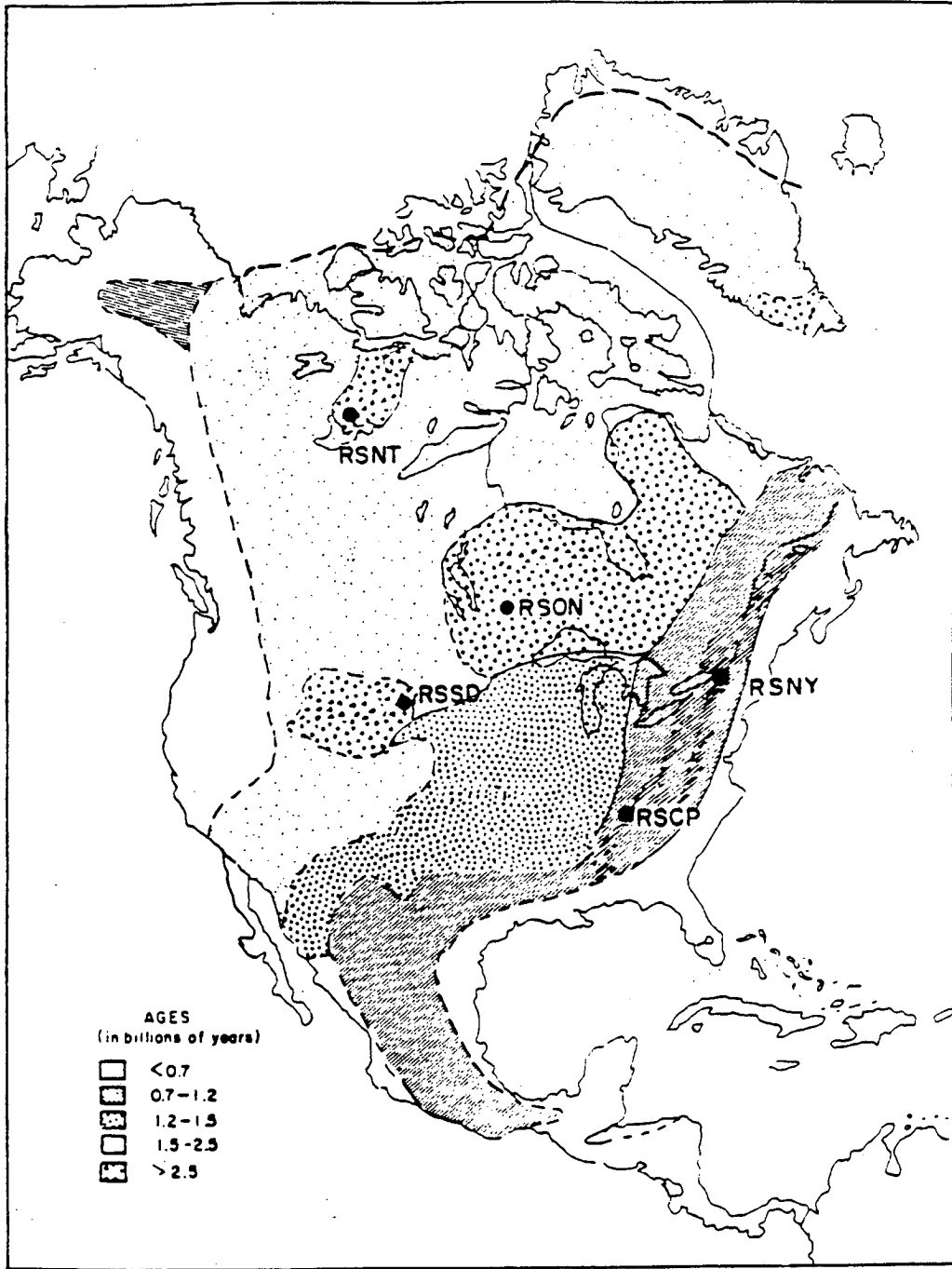


Figure 1

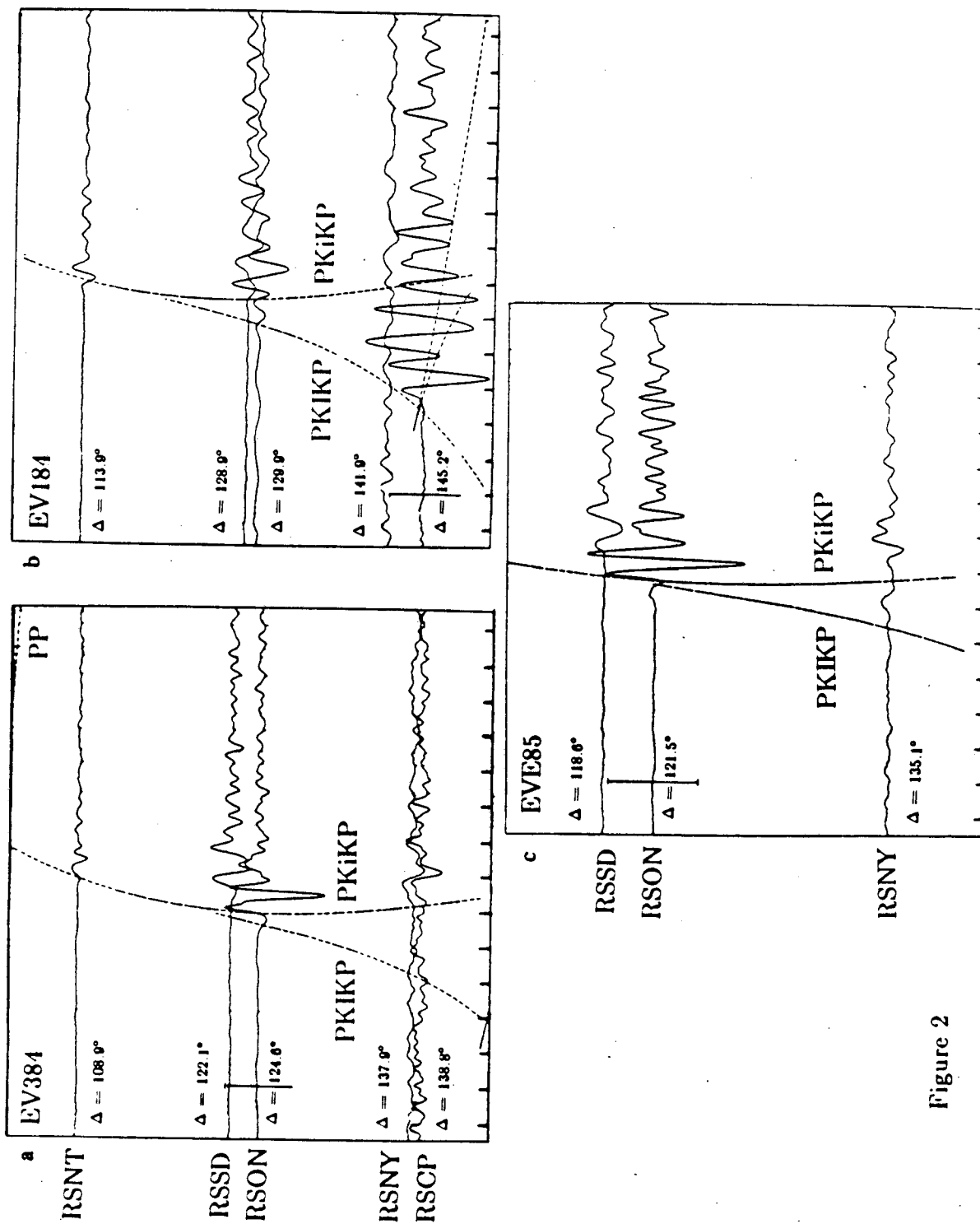


Figure 2

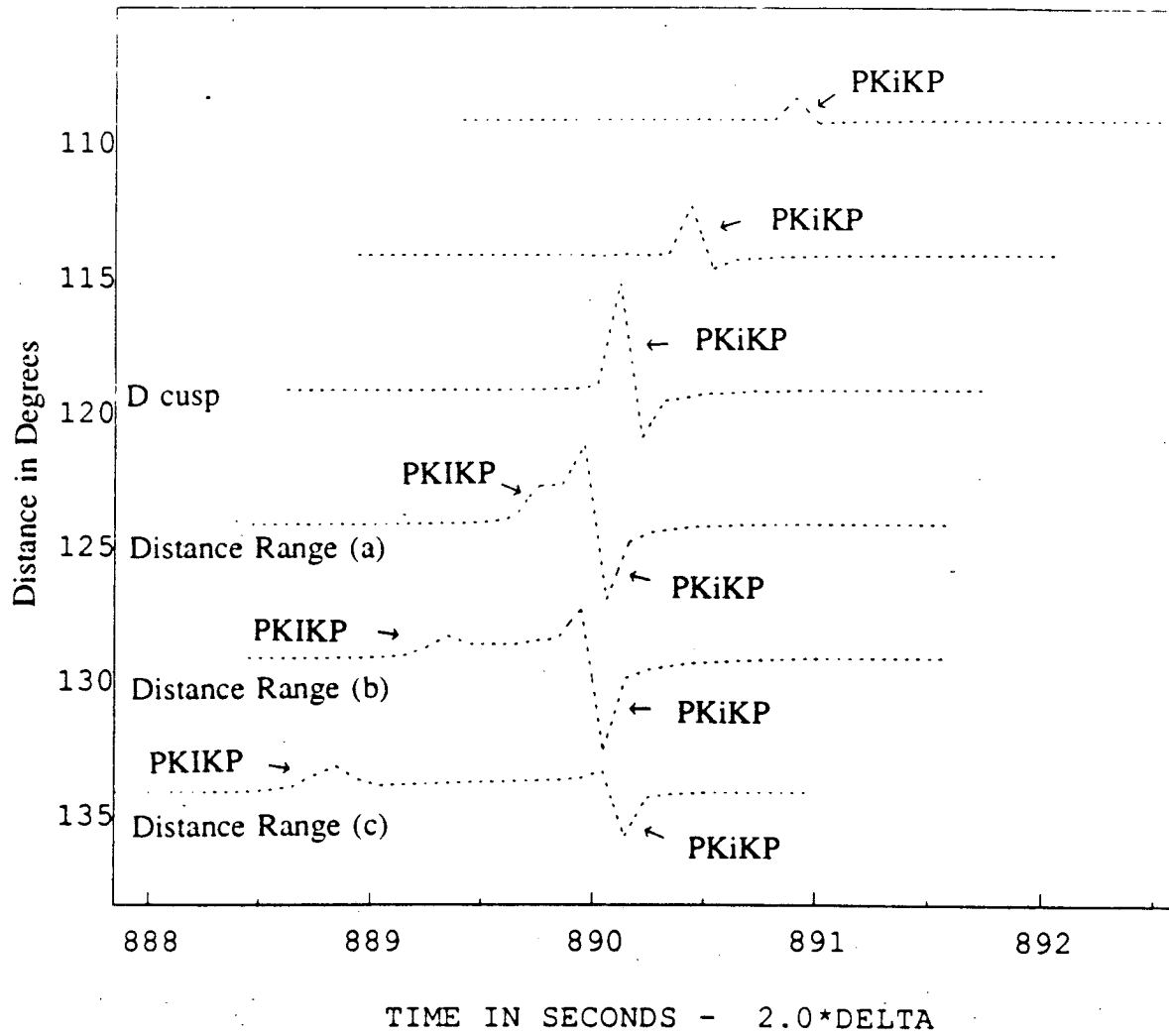


Figure 3

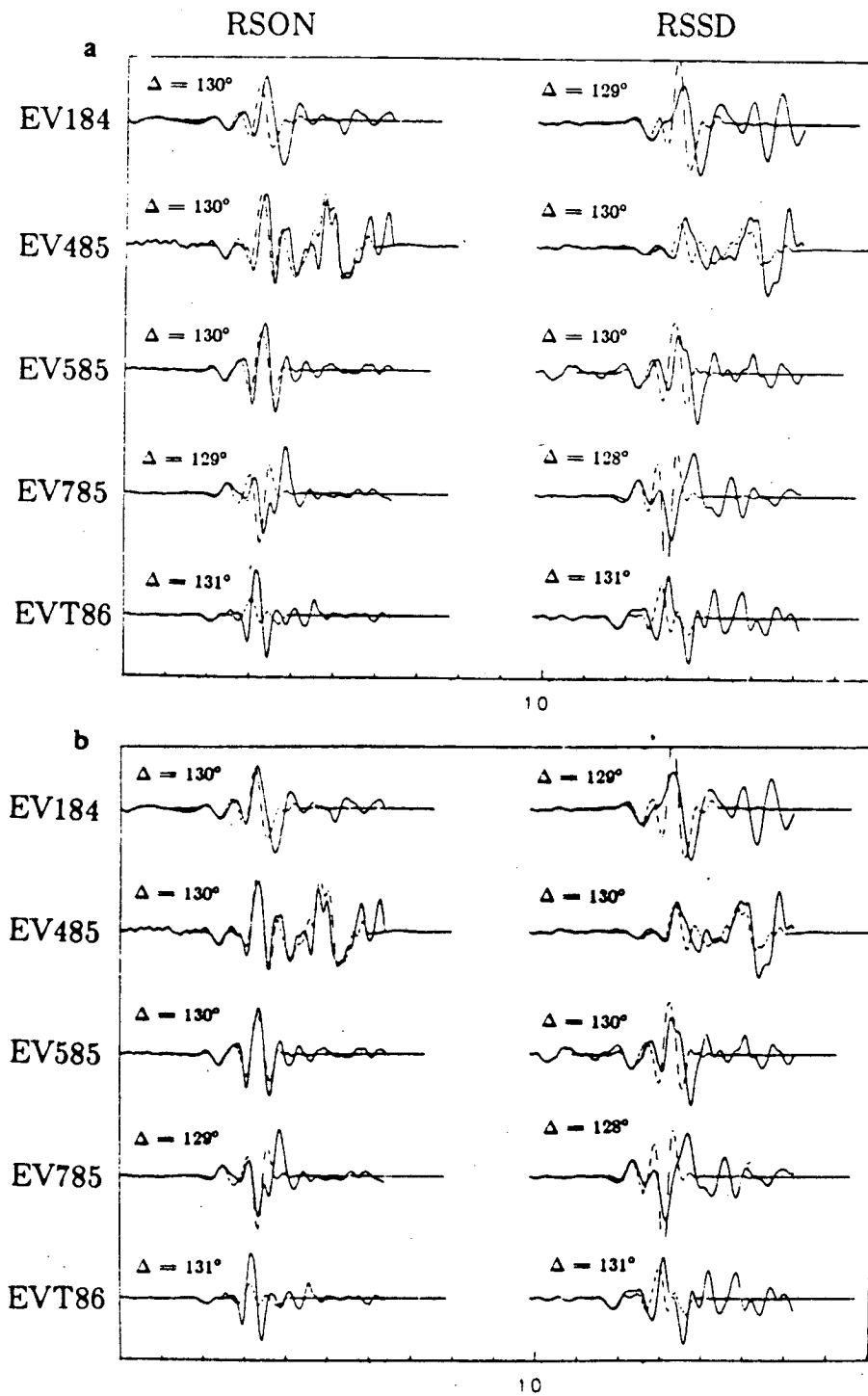


Figure 4

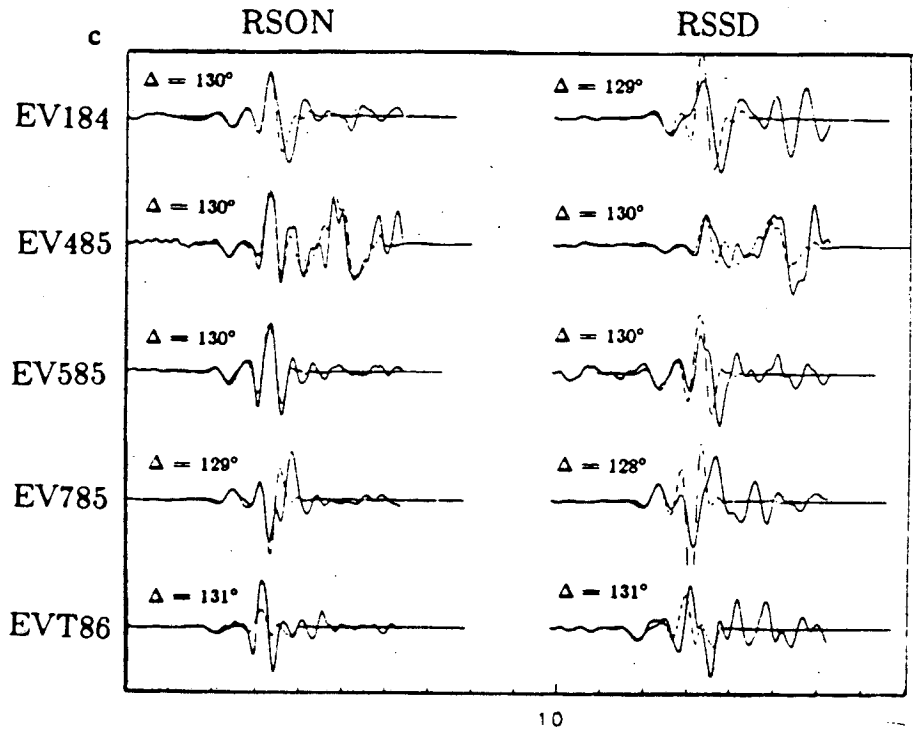


Figure 4

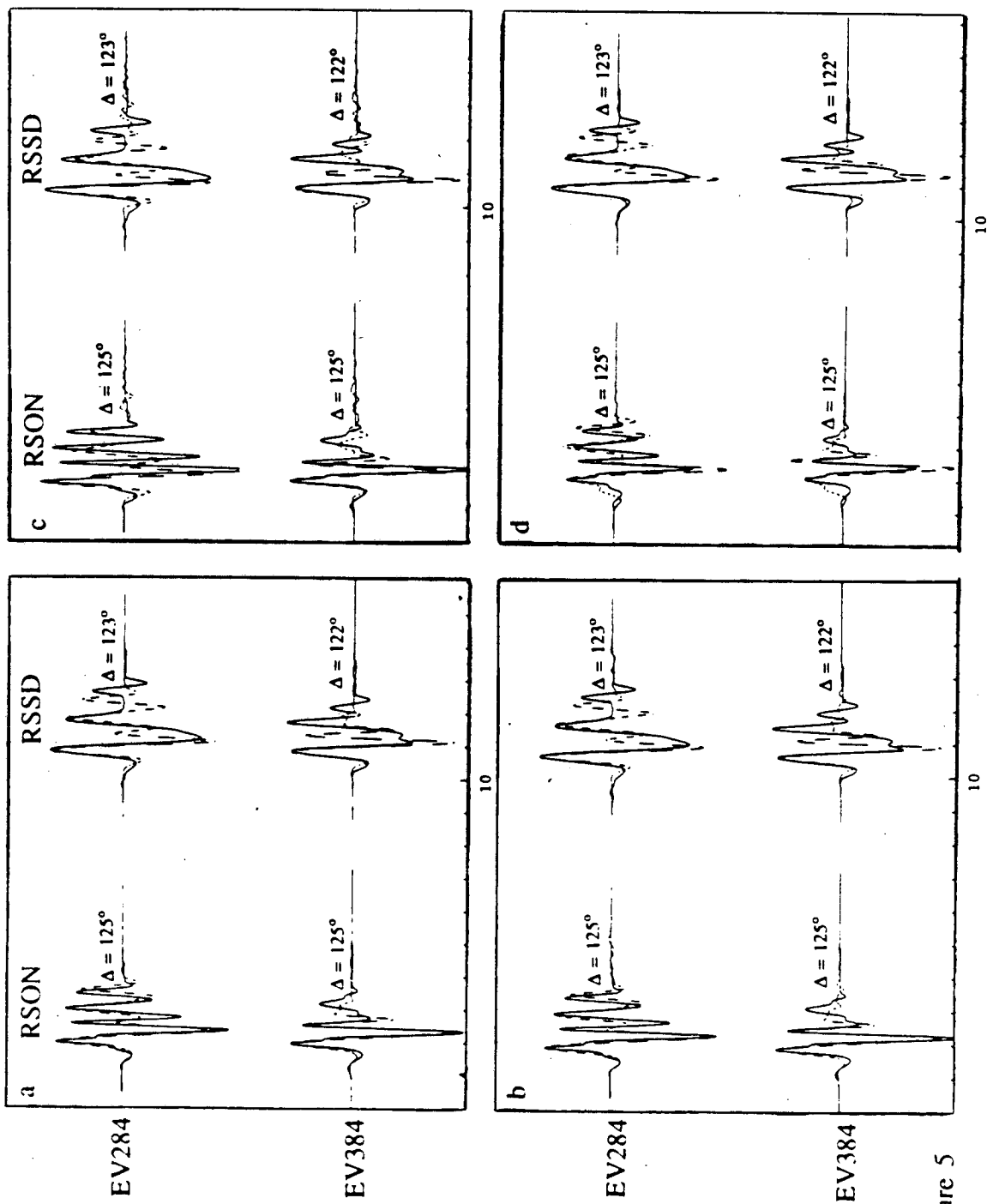


Figure 5

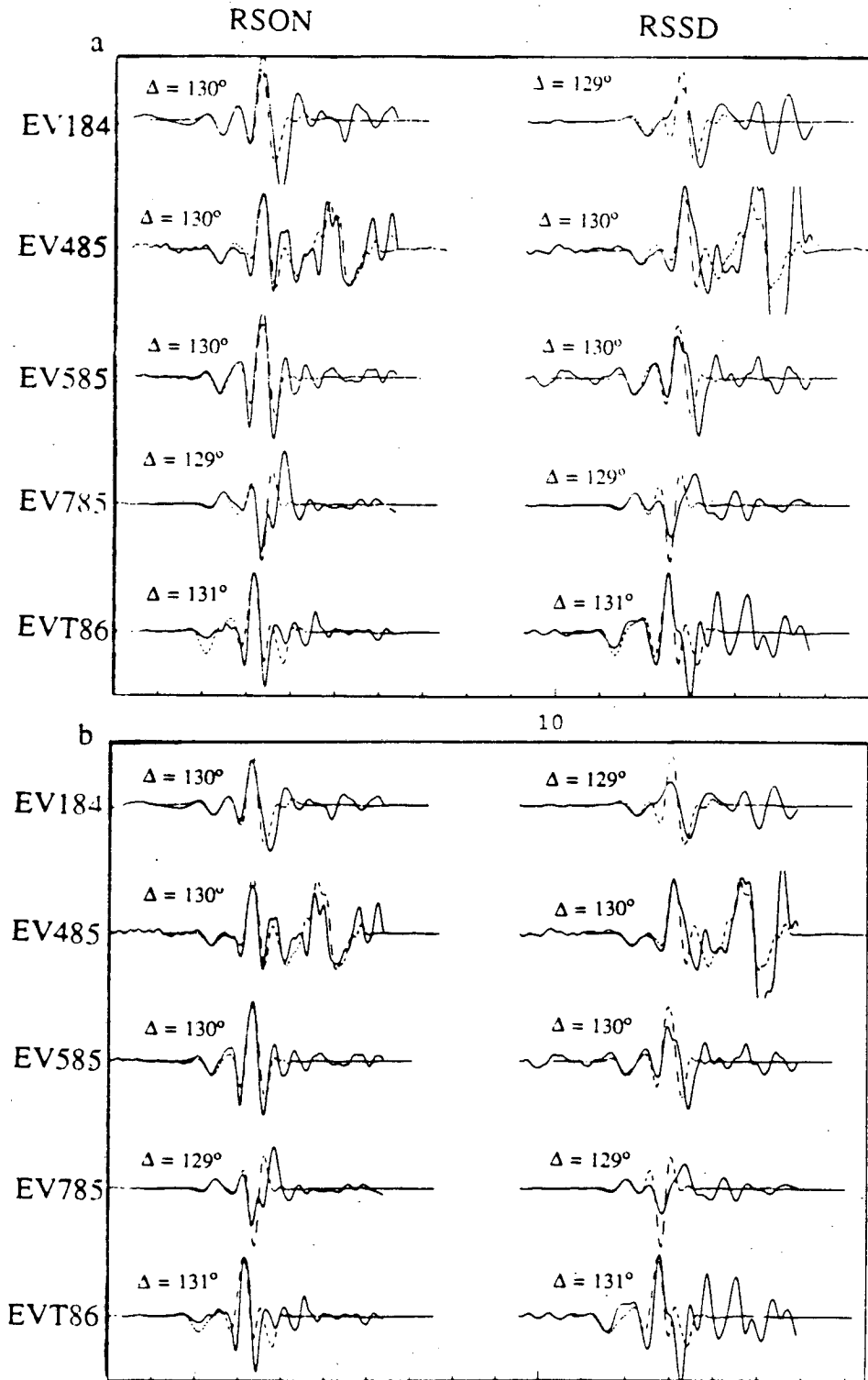


Figure 6

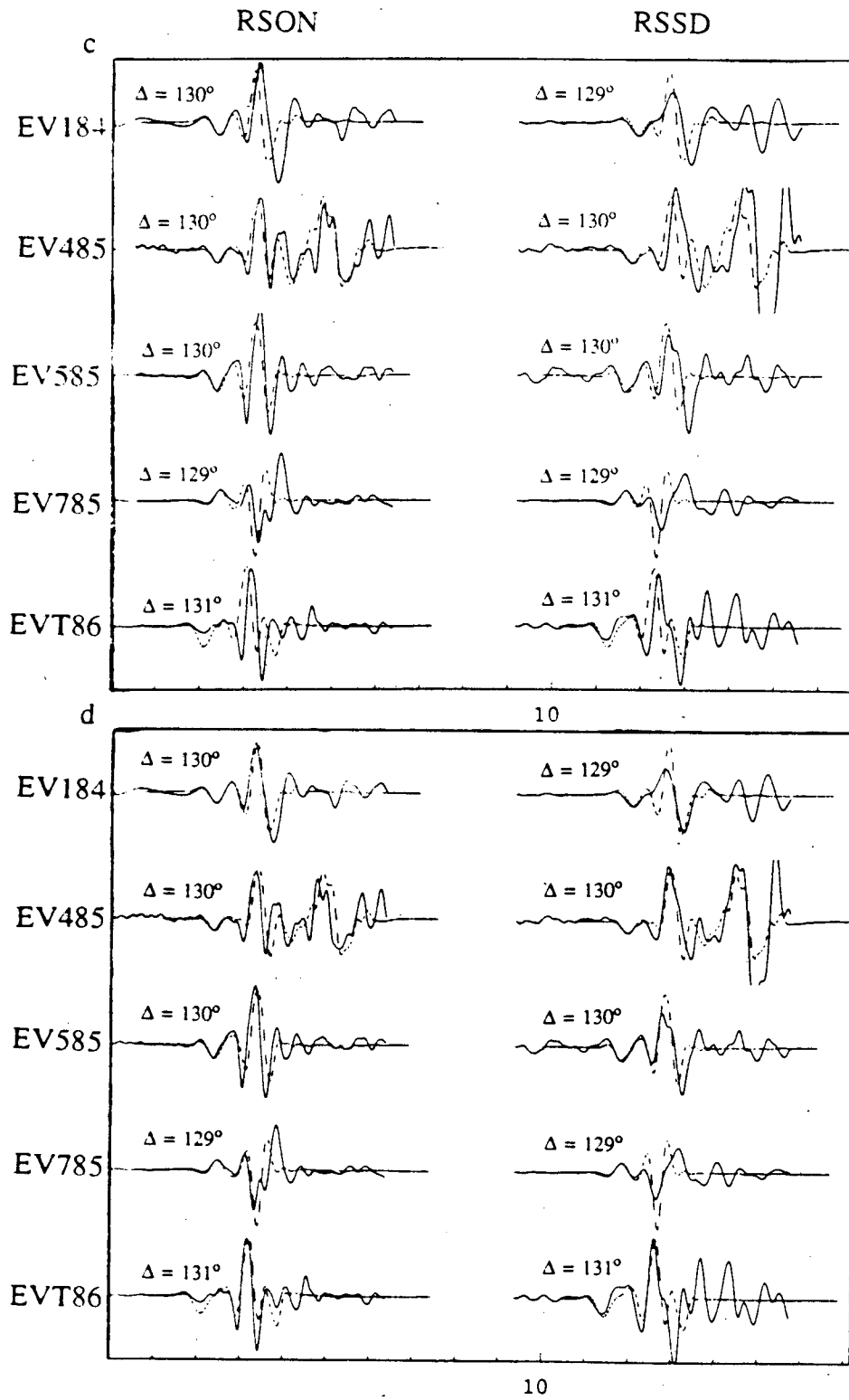


Figure 6

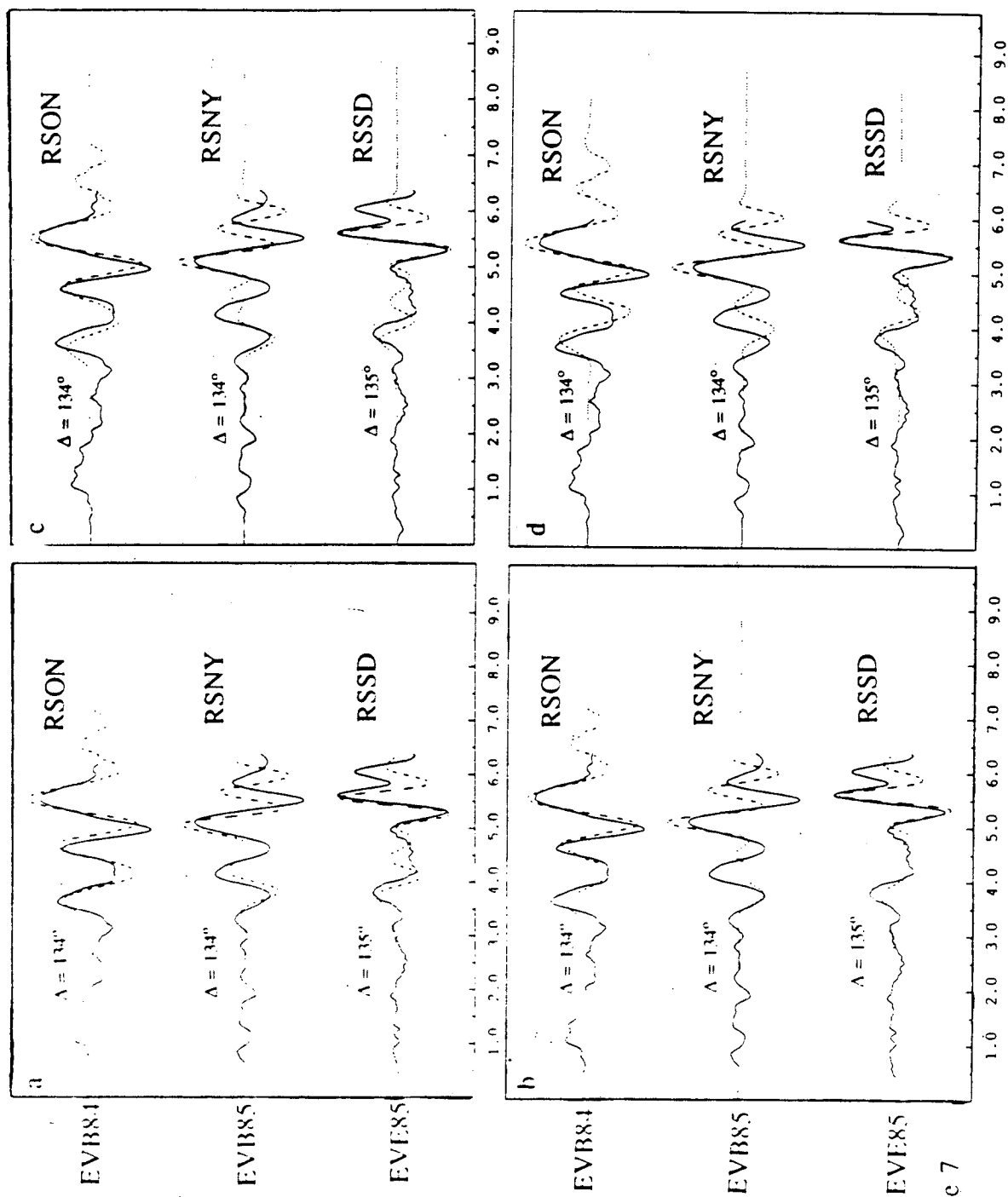


Figure 7

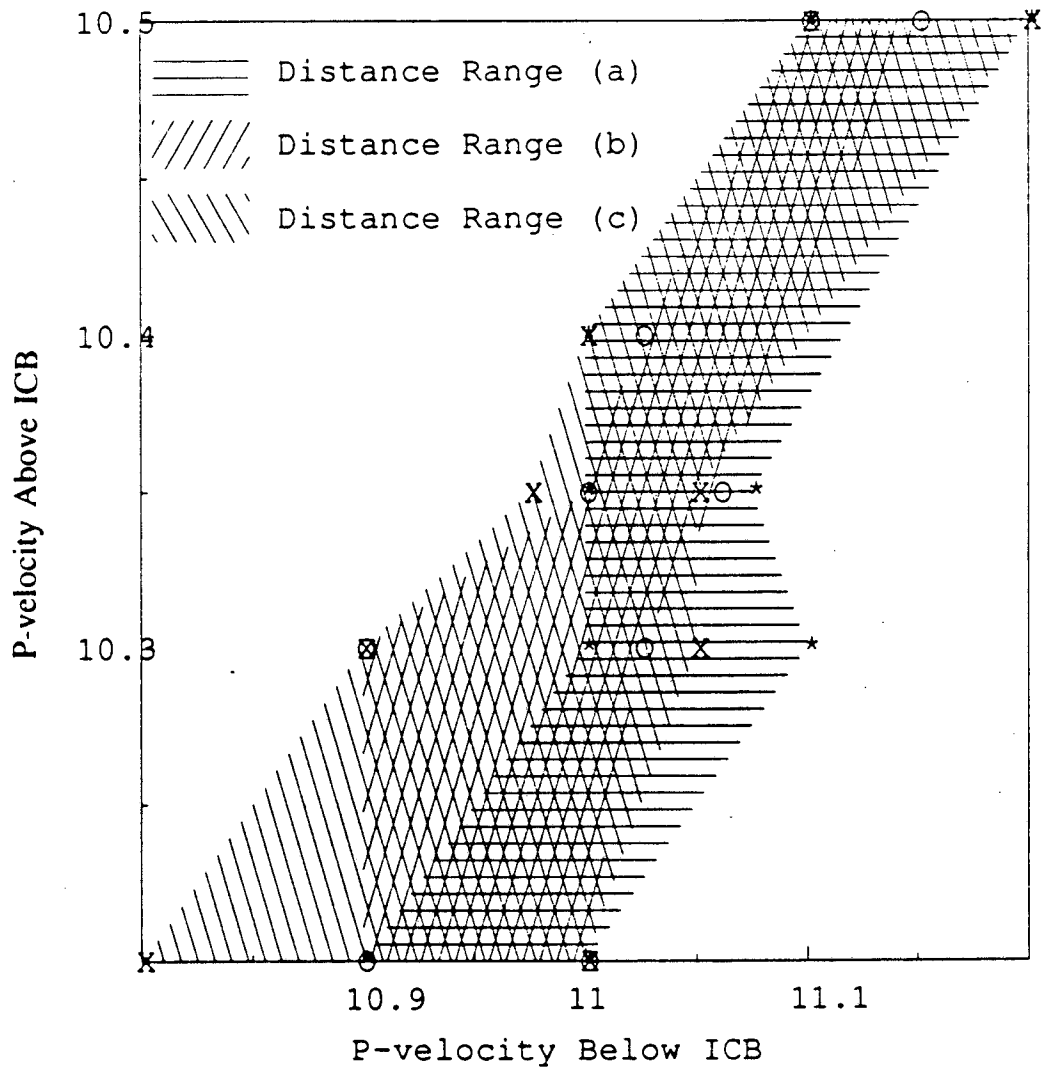


Figure 8

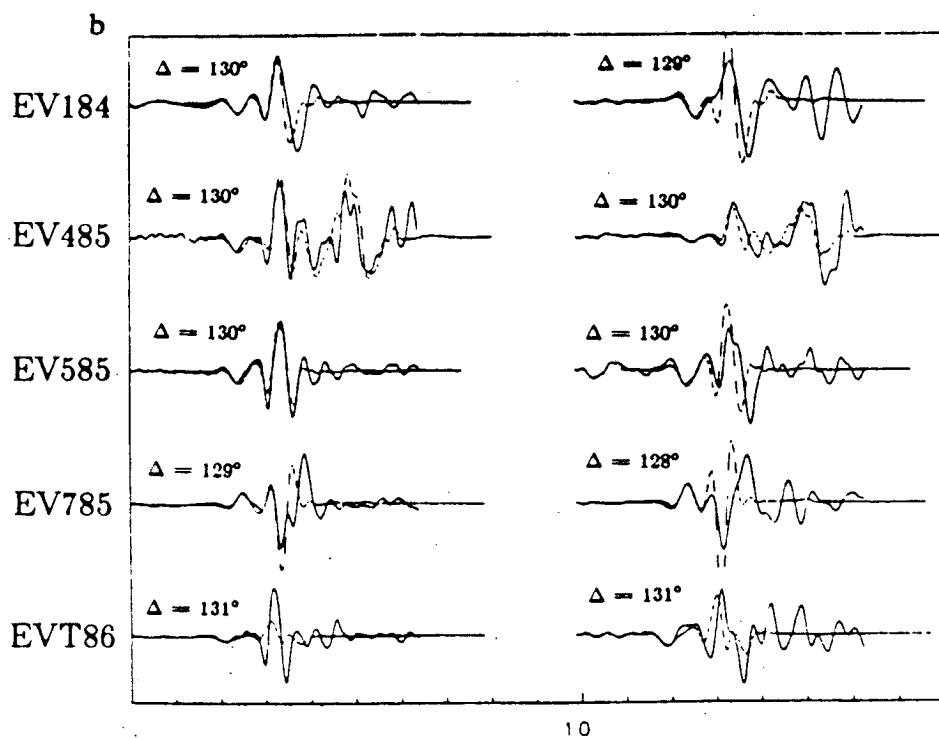
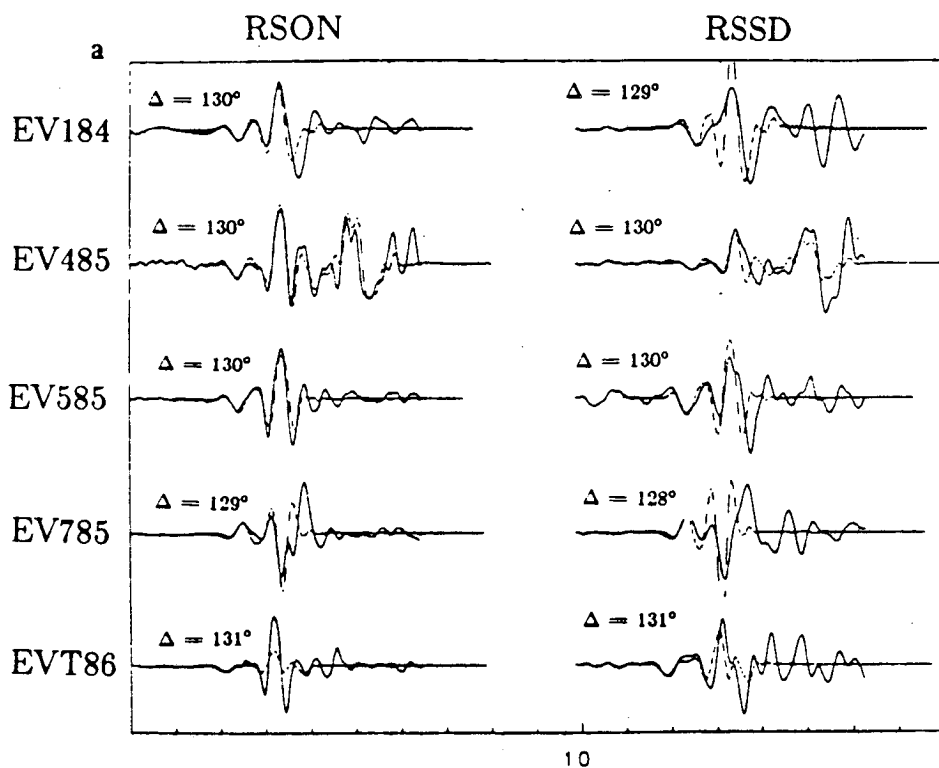


Figure 9

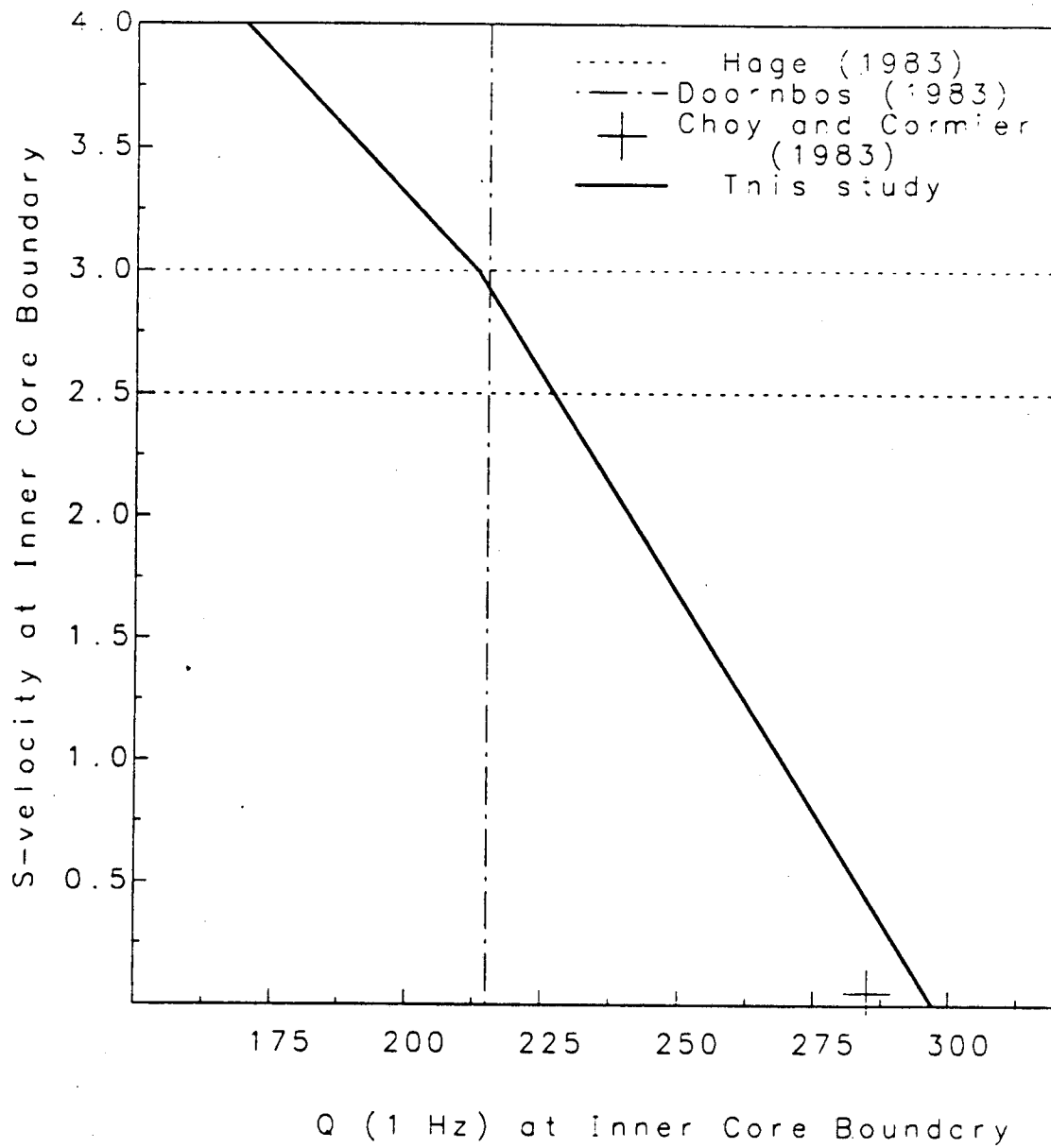


Figure 10

Chapter 4: Conclusions

Most of the conclusions reached in the preceding chapters have been described at length at the end of each chapter, and they will only be summarized here.

In Chapter 1 a hybrid combination of two different methods was developed to calculate short-period body wave seismograms for seismic waves sampling the Earth's deep interior. This represents a significant advance over past modeling studies, where the expense of the computational algorithms precluded the systematic treatment of a large number of Earth models. Also, the development of the hybrid method now makes it possible to take into account the interaction of short-period body waves with laterally homogeneous media of arbitrary complexity with a treatment that is complete in the sense that reverberation and coupling between P and SV motion is included. In the past the expense of such complete algorithms limited their use to long-period seismic waves.

The application of this method to the modeling of previously published data yielded some interesting results regarding the thickness of the inner core-outer core transition. First, it was verified that the observation of undistorted short-period reflections from the ICB at very small distances ($\approx 10^\circ$) constrains the inner core-outer core transition to be less than 5 km thick. While it was previously surmised that this transition must be thin with respect to 1 sec seismic waves, few seismologists had quantified this constraint due to the lack of an efficient modeling algorithm. The most interesting conclusion in Chapter 2, however, pertained to the sudden decrease in amplitude of the pre-critically reflected phase PKiKP in the distance range $70 - 90^\circ$. This is due to coupling of the incident P wave with shear motion in the inner core, and it was found in Chapter 2 that it is very easy to decouple this energy with an extended transition. Although no amplitude measurements are available for PKiKP phases in the distance range $70 - 90^\circ$, there is some evidence that the amplitudes decrease significantly, which would imply that the transition must be very sharp, perhaps no more than 1 or 2 km in thickness. Finally, it was established that the short-period waveform data recorded at epicentral distances of $100 - 140^\circ$ to be used in Chapter 3 were not sensitive to transition thicknesses of

less than 10 km, so that treating the ICB as a simple discontinuity was appropriate.

Application of the technique developed in Chapter 2 to the modeling of some of the best quality short-period waveform data available for this study was undertaken in Chapter 3. The technique facilitated the systematic study of a large number of Earth models as asymptotic calculations for structure outside of the inner core-outer core transition zone were computed only once, and were then combined with a large number of the more complete reflectivity calculations for different models of the transition zone itself. Thus, it was possible to systematically vary 4 parameters describing the transition: the P-velocity above the ICB (α_o), and the P-velocity (α_i), S-velocity (β_i), and attenuation Q_α below the ICB. It was found that by separately considering relative travel times and relative amplitudes it was possible to separate the effects of perturbations of α_o and α_i from those of β_i and Q_α . Further separation of the parameter space was not possible, however, with the result that the data define trade-off regions of the (α_i , α_o) and (β_i , Q_α) parts of the model space that result in synthetics which fit the data. The trade-off region for the (α_i , α_o) part of the model space was particularly well determined by the data, so that e.g., with a P-velocity structure above the ICB given by PREM, the P-velocity below the ICB is $11.03 \pm .03$ km/s. The results of Chapter 2 are consistent with several previous studies, although they are in definite disagreement with one recent study. One explanation offered for this discrepancy is that there may be some degree of lateral heterogeneity in the Earth's core.

There are several geophysical implications of this study. The result in Chapter 2 that the low Q_α in the inner core is due to an absorption band on the high frequency side of the short-period seismic band is not consistent with absorption due to viscous relaxation of a high viscosity fluid. This would require that the relaxed moduli be characteristic of a fluid, and it is clear that the inner core is rigid for body wave frequencies. On the other hand, if the absorption is due to thermal and material diffusion in a fluid-solid mixture at the top of the inner core then the scale length of fluid inclusions would have to be .1 cm or smaller, so that the mixing would not be a large scale phenomenon. At this point it seems worthwhile to point out that these are both bulk mechanisms, neither of which seem likely to dominate the

short-period attenuation in the inner core, as the absence of observations of PKJKP indicate that a substantial part of the attenuation must be due to a shear mechanism.

The trade-off involving the P-velocities above and below the ICB imply that there is some nonuniqueness in any geophysical interpretation. The trade-off curve in Figure 8 of Chapter 3 does indicate, however, that any transitional character in the material properties near the ICB must be manifest both above and below the ICB: if there is a transitional zone of low velocity and strong velocity gradient at the top of the inner core, then there must also be a zone of low velocity and weak velocity gradient above the ICB. Thus, while this study has not independently determined whether or not such transition zones exist, it does make it possible to use the results of other studies indicating the absence of a transition zone at the base of the outer core to argue that there is no transition zone of high velocity gradients below the ICB.

The results of this study suggest several future avenues of research. A procedure similar to that used here may be applicable to the analysis of core phases recorded at other distance ranges, so that the trade-off regions in Figures 8 and 10 in Chapter 3 may be better constrained. Other regions of the Earth may be amenable to this type of analysis, such as D'' at the base of the mantle, although the lateral heterogeneity that may exist in the mantle could make such a procedure difficult. Perhaps the most interesting approach suggested by this study is that of constraining the amplitude-distance curve for pre-critically reflected PKiKP. In particular, observation of the phase reversal predicted by the PREM model at $\approx 80^\circ$ would provide a lower bound on the S-velocity of the inner core.

The fact that some of the elastic and the anelastic material properties below the ICB are fairly well constrained may make it possible to exclude some phenomenological models for the observed attenuation. For example, the frequency dependence and magnitude of Q_α observed in this study constitute enough information, if ascribed to thermal and material diffusion in small fluid inclusions, to estimate the size and volume concentration of the inclusions. It is then a straightforward procedure to calculate the bulk and shear moduli for such a heterogeneous medium using the formulation of Isakovitch (1938, see Appendix C). If such

a calculation results in a predicted P velocity that is inconsistent with the results presented here, then this model could be excluded from consideration as a likely mechanism for the observed seismic wave attenuation. A similar treatment may be possible for other attenuation mechanisms that have been proposed for the inner core, such as fluid-filled cracks and order parameter relaxation.

Finally, it should be noted that all of the results of this study are consistent with an inner core boundary that is a simple, sharp boundary between two very smoothly varying media. While some of the phenomenological models for the inner-core outer core transition consisting of a convoluted mixture of fluid and solid or a 'glassy-type' transition from a low-viscosity to a high-viscosity fluid are not completely ruled out by this study, they are far from being the simplest models that explain the seismic data.

Appendix A: (β_i , Q_α) Waveform Comparisons for Distance Range (b)

The following figures illustrate comparisons of observed (solid traces) and synthetic (dashed traces) waveforms for distance range (b), $128 - 132^\circ$, for perturbations of the S-velocity β_i and attenuation Q_α at the top of the inner core from their respective PREM values. Each figure corresponds to a pair of parameter values (β_i , Q_α) according to the following scheme:

Figure no.	a	b
Figure 1	(175, 4.)	(150, 4.)
Figure 2	(125, 4.)	(100, 4.)
Figure 3	(175, 3.)	(150, 3.)
Figure 4	(125, 3.)	(100, 3.)
Figure 5	(175, 2.)	(150, 2.)
Figure 6	(125, 2.)	(100, 2.)
Figure 7	(175, 1.)	(150, 1.)
Figure 8	(125, 1.)	(100, 1.)
Figure 9	(175, 0.)	(150, 0.)
Figure 10	(125, 0.)	(100, 0.)

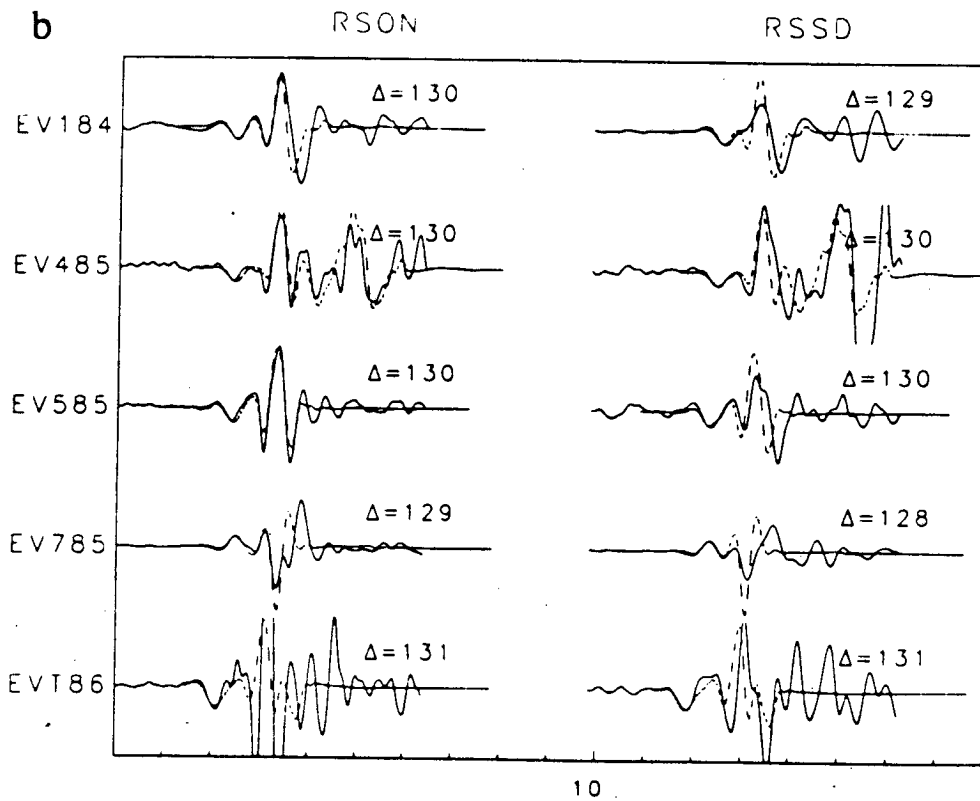
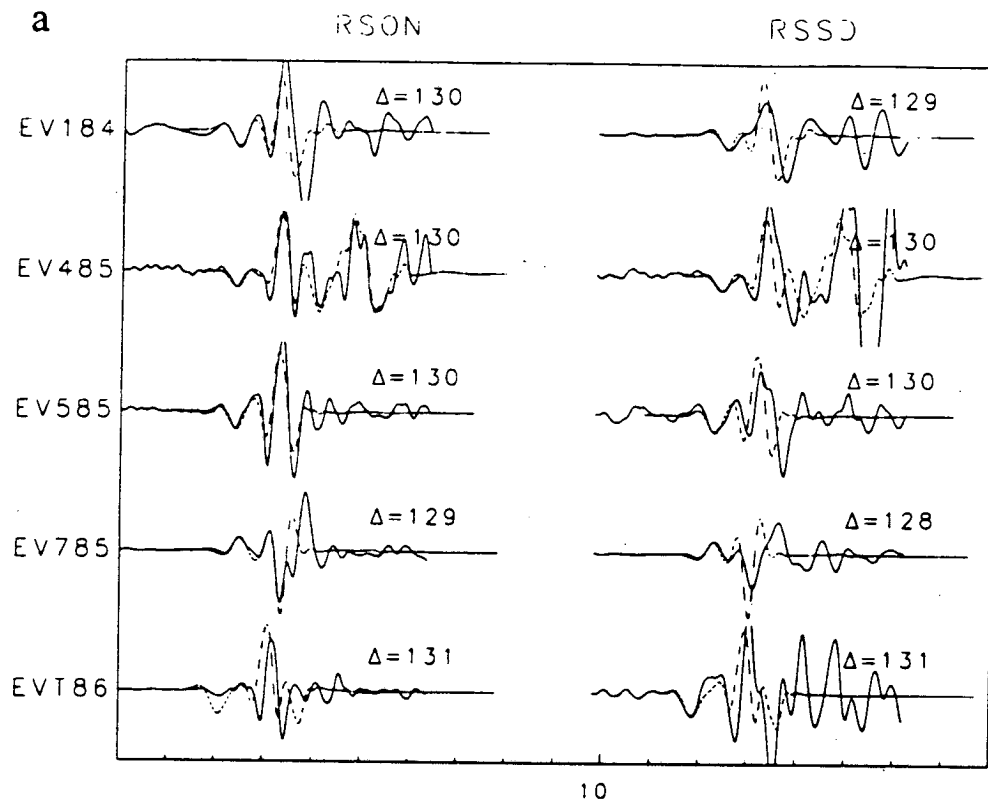


Figure 2

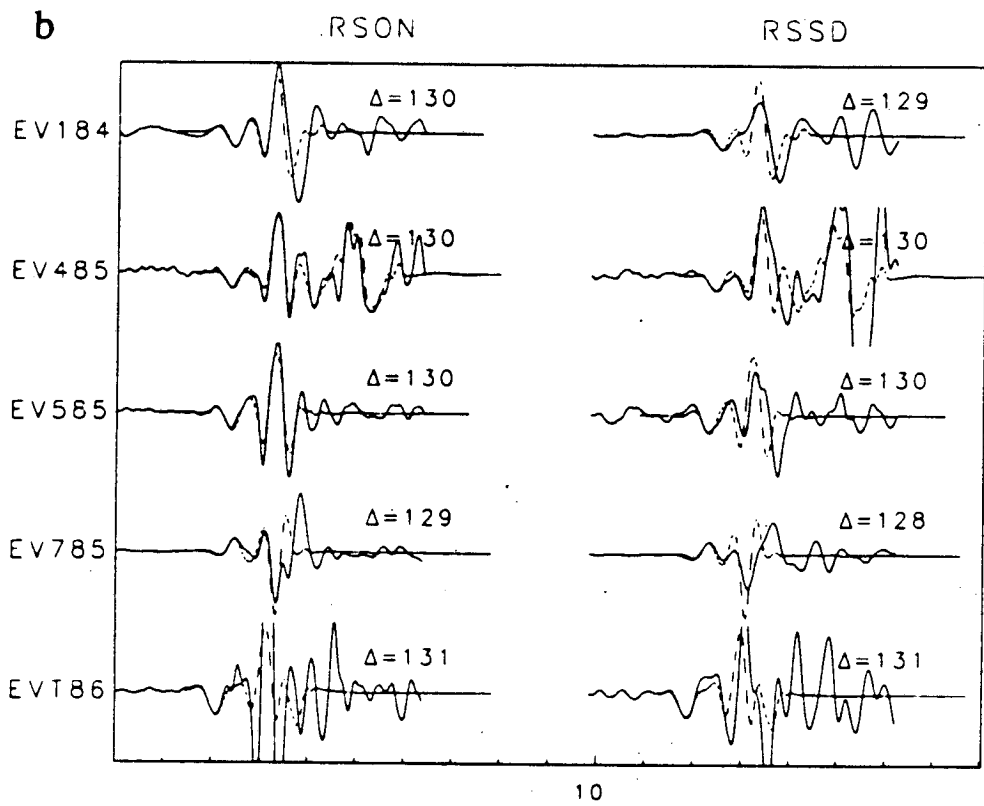
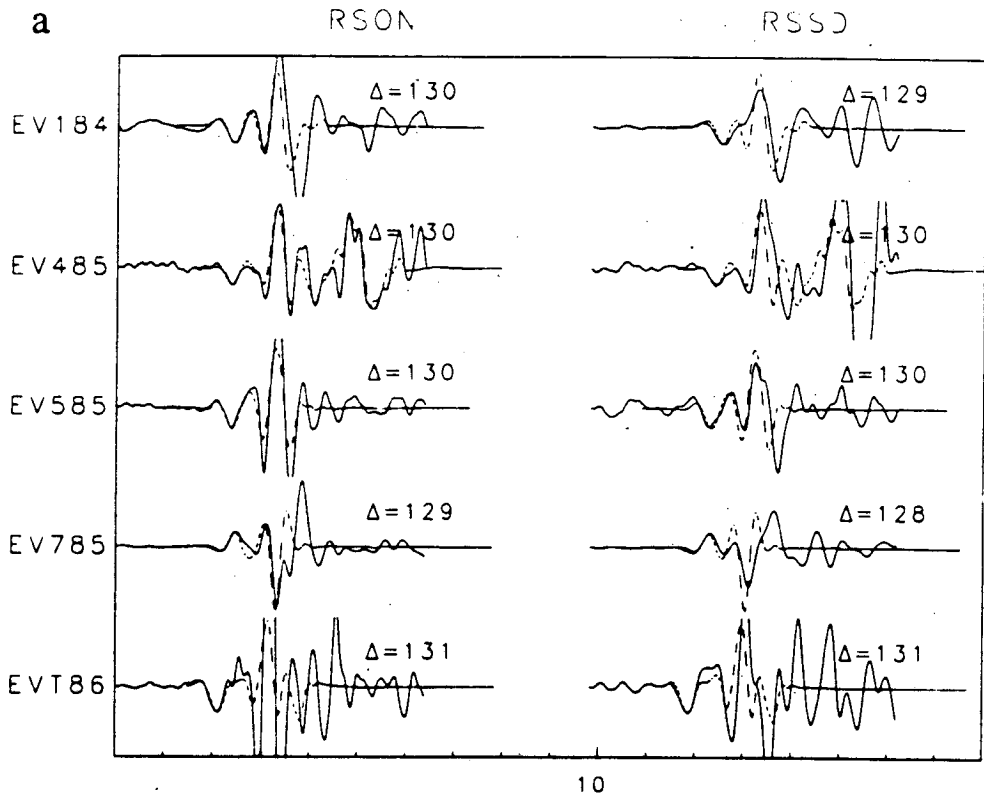


Figure 3

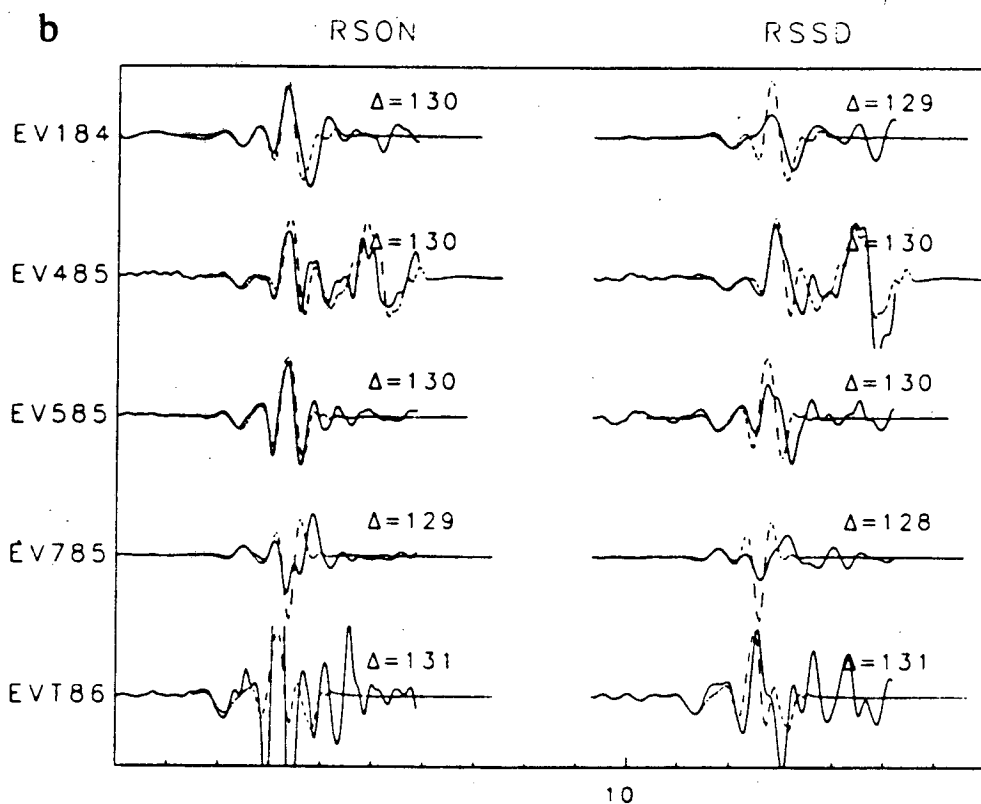
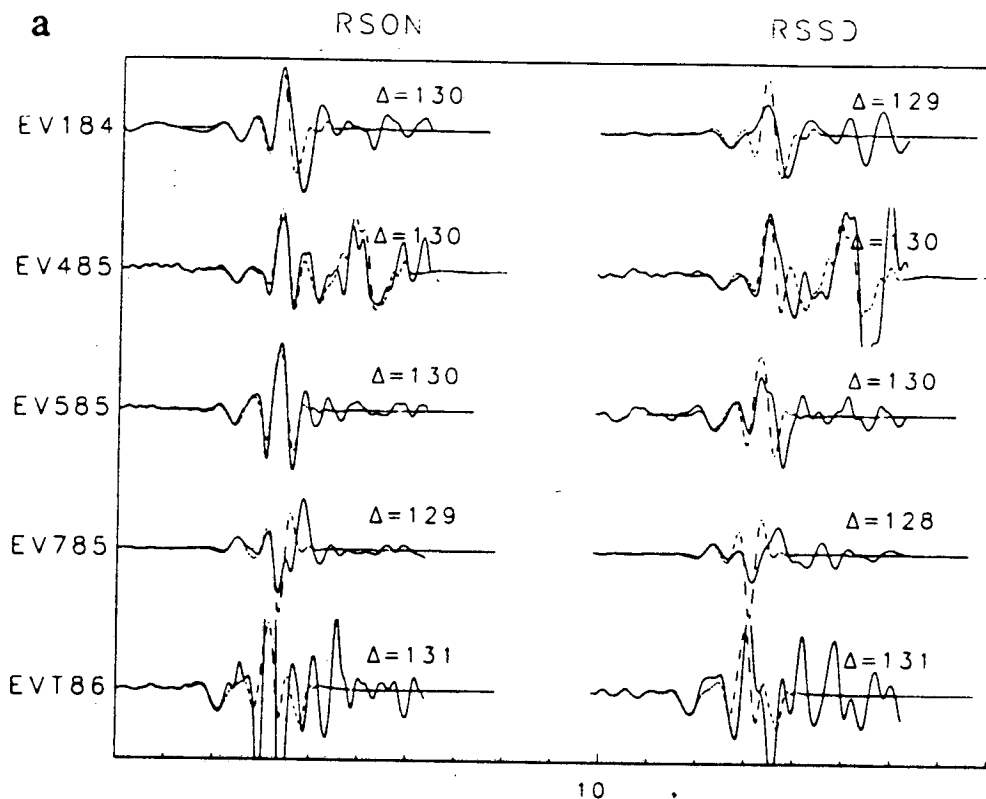


Figure 4

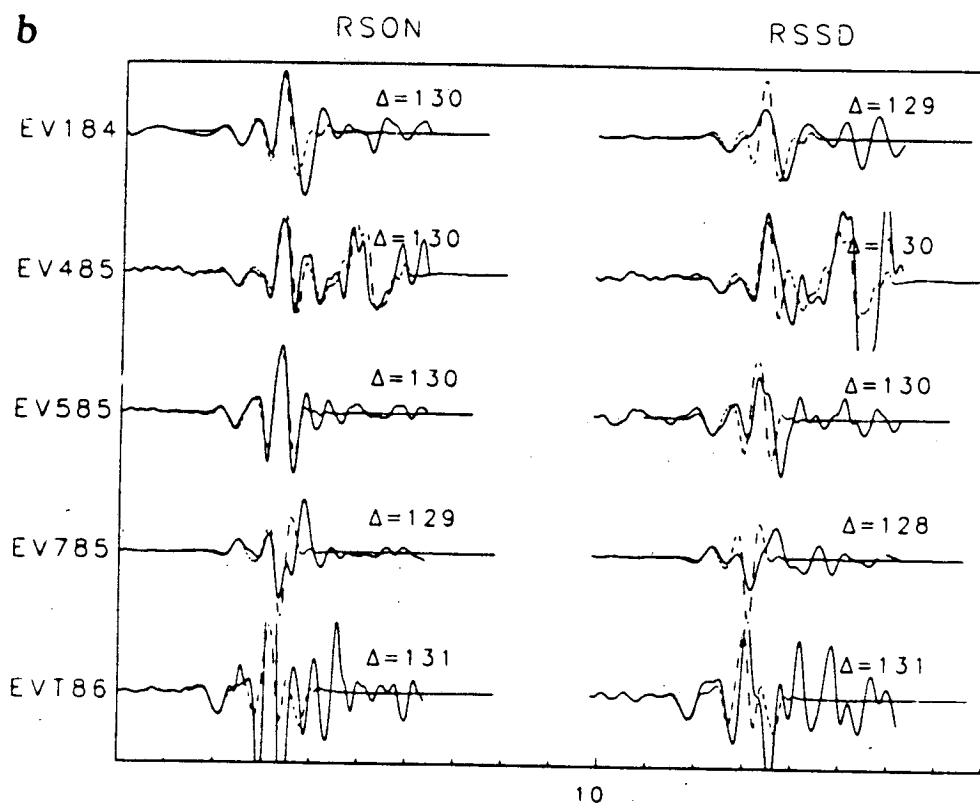
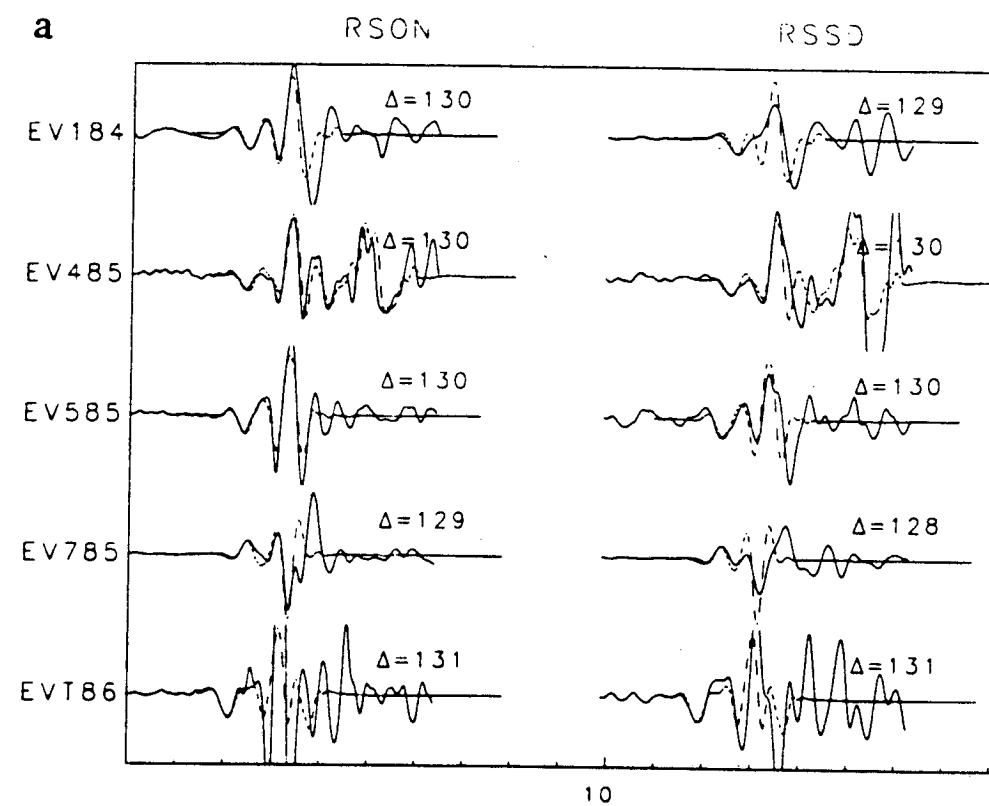


Figure 5

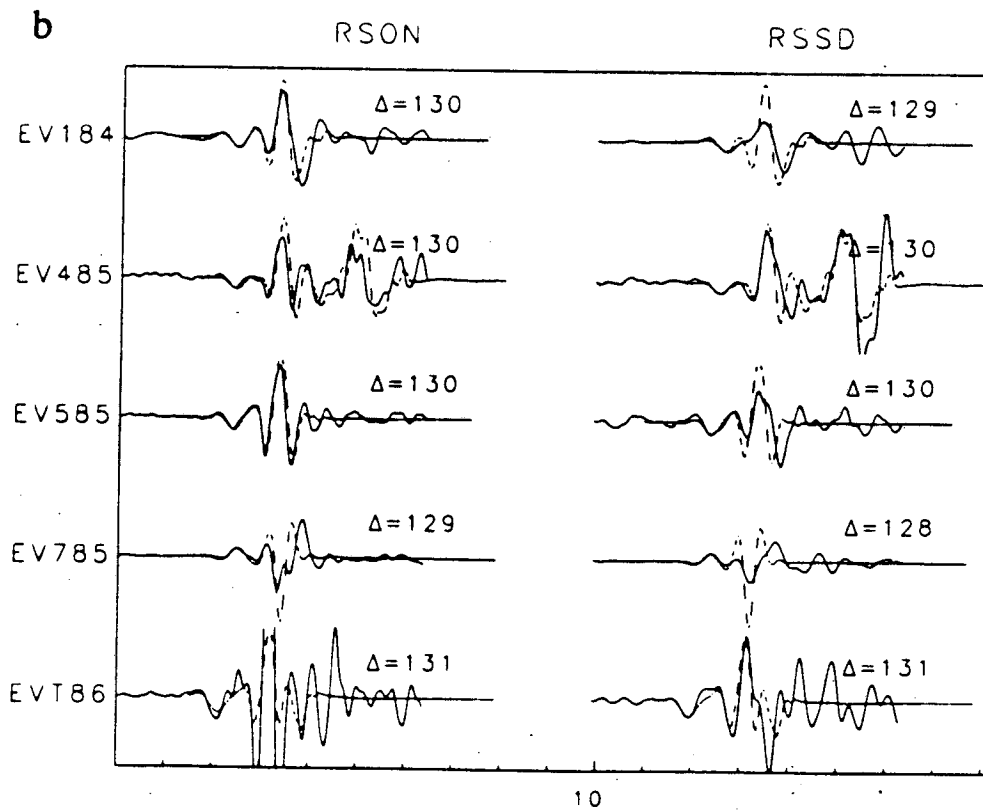
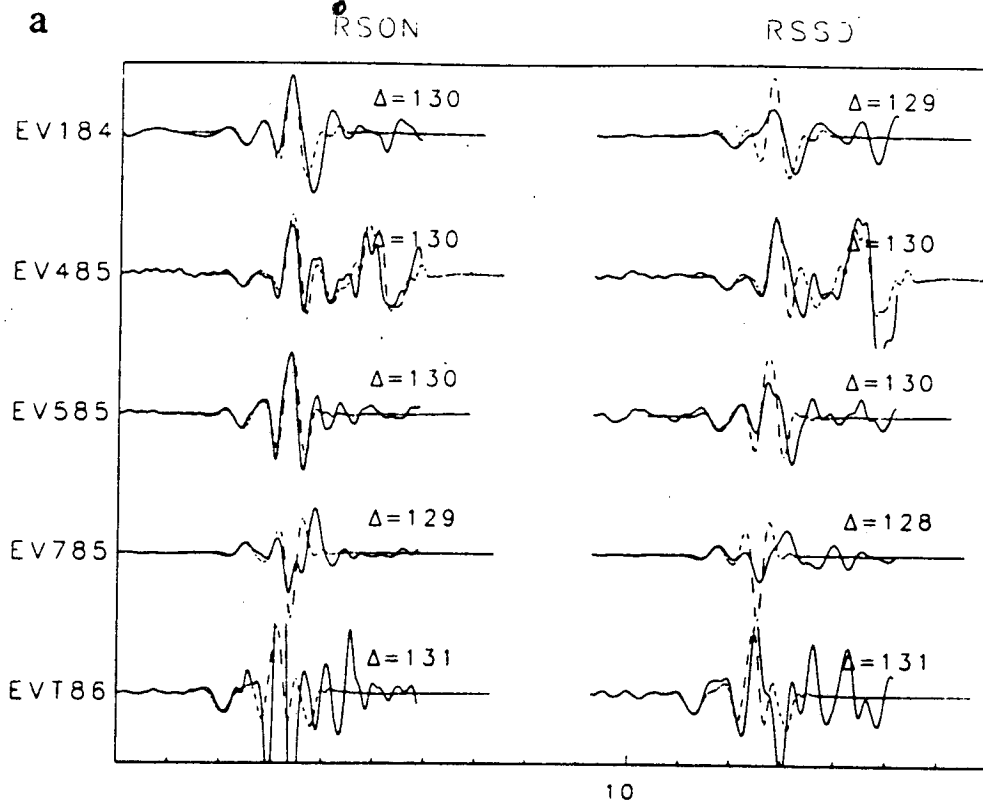


Figure 6

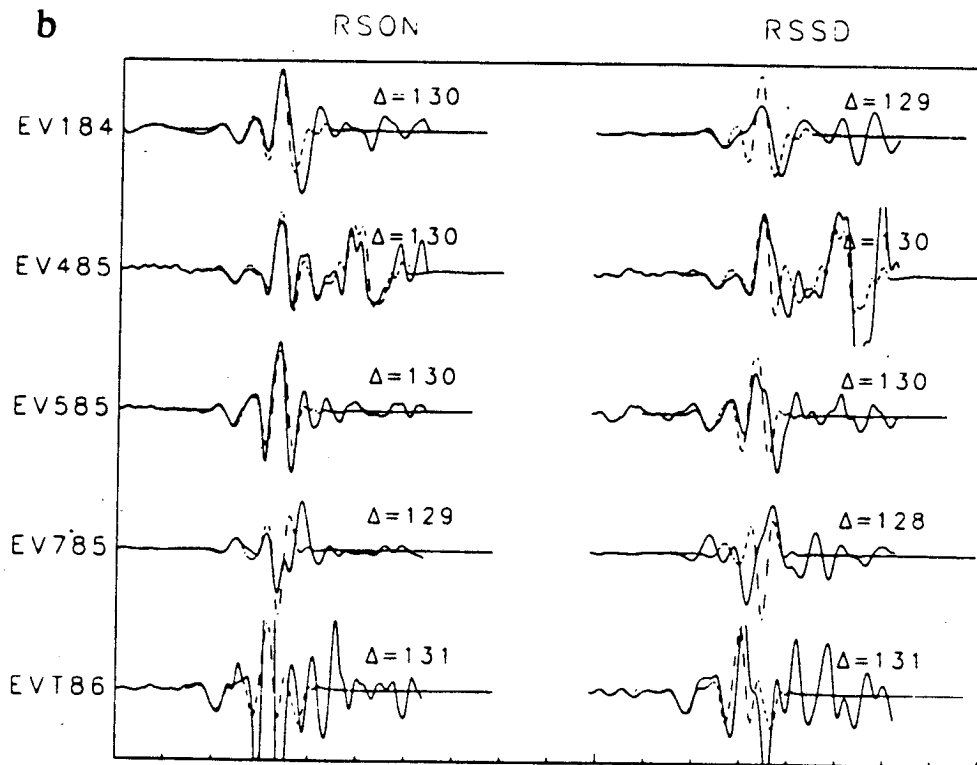
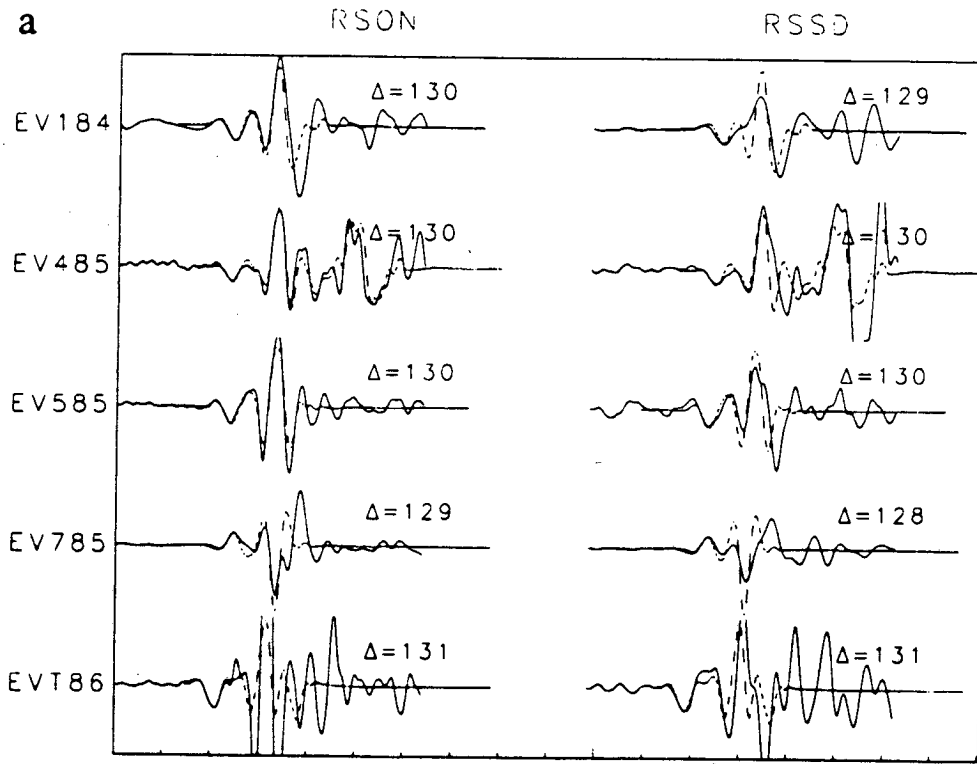


Figure 7

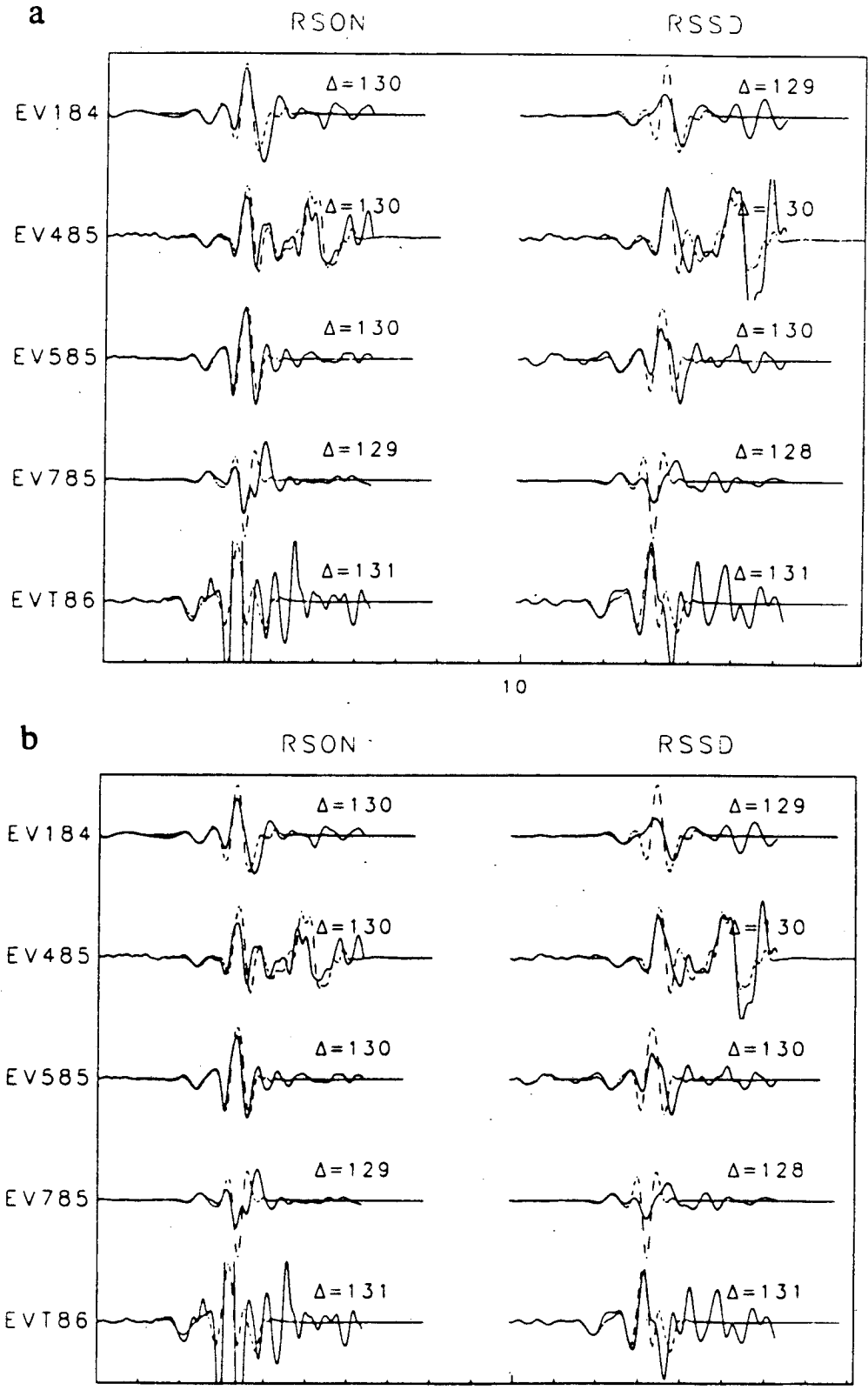


Figure 8

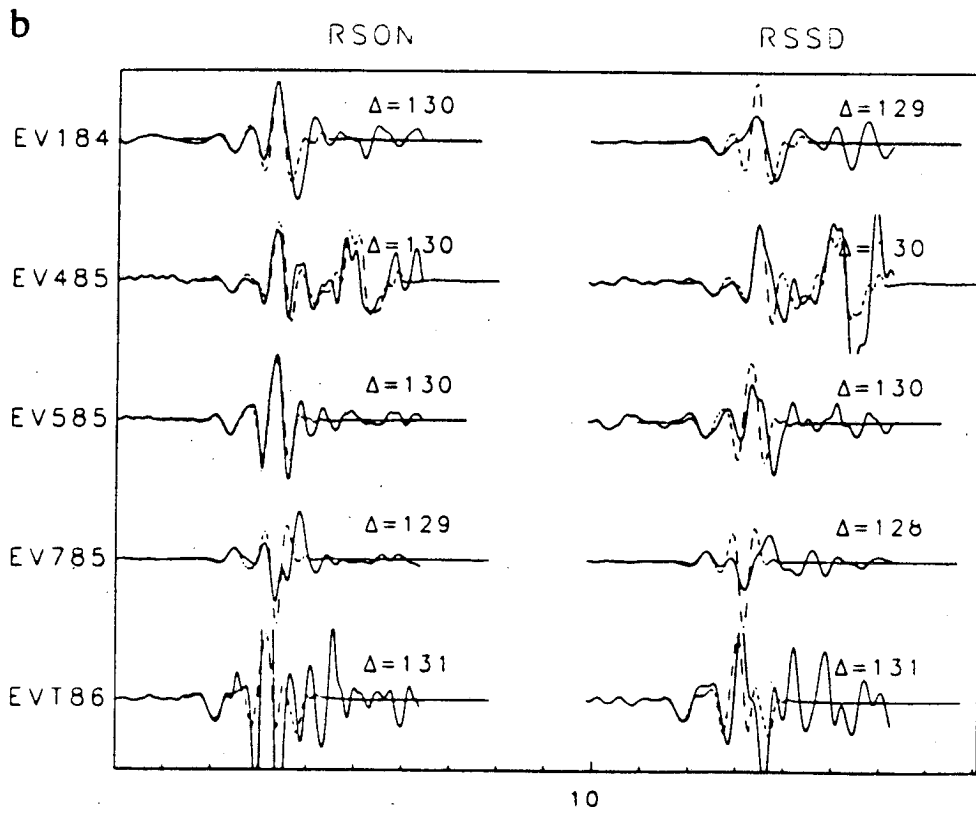
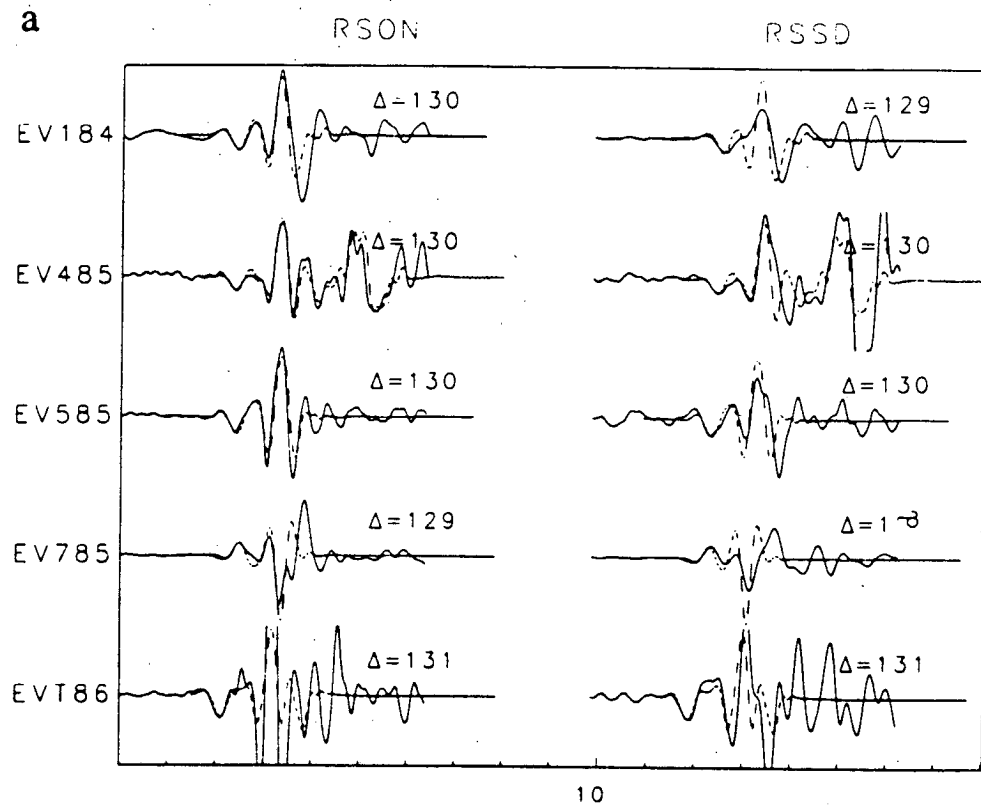
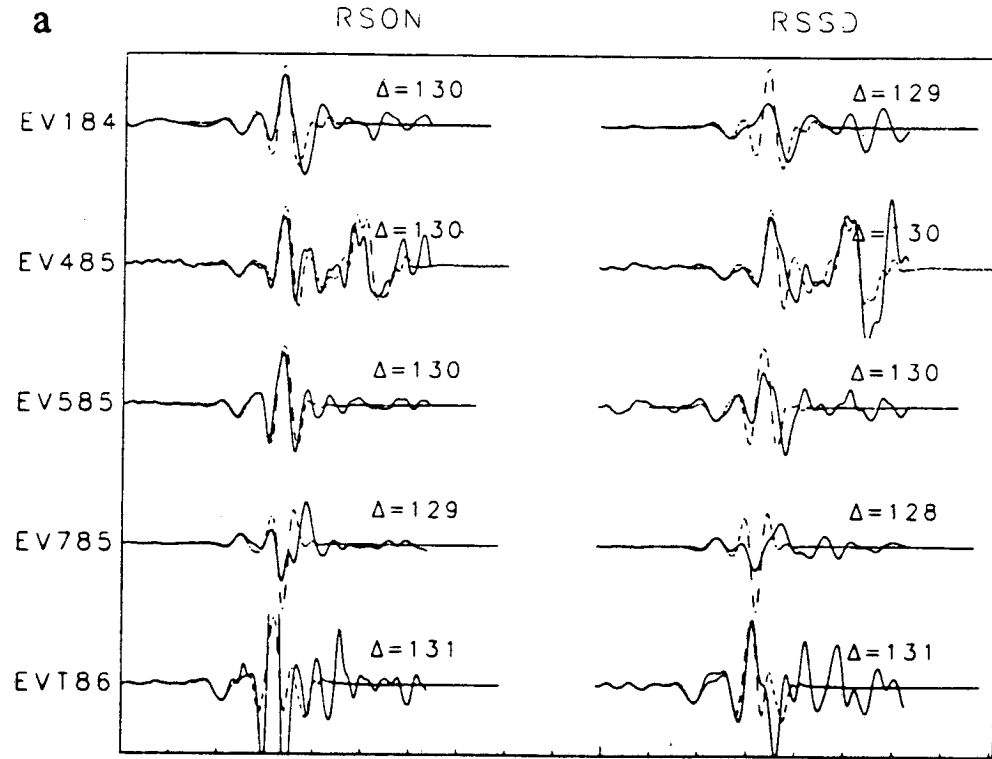
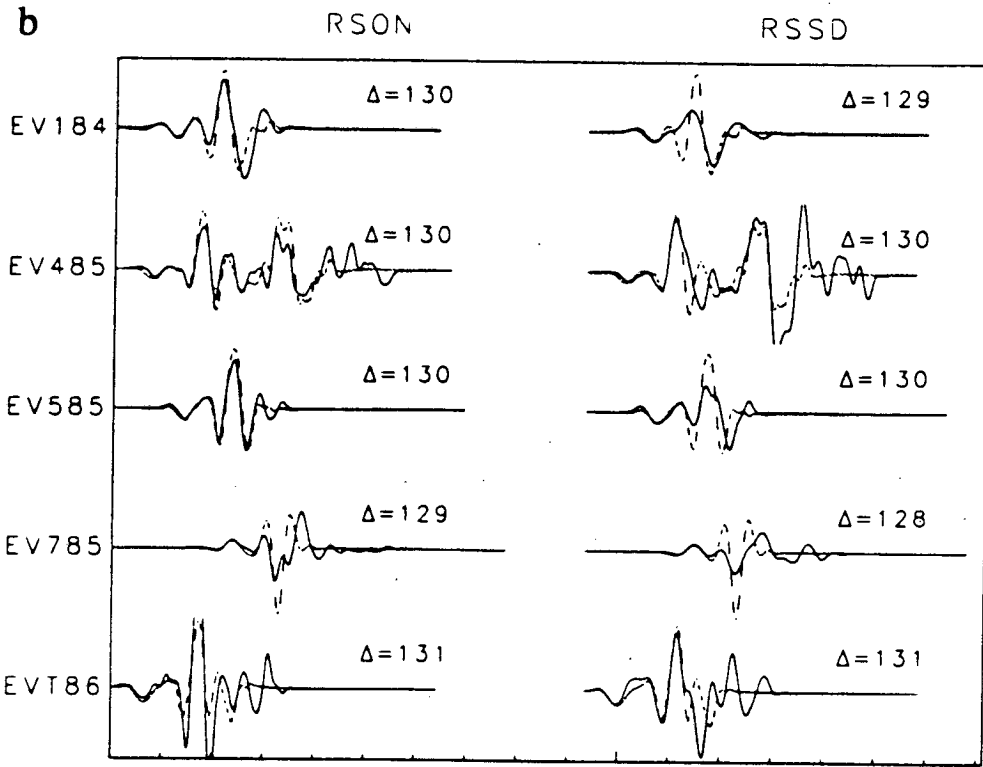


Figure 9



10



10

Figure 10

Appendix B: (α_i , α_o) Waveform Comparisons for Distance Range (b)

The following figures illustrate comparisons of observed (solid traces) and synthetic (dashed traces) waveforms for distance range (b), 128 – 132°, for perturbations of the P-velocities below α_i and above α_o the inner core boundary from their respective PREM values. Each figure corresponds to a pair of parameter values (α_i , α_o) according to the following scheme:

Figure no.	a	b
Figure 1	(11.150 , 10.50)	(11.100 , 10.50)
Figure 2	(11.125 , 10.45)	(11.075 , 10.45)
Figure 3	(11.100 , 10.40)	(11.025 , 10.40)
Figure 4	(11.060 , 10.35)	(11.000 , 10.35)
Figure 5	(11.025 , 10.30)	(10.975 , 10.30)
Figure 6	(11.000 , 10.25)	(10.925 , 10.25)
Figure 7	(10.975 , 10.20)	(10.925 , 10.20)

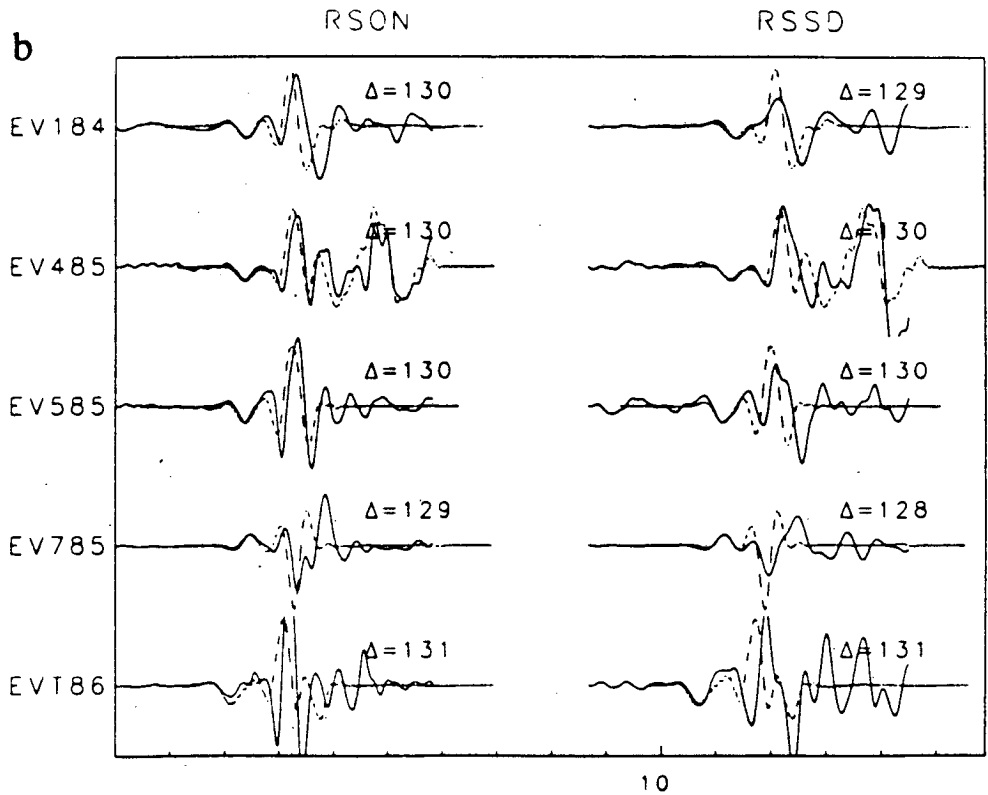
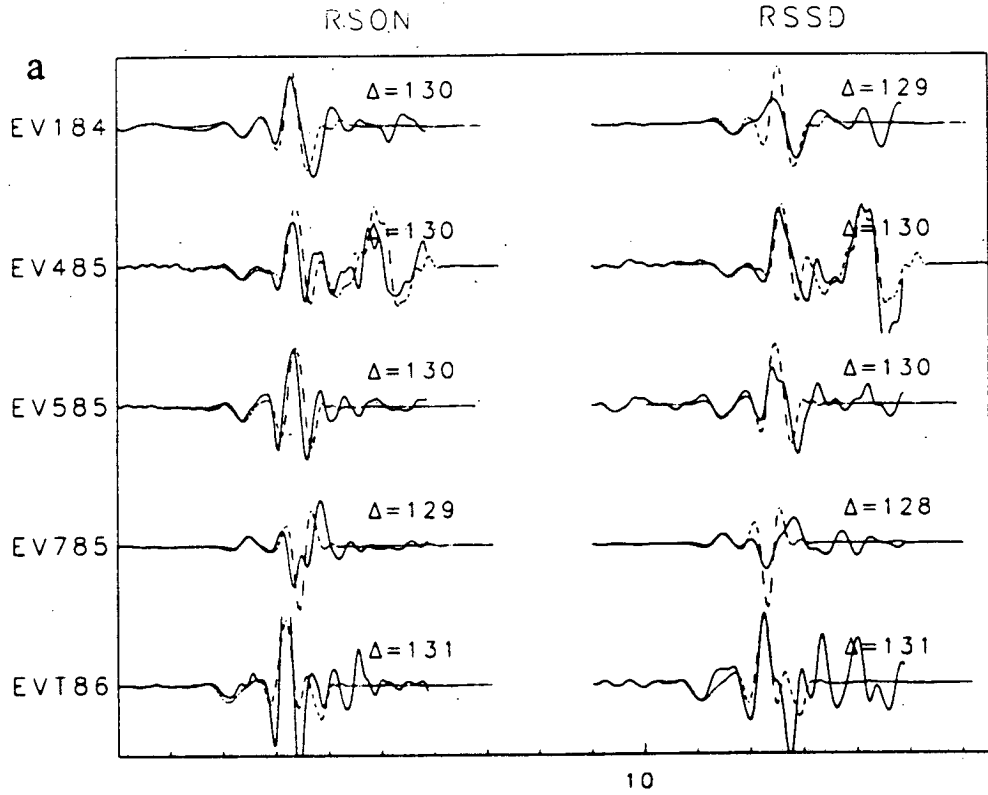


Figure 1

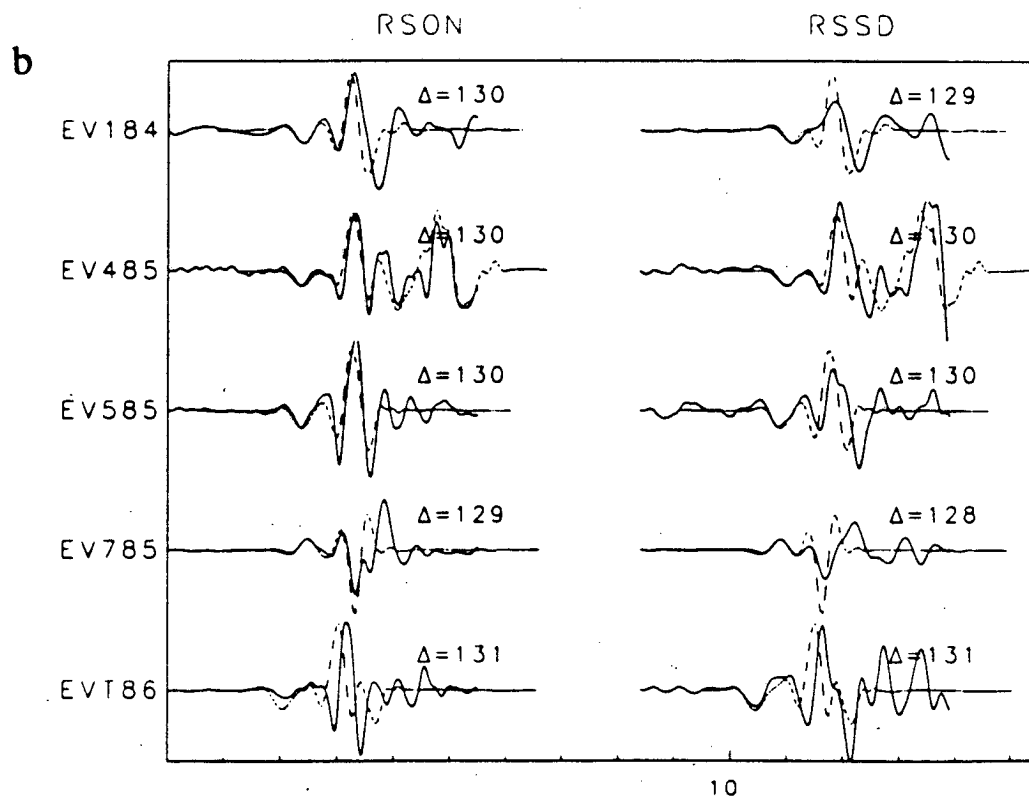
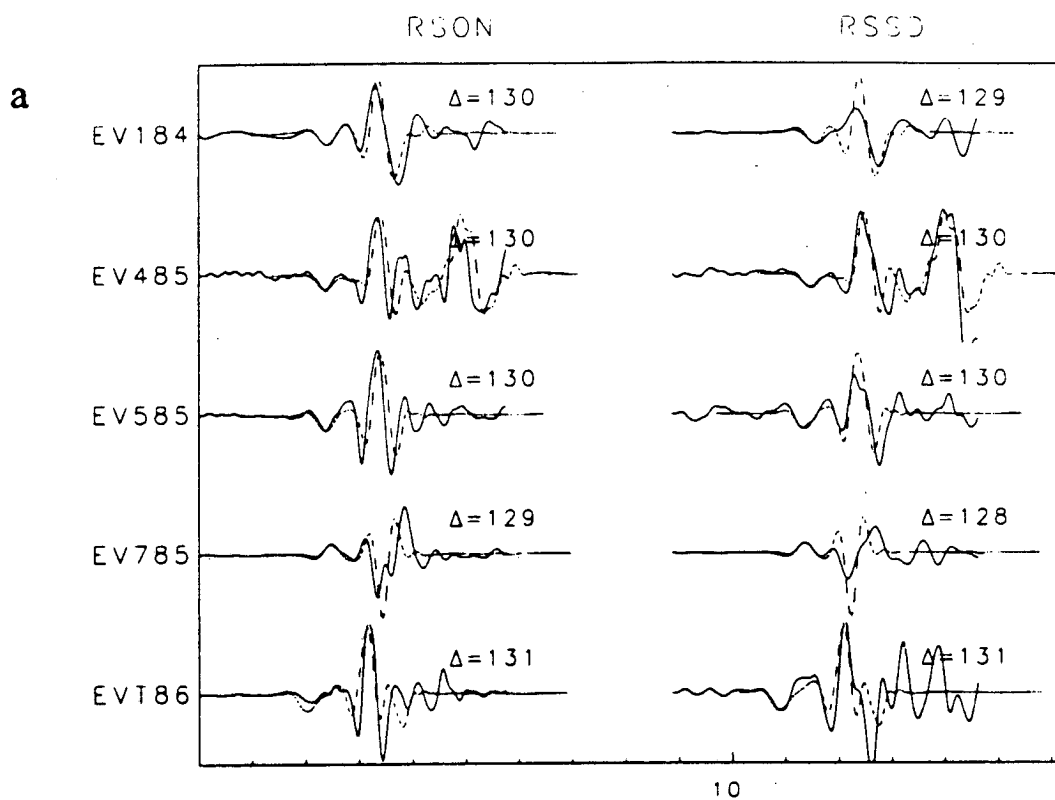


Figure 2

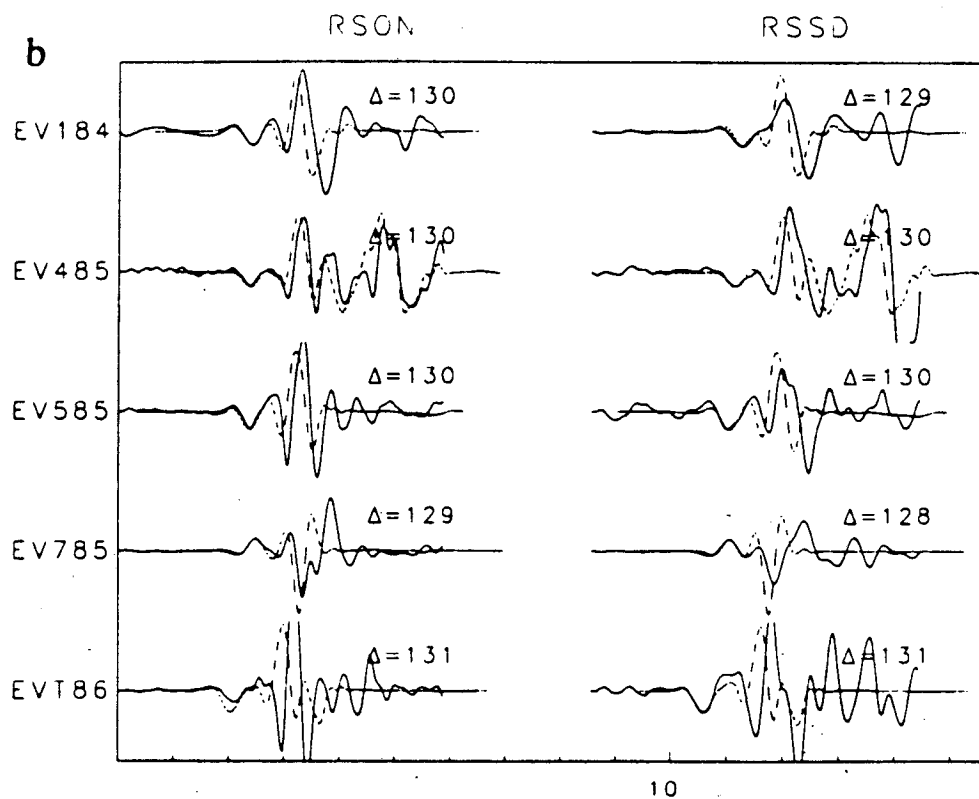
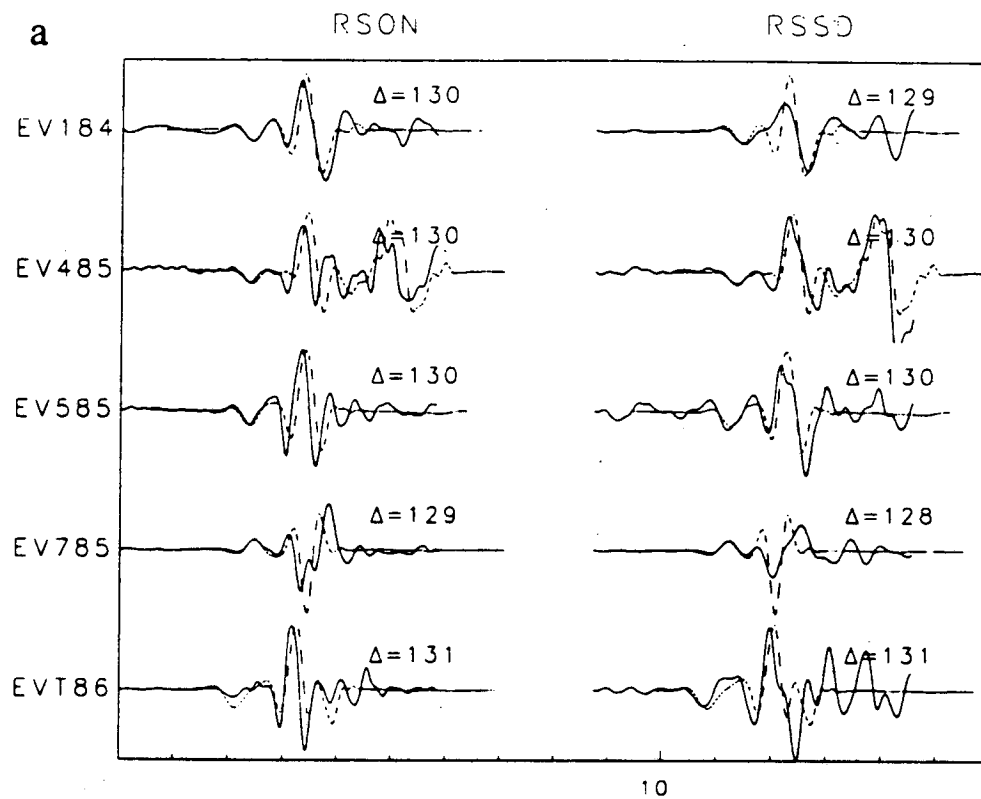


Figure 3

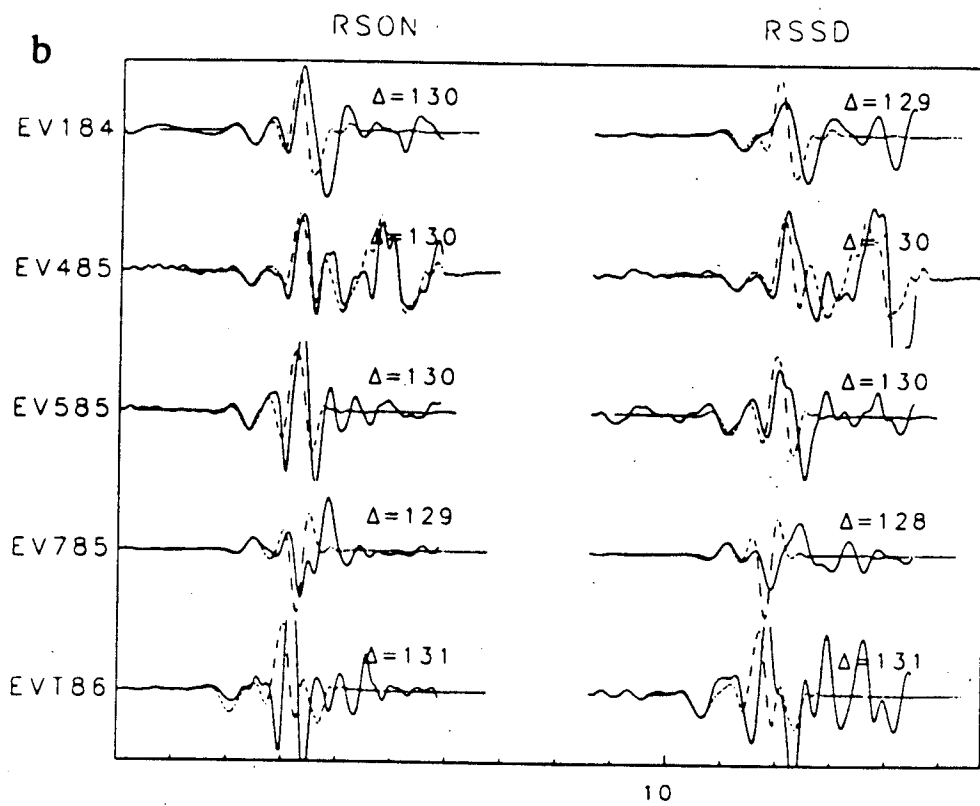
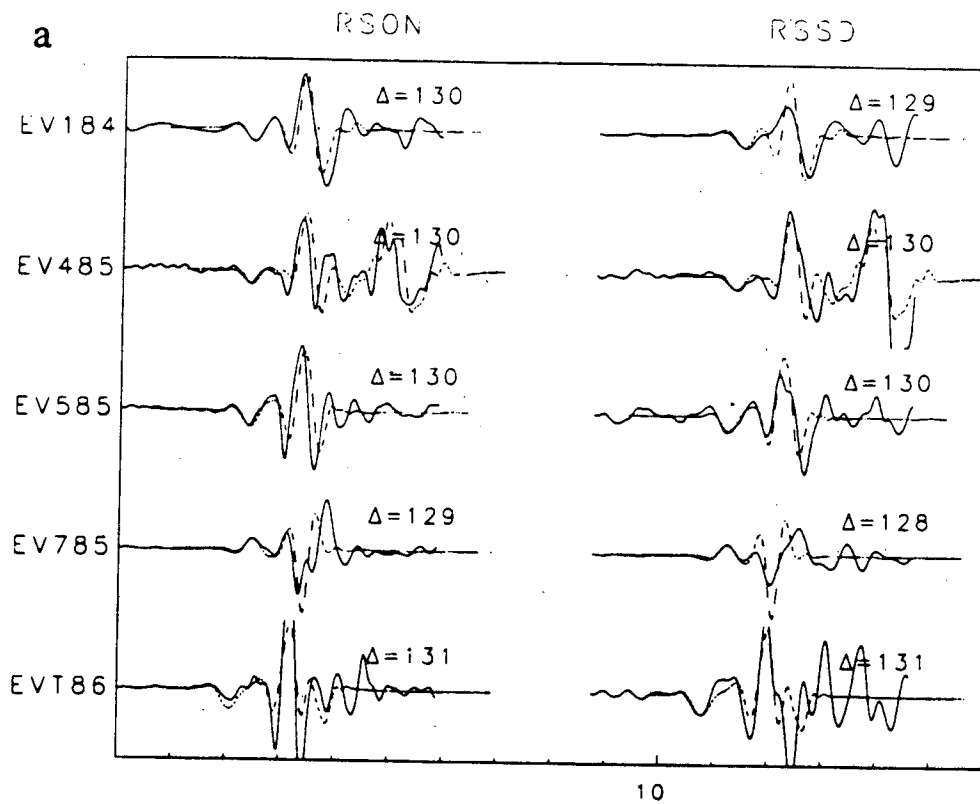


Figure 4

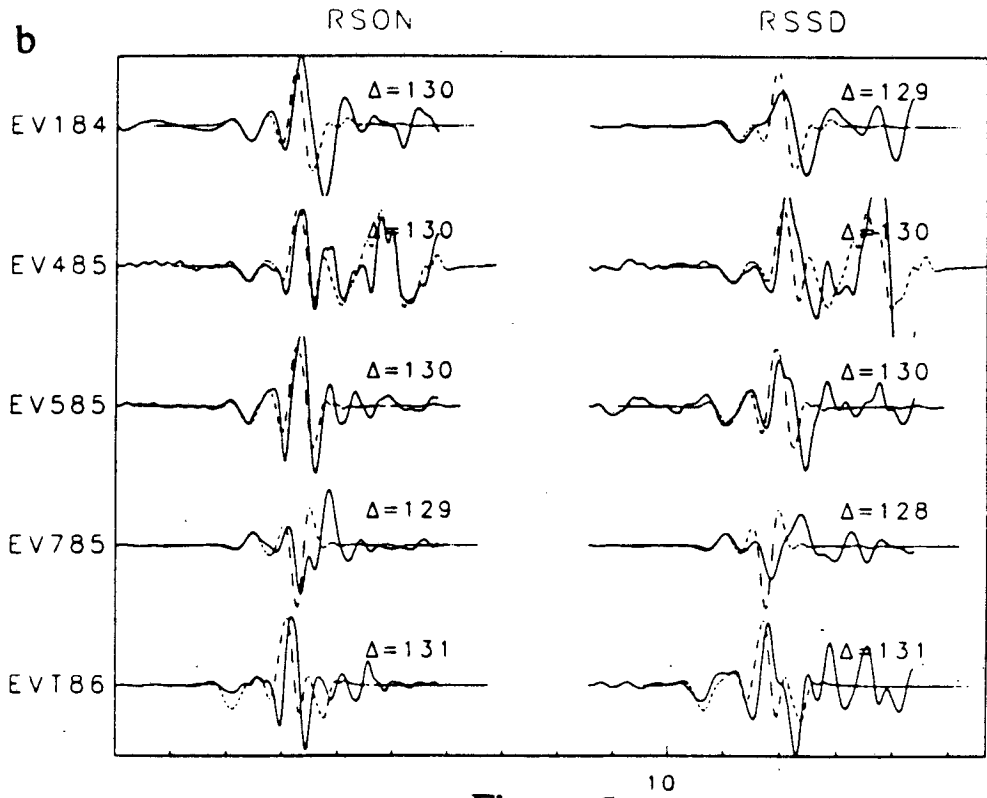
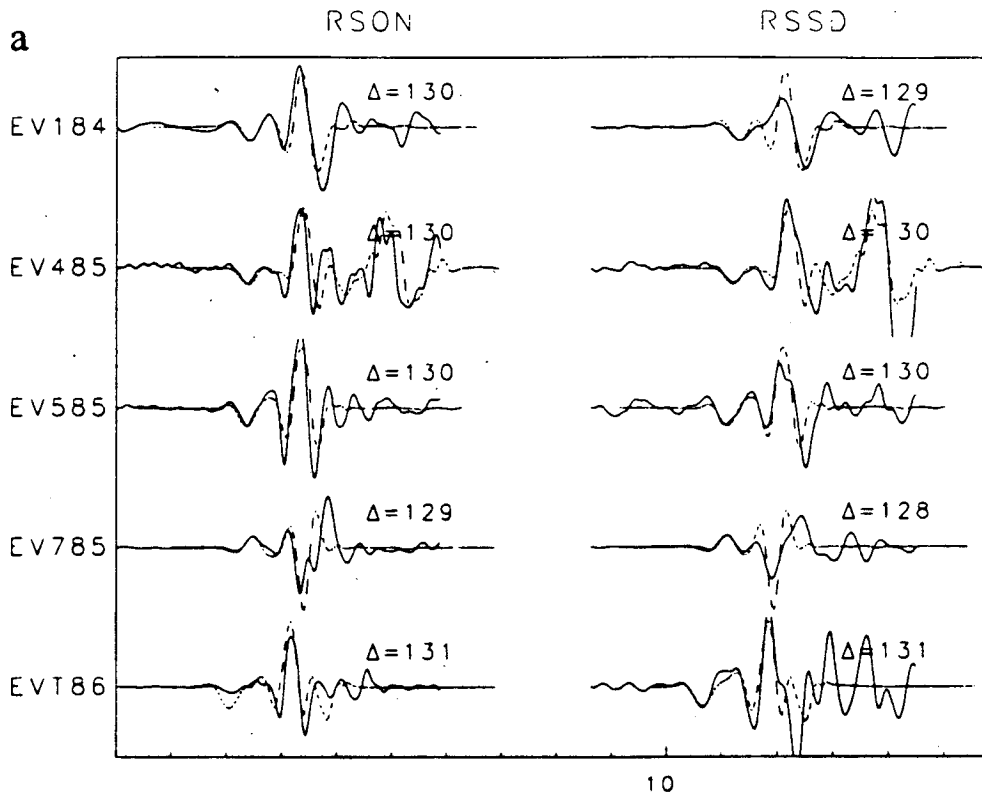


Figure 5

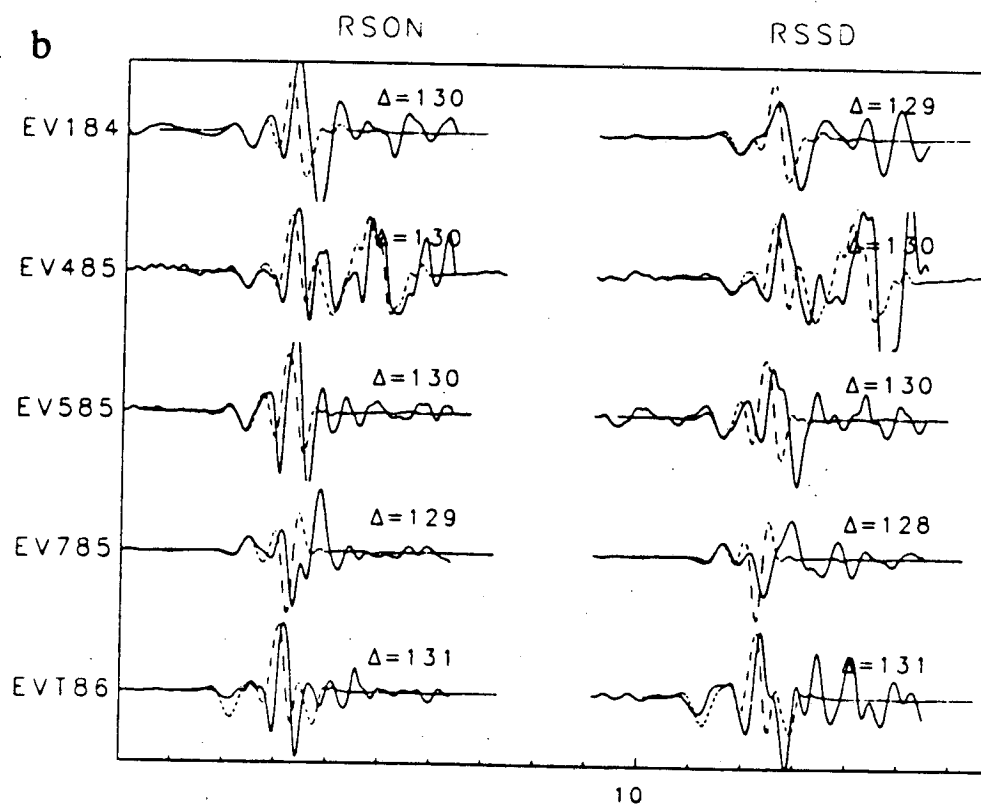
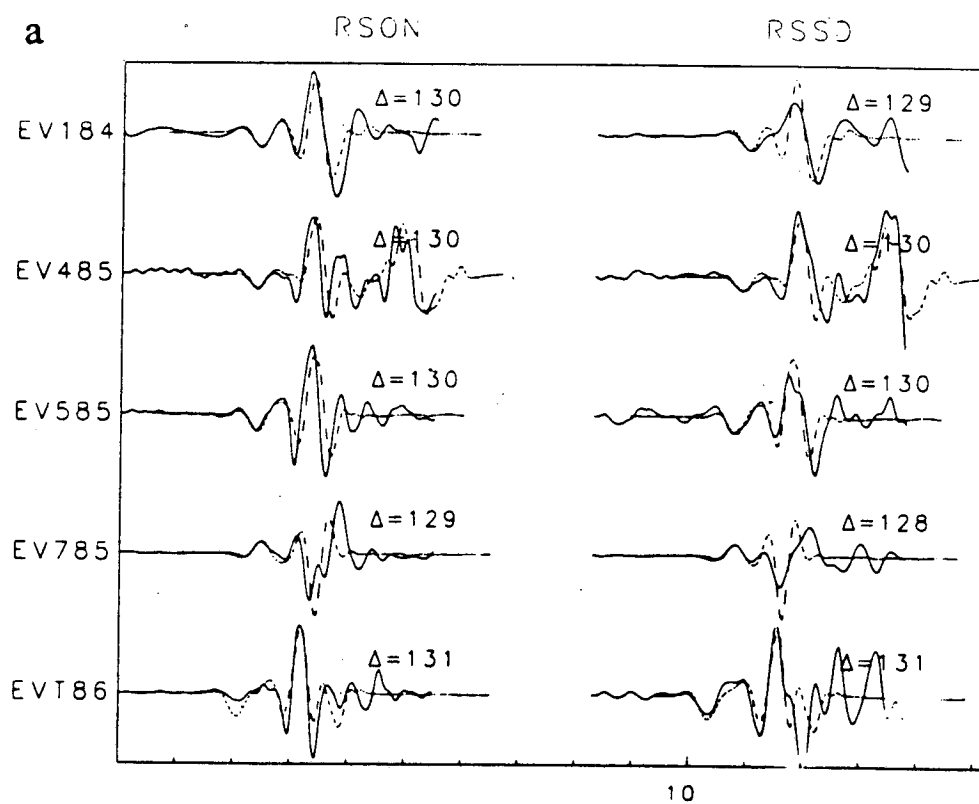


Figure 6

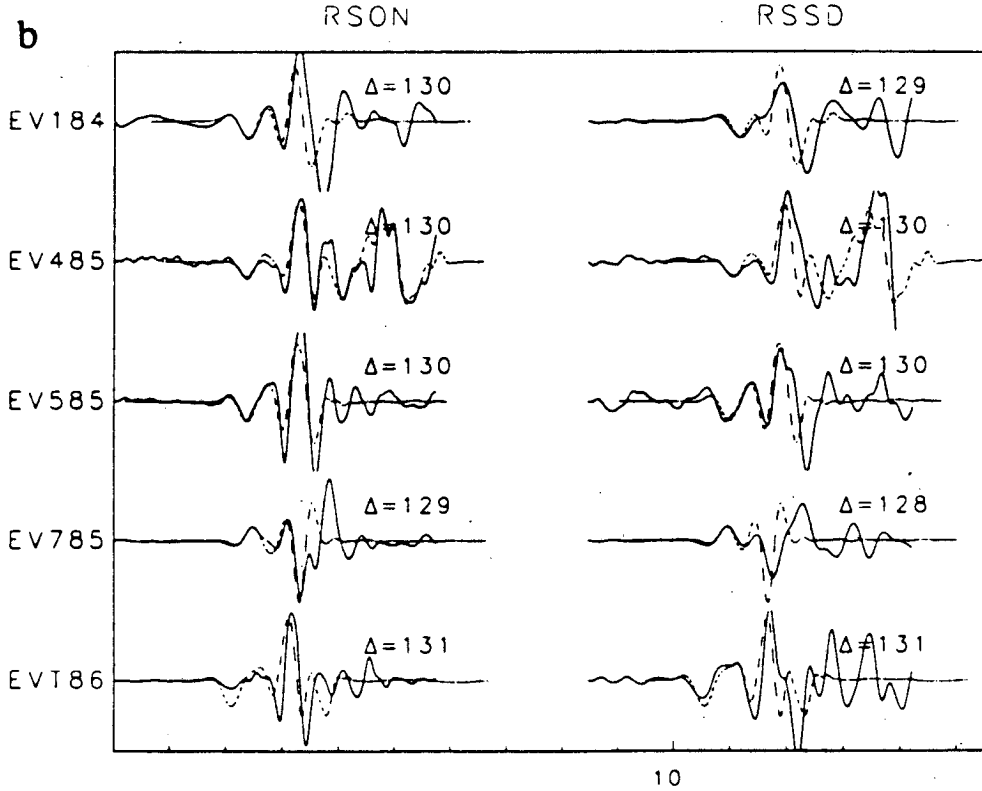
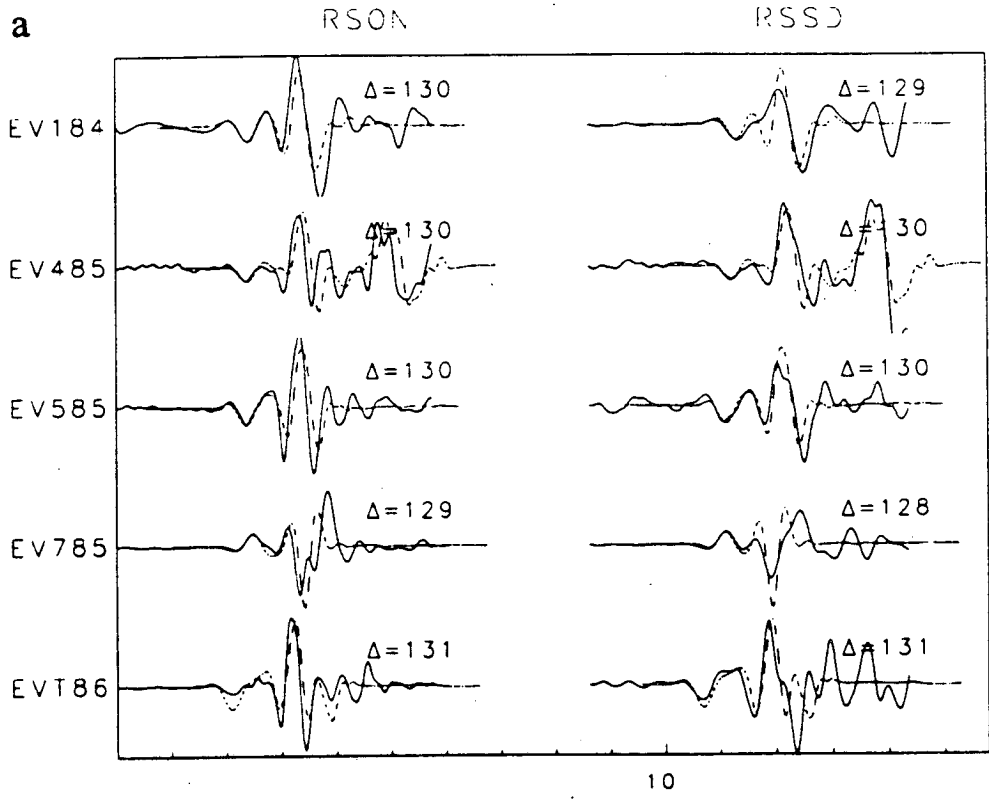


Figure 7

Appendix C: Translation of M.A. Isakovich's

Article on Thermal Dispersion

On the Propagation of Sound in Emulsions*

M. A. Isakovich

P. N. Lebedev Institute of Physics, Academy of Sciences of the USSR

Translated by Phil Cummins

The propagation of sound in emulsions is considered. It is shown that there must be "thermal dispersion" of the acoustic velocity in emulsions, as well as absorption of sound with a characteristic frequency dependence of the coefficient of absorption.

1. Thermal Diffusion in Fluids

It is well known that propagation of sound in fluids generally takes place at the Laplace velocity; alternatively, it may be said that when calculating the speed of sound we may consider changes of temperature in regions of compression and dilatation of the sound wave to take place adiabatically. Actually, "thermal dispersion", that is to say the transition to the Newtonian sound velocity (isothermal expansion and contraction) may become noticeable at

Translated from *Zhurnal Eksperimental'noi i Teoreticheskoi Fiziki*, 18, 907, 1948.

frequencies sufficiently high that thermal wavelengths become comparable to acoustic wavelengths. For fluids, for example, these frequencies are of the order of 10^{12} and higher. But at such high frequencies the propagation of sound effectively ceases as a consequence of strong attenuation. Thus, thermal dispersion in ordinary homogeneous fluids is not observable.

Nevertheless, thermal dispersion may be observed under certain conditions. Here we shall consider the propagation of sound in an emulsion of one fluid in another, assuming (as is always the case in practice) that the grain size of the emulsion is small compared to the acoustic wave length; that is, that the emulsion is "macroscopically" homogeneous. The temperature changes in each component of the emulsion due to the passage of the sound wave will in general be different. "Macroscopic" expansions and contractions will take place adiabatically, as formerly. But at low frequencies the temperature differences between the grains of the emulsion and the surrounding medium will tend to equalize - the process will be "microscopically" isothermal. At higher frequencies this equilibration will not take place and the process will be adiabatic "microscopically" as well. The critical frequency is here that frequency at which the thermal wave length is of the order of the emulsion grain size. At the transition past this frequency the compressibility of the emulsion will change from its "adiabatic-isothermal" to its "adiabatic-adiabatic" value. The sound velocity will change accordingly from the "Laplace-Newton" (LN) to the "Laplace-Laplace" (LL) velocity.

It is well known that the quantity $\gamma = C_p/C_v$ for homogeneous fluids is determined by the ratio of the compressibility obtained by statistical methods to that obtained from the speed of sound (?). It is asserted in what follows that for emulsions this ratio is a function of frequency, which becomes the ratio of heat capacities in the limit of low frequency.

2. "Laplace-Newton" and "Laplace-Laplace" Sound Velocities

Knowing the mechanical and thermodynamic constants of the components, it is not difficult to calculate the limiting values of the compressibility and sound velocity of an emulsion at low and high frequencies.

We introduce the notation: Θ - absolute average temperature, α - coefficient of thermal expansion, β - isothermal compressibility, ρ - density, χ - thermal conductivity, ε - emulsion concentration. We will use indices to distinguish values pertaining to the first and second components of the emulsion. We will use letters without indices to denote values averaged over volume; furthermore, we will omit indices also in written expressions that pertain equally to both components.

The adiabatic compressibility of either component is equal to β/γ ; employing the thermodynamic relation $C_p - C_v = \Theta\alpha/\rho\beta$, we may write the adiabatic compressibilities in the form:

$$\beta - \Theta\alpha^2/\rho C_p \quad (1)$$

The values α, β, ρ, C_p for the emulsion are obtained by adding the values for each component.

The "adiabatic-adiabatic" compressibility of the emulsion can be expressed in the form:

$$\varepsilon\beta_1/\gamma_1 + (1-\varepsilon)\beta_2/\gamma_2 = \varepsilon(\beta_1 - \Theta\alpha_1^2/\rho_1 C_{p1}) + (1-\varepsilon)(\beta_2 - \Theta\alpha_2^2/\rho_2 C_{p2})$$

The "adiabatic-isothermal" compressibility may be found from the expression (1),

$$\varepsilon\beta_1 + (1-\varepsilon)\beta_2 - \Theta \frac{[\varepsilon\alpha_1 + (1-\varepsilon)\alpha_2]^2}{[\varepsilon\rho_1 + (1-\varepsilon)\rho_2][\varepsilon C_{p1} + (1-\varepsilon)C_{p2}]}$$

From this we get the expression for the LN velocity c_{LN} and the LL velocity c_{LL} :

$$c_{LN} = \left\{ [\varepsilon\rho_1 + (1-\varepsilon)\rho_2][\varepsilon\beta_1 + (1-\varepsilon)\beta_2] - \Theta \frac{[\varepsilon\alpha_1 + (1-\varepsilon)\alpha_2]^2}{[\varepsilon C_{p1} + (1-\varepsilon)C_{p2}]} \right\}^{-1/2} \quad (2)$$

$$c_{LL} = \left\{ [\varepsilon\rho_1 + (1-\varepsilon)\rho_2][\varepsilon\beta_1/\gamma_1 + (1-\varepsilon)\beta_2/\gamma_2] \right\}^{-1/2} \quad (3)$$

For example, for a 50% emulsion of spherical benzol particles in water, $c_{LN}=1260m/s$, and $c_{LL}=1350m/s$. The critical frequency is of order $\omega = 3 \times 10^5$, which is in the frequency range where ordinary attenuation is not yet strong.

Thus, the experimental determination of the dispersion curve is not necessarily difficult. As far as we know, up to the present the experimental determination of the velocity of sound in emulsions has been carried out only for high frequencies (*LL* velocity) [1].

3. General Equations

With the existence of such strong dispersion it is of interest to trace in detail the variation of the dispersion curve, which is bounded by the upper and lower values of the calculated asymptotic velocities. Furthermore, as discovered by N.N. Andreev, we may also expect an increase in attenuation.

For convenience in the computations we introduce the complex wave number $k-i\delta$, the imaginary part of which gives the attenuation. It is expressed by the formula:

$$k-i\delta = \omega\sqrt{\rho s/p}, \quad (4)$$

where $p = e^{i\omega x}$ is the acoustic pressure, ρ - average density, and s - the average complex compression of the emulsion. s is the result of averaging the compression over a volume small compared to a wavelength, but which encloses a sufficient number of heterogeneous sections so that the average characteristics of this volume element would be the same as those for the medium as a whole. A volume so defined may be considered to exist in a uniform oscillating pressure field $p \approx e^{i\omega x}$.

If heat exchange between adjoining portions of the emulsion did not take place, then the compression in every portion would be identical, and the average compression would be real: $s = \epsilon s_1 + (1-\epsilon)s_2$. The compression s_1 and s_2 must in this case be determined by the adiabatic compressibilities of the components.

In the presence of heat exchange it is necessary to solve the problem of heat transfer between emulsion components. The compression at every point is obtained from the equations of state for each component:

$$s_1 = \beta_1 p - \alpha_1 T_1, \quad s_2 = \beta_2 p - \alpha_2 T_2 \quad (5)$$

Here T_1 and T_2 are the increases in temperature due to the oscillating acoustic pressure and heat conduction. The average compression will now be complex and is given by the formula:

$$s = \epsilon \bar{s}_1 + (1-\epsilon) \bar{s}_2 = \frac{1}{V_1+V_2} \left[\int_{V_1} s_1 dV_1 + \int_{V_2} s_2 dV_2 \right] \quad (6)$$

Here V_1 and V_2 are the volumes occupied by each component, and the overbars denote averages over the corresponding volumes.

We note that such a treatment does not take into account the Kirchoff absorption which is due to "macroscopic" heat exchange between regions of dilatation and compression in the sound wave.

The spatial distribution of temperature T for each component is obtained from the appropriate equation of heat conduction: $\rho q = \chi \nabla^2 T$. Here q is the heat flow per unit time. To eliminate q we use the energy equation:

$$q = C_p \left[\frac{\partial T}{\partial t} \right] - \left[\Theta \alpha / \rho \right] \frac{\partial p}{\partial t}$$

Which yields:

$$\frac{\partial T}{\partial t} - \frac{\chi}{\rho C_p} \nabla^2 T - \Theta \frac{\alpha}{\rho C_p} \frac{\partial p}{\partial t} = 0$$

For sound of frequency ω we may take $T = e^{i\omega t} T'$, where T' depends only on the spatial coordinates. Omitting the prime, we get for unit pressure amplitude:

$$\nabla^2 T - 2in^2 T + 2in^2 \frac{\Theta \alpha}{\rho C_p} = 0 \quad (7)$$

Here, $(1+i)n = (1+i) \left(\frac{\omega \rho C_p}{2\chi} \right)^{1/2}$ is the complex wavenumber of the temperature wave.

The general solution of the inhomogeneous equation (7) is equal to the sum of the particular integral $T = \frac{\Theta \alpha}{\rho C_p}$ and the general solution of the homogeneous equation $\nabla^2 T - 2in^2 T = 0$. The arbitrary constants are chosen to satisfy the boundary conditions. For example, on the boundaries between volume elements the equalities

$$T_1 = T_2 \quad , \quad \chi_1 \frac{\partial T_1}{\partial v} = \chi_2 \frac{\partial T_2}{\partial v}$$

must hold, where v is the normal to the boundary.

By finding the integral of equation (7) which satisfies the boundary conditions we obtain the complex compression at every point in the medium:

$$s_1 = p(\beta_1 - \alpha_1 T_1) \quad , \quad s_2 = p(\beta_2 - \alpha_2 T_2) \quad (8)$$

Finally, the wave number is determined by the formula:

$$\begin{aligned} k - i\delta &= \omega \left\{ [\epsilon \rho_1 + (1-\epsilon)\rho_2] [\epsilon s_1 + (1-\epsilon)s_2] \right\}^{1/2} \\ &= \frac{\omega}{V_1 + V_2} [(V_1 \rho_1 + V_2 \rho_2) (\int_{V_1} s_1 dV_1 + \int_{V_2} s_2 dV_2)]^{1/2} \end{aligned} \quad (9)$$

4. One-Dimensional Emulsion

As a simple example we first consider a one-dimensional problem, assuming that the components of the emulsion are distributed in alternating layers of thicknesses $2h_1$ and $2h_2$. The layer thicknesses will be taken to be small compared to the acoustic wave length.

Obviously, in equalizing the temperature difference generated between layers by a change in pressure, the centers of the plane layers are adiabatic boundaries. Therefore, to obtain the average compression in a region small compared to an acoustic wave length, it is sufficient to find the average compression in the region between two adjacent adiabatic boundaries. If we take the plane $x = 0$ as the plane dividing two adjacent layers, then such a region may be taken as the section situated between the planes $x = -h_1$ and $x = +h_2$.

In equation (7) we must now set $\nabla^2 = \frac{d^2}{dx^2}$, and the boundary conditions take the form:

$$T_1 = T_2 \quad , \quad \chi_1 \frac{dT_1}{dx} = \chi_2 \frac{dT_2}{dx} \quad \text{at } x = 0$$

$$\frac{dT_1}{dx} = 0 \quad \text{at } x = -h_1, \quad \frac{dT_2}{dx} = 0 \quad \text{at } x = +h_2$$

The general integral of equation (7) may be written in the form:

$$T_1 = \left(\frac{\Theta \alpha_1}{\rho_1 C_{p1}} \right) + A_1 e^{(1+i)n_1 x} + B_1 e^{-(1+i)n_1 x}$$

and analogously for T_2 . The constants A_1, B_1, A_2, B_2 are determined from the boundary conditions. A simple calculation leads to the following expression for the average compression:

$$s = \frac{p}{h_1+h_2} \left\{ h_1 \frac{\beta_1}{\gamma_1} + h_2 \frac{\beta_2}{\gamma_2} + (1-i) \frac{\Theta}{\omega} \left(\frac{\alpha_1}{\rho_1 C_{p1}} - \frac{\alpha_2}{\rho_2 C_{p2}} \right)^2 \right. \\ \left. \times \frac{\chi_1 \chi_2 n_1 n_2 \tanh[(1+i)n_1 h_1] \tanh[(1+i)n_2 h_2]}{\chi_1 n_1 \tanh[(1+i)n_1 h_1] + \chi_2 n_2 \tanh[(1+i)n_2 h_2]} \right\}$$

Assuming the attenuation and dispersion to be small, we obtain in accordance with (3) and (4):

$$k - i\delta = k_{LL} + \frac{(1-i)}{2h_1+h_2} \Theta \rho c_{LL} \left(\frac{\alpha_1}{\rho_1 C_{p1}} - \frac{\alpha_2}{\rho_2 C_{p2}} \right)^2 \\ \times \frac{\chi_1 \chi_2 n_1 n_2 \tanh[(1+i)n_1 h_1] \tanh[(1+i)n_2 h_2]}{\chi_1 n_1 \tanh[(1+i)n_1 h_1] + \chi_2 n_2 \tanh[(1+i)n_2 h_2]} \quad (10)$$

Here $k_{LL} = \frac{\omega}{c_{LL}}$ is the real wave number for the LL velocity.

Analysis of the above expression has lead to a simpler expression in the case when the values of h, ρ, C_p , and χ are the same for both components. Then (10) takes the form:

$$k - i\delta = k_{LL} + \frac{(1-i)}{8h} \Theta c_{LL} \frac{(\alpha_1 - \alpha_2)^2}{\rho C_p^2} \chi n \tanh[(1+i)nh]$$

From which we obtain the phase velocity:

$$c = c_{LL} \left\{ 1 - \frac{\Theta c_{LL}^2 (\alpha_1 - \alpha_2)^2}{16nh C_p} (\text{Re} + \text{Im}) \tanh[(1+i)nh] \right\}$$

and the attenuation:

$$\delta = \frac{\omega \Theta c_{LL}^2 (\alpha_1 - \alpha_2)^2}{16nhC_p} (\text{Re} - \text{Im}) \tanh[(1+i)nh]$$

The curves in figure 1 show the dependence of dispersion and attenuation on the parameter nh . For small frequencies ($nh \ll 1$, that is, the thermal wavelength is much larger than the layer thickness) c becomes the LN velocity $c_{LN} = \sqrt{\gamma\rho\beta}$ where

$$\gamma = \left[1 - \Theta \frac{(\alpha_1 + \alpha_2)^2}{4\rho\beta C_p} \right]^{-1}$$

appears as the ratio of the macroscopic heat capacities of the emulsion (?).

The attenuation for small frequencies is given by:

$$\delta = \Theta \frac{(\alpha_1 - \alpha_2)^2 \rho c_{LL} h^2 \omega^2}{24\chi}$$

This has the same quadratic frequency dependence as ordinary Kirchoff absorption. On the other hand the dependence on the thermal conductivity is different: with increasing thermal conductivity the attenuation decreases. Introducing the "effective" thermal conductivity χ^* , we may write the attenuation coefficient in the same form as for the Kirchoff case:

$$\delta = \frac{\omega^2 \chi^* (\gamma - 1)}{2\rho c^3 C_p}$$

where to a good approximation

$$\chi^* \approx \frac{(ch\rho C_p)^2}{\chi} = \chi \left(\frac{\lambda h}{\Lambda} \right)^2$$

Here $\lambda = 2\pi/k$ is the acoustic wave length, and $\Lambda = 2\pi\sqrt{2\chi/\omega\rho C_p}$ is the thermal wave length.

At high frequencies ($nh \gg 1$) the propagation speed approaches the LL value:

$$c = c_{LL} \left[1 - \frac{\Theta c_{LL}^2 (\alpha_1 - \alpha_2)^2}{16nh\chi C_p} \right]$$

The attenuation increases in proportion to the square root of the frequency:

$$\delta = \frac{\Theta c_{LL} (\alpha_1 - \alpha_2)^2 \chi n}{8h\rho C_p^2}$$

As was shown elsewhere [2], this frequency dependence is also consistent with other cases of sound wave propagation in heterogeneous media.

Here we may likewise, purely as a matter of convention, introduce an "effective" thermal conductivity, which is given approximately by:

$$\chi^* = (c^2/h)(\chi\rho C_p)^{1/2}\omega^{-3/2} \approx \chi(\lambda^2/h\Lambda)$$

Here, however, χ^* is not constant, but decreases with increasing frequency as $\omega^{-3/2}$.

5. Emulsion with Spherical Particles

For a situation easily realized in practice - that of one fluid in another - the calculation may be carried out provided that there is no thermal interaction between the emulsion grains (the distance between the emulsion grains is larger than the thermal wave length in the surrounding medium), i. e., for sufficiently dilute emulsions. Then the temperature distribution near the individual grains will be the same as if an isolated grain of one component were embedded in an infinite medium of the other component.

If an emulsion grain has spherical form, then the solution to equation (7) takes the form:

$$T_1 = \frac{\Theta\alpha_1}{\rho_1 C_{p1}} + \frac{A}{r} \sinh[(1+i)n_1 r]$$

in the emulsion grain, and

$$T_2 = \frac{\Theta\alpha_2}{\rho_2 C_{p2}} + \frac{B}{r} e^{-(1+i)n_2 r}$$

in the surrounding medium. Here r denotes distance from the center of the emulsion grain.

The boundary conditions have the form: $T_1 = T_2$, $\chi_1 \frac{dT_1}{dr} = \chi_2 \frac{dT_2}{dr}$ at $r=R$, where R is the emulsion grain radius.

The solution, expressed according to the scheme of the preceding section, is:

$$k-i\delta = k_{LL} - i\frac{3}{2R^2} \epsilon \Theta \rho C_{LL} \left(\frac{\alpha_1}{\rho_1 C_{p1}} - \frac{\alpha_2}{\rho_2 C_{p2}} \right)^2$$

$$\times \frac{\chi_1 \chi_2 \left\{ [(1+i)n_2 R + 1](1+i)n_1 R - \tanh[(1+i)n_1 R] \right\}}{\chi_1 \left\{ (1+i)n_1 R - \tanh[(1+i)n_1 R] \right\} + \chi_2 [(1+i)n_2 R + 1] \tanh[(1+i)n_1 R]}$$

For small frequencies ($n_1 R \ll 1$), we get:

$$c_{LN} = c_{LL} \left[1 - 1/2 \varepsilon \Theta c_{LL}^2 \rho \rho_1 C_{p1} \left(\frac{\alpha_1}{\rho_1 C_{p1}} - \frac{\alpha_2}{\rho_2 C_{p2}} \right)^2 \right]$$

$$\delta = \left(\frac{1}{6\chi_1} \right) \varepsilon \Theta c_{LL} \rho \rho_1^2 C_{p1}^2 (1/5 + \chi_1/\chi_2) R^2 \omega^2$$

For large frequencies ($n_1 R \gg 1$), we find:

$$c = c_{LL} \left[1 - \frac{3}{2R\sqrt{2}\omega} \varepsilon \Theta \rho c_{LL}^2 \left(\frac{\alpha_1}{\rho_1 C_{p1}} - \frac{\alpha_2}{\rho_2 C_{p2}} \right)^2 \frac{(\chi_1 \chi_2 \rho_1 \rho_2 C_{p1} C_{p2})^{1/2}}{(\chi_1 \rho_1 C_{p1})^{1/2} + (\chi_2 \rho_2 C_{p2})^{1/2}} \right]$$

$$\delta = \sqrt{\omega} \frac{3}{2\sqrt{2}R} \varepsilon \Theta \rho c_{LL} \left(\frac{\alpha_1}{\rho_1 C_{p1}} - \frac{\alpha_2}{\rho_2 C_{p2}} \right)^2 \frac{(\chi_1 \chi_2 \rho_1 \rho_2 C_{p1} C_{p2})^{1/2}}{(\chi_1 \rho_1 C_{p1})^{1/2} + (\chi_2 \rho_2 C_{p2})^{1/2}}$$

These characteristic forms for the dependence of absorption and dispersion on the medium parameters and frequency are the same as for a one-dimensional emulsion.

In conclusion we emphasize that the attenuation of sound in an emulsion may be strong even at moderate frequencies. For example, for a 10% emulsion of benzol in water, with grain size $\approx 5\mu$, attenuation is $\delta = 1.5 \times 10^{-5} \omega^{1/2}$, at frequencies higher than 10^5 Hz. Thus, at a frequency of 1.5×10^5 Hz, $\delta \approx 1.5 \times 10^{-2}$ (?), which is typically 100 times greater than the attenuation of pure benzol at this frequency.

[1] Urick. Journ. Appl. Phys., 18, 983, 1947.

[2] Isakovich. JETP, 18, 386, 1948.

Appendix D: A Detailed Derivation of Isakovich's

Formulas in Section 5

The solutions for the temperature distribution in the spherical emulsion grains and in the surrounding medium are:

$$T_1 = \frac{\Theta\alpha_1}{\rho_1 C_{p1}} + \frac{A}{r} \sinh[(1+i)n_1 r] \quad , \quad T_2 = \frac{\Theta\alpha_2}{\rho_2 C_{p2}} + \frac{B}{r} e^{-(1+i)n_2 r}$$

The boundary conditions $T_1 = T_2$, $\chi_1 \frac{dT_1}{dr} = \chi_2 \frac{dT_2}{dr}$ at $r=R$ determine A and B :

$$A = R \Theta \left(\frac{\alpha_1}{\rho_1 C_{p1}} - \frac{\alpha_2}{\rho_2 C_{p2}} \right)$$

$$\times \frac{\chi_2[(1+i)n_2 R + 1]}{\chi_1(\sinh[(1+i)n_1 R] - (1+i)n_1 R \cosh[(1+i)n_1 R]) - \chi_2[(1+i)n_2 R + 1] \sinh[(1+i)n_1 R]}$$

$$B = R \Theta \left(\frac{\alpha_1}{\rho_1 C_{p1}} - \frac{\alpha_2}{\rho_2 C_{p2}} \right)$$

$$\times \frac{\chi_1(\sinh[(1+i)n_1 R] - (1+i)n_1 R \cosh[(1+i)n_1 R]) e^{(1+i)n_2 R}}{\chi_1(\sinh[(1+i)n_1 R] - (1+i)n_1 R \cosh[(1+i)n_1 R]) - \chi_2[(1+i)n_2 R + 1] \sinh[(1+i)n_1 R]}$$

For the average compression s,

$$s = \frac{1}{V_1 + V_2} \left[\int_{V_1} s_1 dV_1 + \int_{V_2} s_2 dV_2 \right]$$

$$= \beta_1 \frac{V_1}{V_1 + V_2} + \beta_2 \frac{V_2}{V_1 + V_2} - \frac{1}{V_1 + V_2} \left[\alpha_1 \int_{V_1} T_1 dV_1 + \alpha_2 \int_{V_2} T_2 dV_2 \right]$$

Now, the above solutions for T_1 and T_2 yield:

$$\begin{aligned} \int_{V_1} T_1 dV_1 &= 4\pi \int_0^R r^2 T_1(r) dr = V_1 \Theta \frac{\alpha_1}{\rho_1 C_{p1}} + 4\pi \int_0^R r \sinh[(1+i)n_1 r] dr \\ &= V_1 \Theta \frac{\alpha_1}{\rho_1 C_{p1}} + 4\pi A \left[\frac{R}{(1+i)n_1} \cosh[(1+i)n_1 R] - \frac{1}{[(1+i)n_1]^2} \sinh[(1+i)n_1 R] \right] \end{aligned}$$

$$\begin{aligned} \int_{V_2} T_2 dV_2 &= 4\pi \int_R^{\infty} r^2 T_2(r) dr = V_2 \Theta \frac{\alpha_2}{\rho_2 C_{p2}} + 4\pi \int_R^{\infty} r e^{-(1+i)n_2 r} dr \\ &= V_2 \Theta \frac{\alpha_2}{\rho_2 C_{p2}} + 4\pi B \left[\frac{R}{(1+i)n_2} + \frac{1}{[(1+i)n_2]^2} \right] e^{-(1+i)n_2 R} \end{aligned}$$

where R_{∞} is some distance large compared to the thermal wave length but small compared to the distance between emulsion grains. Thus,

$$\begin{aligned} \frac{s}{p} &= \varepsilon \beta_1 + (1-\varepsilon) \beta_2 - \Theta \left[\varepsilon \frac{\alpha_1^2}{\rho_1 C_{p1}} + (1-\varepsilon) \frac{\alpha_2^2}{\rho_2 C_{p2}} \right] \\ &\quad - \frac{4\pi}{V_1 + V_2} \left[\alpha_1 A \left[\frac{R}{(1+i)n_1} \cosh[(1+i)n_1 R] - \frac{1}{[(1+i)n_1]^2} \sinh[(1+i)n_1 R] \right] \right. \\ &\quad \left. + \alpha_2 B \left[\frac{R}{(1+i)n_2} + \frac{1}{[(1+i)n_2]^2} \right] e^{-(1+i)n_2 R} \right] \end{aligned}$$

where $\varepsilon = \frac{V_1}{V_1 + V_2}$. From Isakovich's eqs. (1) - (3),

$$1/c_L^2 = \rho \left[\varepsilon \left(\beta_1 - \Theta \frac{\alpha_1^2}{\rho_1 C_{p1}} \right) + (1-\varepsilon) \left(\beta_2 - \Theta \frac{\alpha_2^2}{\rho_2 C_{p2}} \right) \right]$$

and using $V_1 = 4\pi R^3/3$, the complex compression can be expressed in terms of the high frequency sound velocity c_{LL} :

$$s/p = 1/\rho c^2 = \frac{1}{\rho c_{LL}^2} - \frac{3\epsilon}{R^2} \left[\frac{\alpha_1 A}{(1+i)n_1} (\cosh[(1+i)n_1 R] - \frac{\sinh[(1+i)n_1 R]}{[(1+i)n_1 R]}) \right. \\ \left. + \frac{\alpha_2 B}{(1+i)n_2} e^{-(1+i)n_2 R} \left(1 + \frac{1}{[(1+i)n_2]R}\right) \right]$$

$$\frac{1}{c^2} = \frac{1}{c_{LL}^2} - \frac{3\epsilon\rho\Theta}{R^2} \left(\frac{\alpha_1}{\rho_1 C_{p1}} - \frac{\alpha_2}{\rho_2 C_{p2}} \right)$$

$$\left[\frac{\alpha_1 \chi_2 R [(1+i)n_2 R + 1]}{(1+i)n_1} (\cosh[(1+i)n_1 R] - \frac{\sinh[(1+i)n_1 R]}{[(1+i)n_1]R}) \right. \\ \left. + \frac{\alpha_2}{(1+i)n_2} \left(1 + \frac{1}{(1+i)n_2 R}\right) R \chi_1 (\sinh[(1+i)n_1 R] - (1+i)n_1 R \cosh[(1+i)n_1 R]) \right] \\ \times \frac{-1}{\chi_1 ((1+i)n_1 R \cosh[(1+i)n_1 R] - \sinh[(1+i)n_1 R]) + \chi_2 [(1+i)n_2 R + 1] \sinh[(1+i)n_1 R]}$$

or, using $n^2 = \frac{\omega\rho C_p}{2\chi}$:

$$\frac{1}{c^2} = \frac{1}{c_{LL}^2} + \frac{3\epsilon\rho\Theta}{R^2} \frac{2}{(1+i)\omega} \left(\frac{\alpha_1}{\rho_1 C_{p1}} - \frac{\alpha_2}{\rho_2 C_{p2}} \right) \left[\frac{n_1 \alpha_1 [(1+i)n_2 R + 1]}{\rho_1 C_{p1} (1+i)n_1 R} - \frac{n_2 \alpha_2}{\rho_2 C_{p2}} \left[1 + \frac{1}{(1+i)n_2 R}\right] \right] \\ \times \frac{[(1+i)n_1 R - \tanh[(1+i)n_1 R]] R \chi_1 \chi_2}{\chi_1 ((1+i)n_1 R - \tanh[(1+i)n_1 R]) + \chi_2 [(1+i)n_2 R + 1] \tanh[(1+i)n_1 R]}$$

$$\begin{aligned}
&= \frac{1}{c_{L2}^2} + \frac{3\epsilon\rho\Theta}{R^2} \frac{2R\chi_1\chi_2}{(1+i)\omega} \left(\frac{\alpha_1}{\rho_1 C_{p1}} - \frac{\alpha_2}{\rho_2 C_{p2}} \right) \left[n_2 \left(\frac{\alpha_1}{\rho_1 C_{p1}} - \frac{\alpha_2}{\rho_2 C_{p2}} \right) + \frac{1}{(1+i)R} \left(\frac{\alpha_1}{\rho_1 C_{p1}} - \frac{\alpha_2}{\rho_2 C_{p2}} \right) \right] \\
&\quad \times \frac{-((1+i)n_1R - \tanh[(1+i)n_1R])}{\chi_1((1+i)n_1R - \tanh[(1+i)n_1R]) + \chi_2[(1+i)n_2R + 1]\tanh[(1+i)n_1R]} \\
&= \frac{1}{c_{L2}^2} - i \frac{3\epsilon\rho\Theta}{\omega R^2} \times \left(\frac{\alpha_1}{\rho_1 C_{p1}} - \frac{\alpha_2}{\rho_2 C_{p2}} \right)^2 \\
&\quad \frac{\chi_1\chi_2((1+i)n_2R+1)((1+i)n_1R - \tanh[(1+i)n_1R])}{\chi_1((1+i)n_1R - \tanh[(1+i)n_1R]) + \chi_2[(1+i)n_2R + 1]\tanh[(1+i)n_1R]}
\end{aligned}$$

which is equivalent to Isakovich's dispersion formula, although Isakovich has used a "low-loss" approximation. No such approximation has been used in the above derivation.

Unfortunately, the above dispersion formula is referenced to the high frequency velocity. To reference this formula to the low frequency velocity, it is necessary to take the limit of the above expression as $\omega \rightarrow 0$. This is obtained from the following:

$$\begin{aligned}
&\frac{1}{\omega} \frac{[(1+i)n_2R+1][(1+i)n_1R - \tanh[(1+i)n_1R])}{\chi_1((1+i)n_1R - \tanh[(1+i)n_1R]) + \chi_2[(1+i)n_2R + 1]\tanh[(1+i)n_1R]} \\
&= \frac{1}{\omega} \frac{[(1+i)n_2R+1][(1+i)n_1R \cosh[(1+i)n_1R] - \sinh[(1+i)n_1R])}{\chi_1((1+i)n_1R \cosh[(1+i)n_1R] - \sinh[(1+i)n_1R]) + \chi_2[(1+i)n_2R + 1]\sinh[(1+i)n_1R]} \\
&\rightarrow_{\omega \rightarrow 0} \frac{1}{\omega} \frac{[(1+i)n_2R+1] \left[(1+i)n_1R \left(1 + \frac{1}{2}[(1+i)n_1R]^2 + \dots \right) \right]}{\chi_1 \left[(1+i)n_1R \left(1 + \frac{1}{2}[(1+i)n_1R]^2 + \dots \right) - ((1+i)n_1R + \dots) \right]}
\end{aligned}$$

$$\frac{\dots \left[-((1+i)n_1R + \frac{1}{6}[(1+i)n_1R]^3 + \dots) \right]}{+\chi_2 \left[[(1+i)n_2R + 1] \frac{1}{2}((1+i)n_1R + \dots) \right]}$$

$$\rightarrow \frac{1}{3\chi_2\omega} [(1+i)n_1R]^2 = i \frac{R^2 \rho_1 C_{p1}}{3\chi_1 \chi_2}$$

Thus,

$$\lim_{\omega \rightarrow 0} \frac{1}{c^2} = \frac{1}{c_{LN}^2} = \frac{1}{c_{LL}^2} + \epsilon \Theta \rho \rho_1 C_{p1} \left[\frac{\alpha_1}{\rho_1 C_{p1}} - \frac{\alpha_2}{\rho_2 C_{p2}} \right]^2$$

This agrees with Isakovich's formula. Finally, the dispersion formula referenced to the low frequency velocity is:

$$\frac{1}{c^2} = \frac{1}{c_{LN}^2} - \epsilon \Theta \rho \rho_1 C_{p1} \left(\frac{\alpha_1}{\rho_1 C_{p1}} - \frac{\alpha_2}{\rho_2 C_{p2}} \right)^2$$

$$\times \left[1 + \frac{3i}{\omega R^2 \rho_1 C_{p1}} \frac{\chi_1 \chi_2 ((1+i)n_2R + 1) ((1+i)n_1R - \tanh[(1+i)n_1R])}{\chi_1 ((1+i)n_1R - \tanh[(1+i)n_1R]) + \chi_2 ((1+i)n_2R + 1) \tanh[(1+i)n_1R]} \right]$$

In the case when $\chi_1 = \chi_2$, this expression takes the slightly simpler form:

$$\frac{1}{c^2} = \frac{1}{c_{LN}^2} -$$

$$A \times \left[1 + i \frac{3}{2\omega\tau_1} \frac{((1+i)\sqrt{\omega\tau_2+1})(1+i)\sqrt{\omega\tau_1} - \tanh[(1+i)\sqrt{\omega\tau_1}]}{((1+i)\sqrt{\omega\tau_1} - \tanh[(1+i)\sqrt{\omega\tau_1}]) + [(1+i)\sqrt{\omega\tau_2+1}] \tanh[(1+i)\sqrt{\omega\tau_1}]} \right]$$

where $A = \frac{3}{2} \epsilon \Theta \rho \rho_1 C_{p1} \left(\frac{\alpha_1}{\rho_1 C_{p1}} - \frac{\alpha_2}{\rho_2 C_{p2}} \right)^2$ and $\tau = \frac{R^2 \rho C_p}{2\chi}$.

LAWRENCE BERKELEY LABORATORY
TECHNICAL INFORMATION DEPARTMENT
UNIVERSITY OF CALIFORNIA
BERKELEY, CALIFORNIA 94720